University of Bremen
Geoscience

Alfred Wegener Institute
Helmholtz Center for Polar and Marine Research

Dissertation zur Erlangung des Grades

Dr. rer. nat

The role of atmospheric circulation patterns on the variability of ice core constituents in coastal Dronning Maud Land, Antarctica

vorgelegt von

Kerstin Schmidt

20.10.2015

Erklärung

Hiermit versichere ich, dass ich diese Dissertation selbständig verfasst und keine anderen als die angegebenen Quellen und Hilfsmittel benutzt habe. Die Stellen meiner Arbeit, die dem Wortlaut oder dem Sinn nach anderen Werken entnommen sind, habe ich in jedem Fall unter Angabe der Quelle als Entlehnung kenntlich gemacht. Dasselbe gilt für Tabellen, Karten und Abbildungen. Diese Arbeit hat in dieser oder einer ähnlichen Form noch nicht im Rahmen einer anderen Prüfung vorgelegen. Einer Veröffentlichung durch die Bibliothek stimme ich zu.

Hamburg den 20. Oktober 2015

Kerstin Schmidt

Die vorliegende Dissertation wurde am 03.05.2017 an der Universität Bremen verteidigt. Der Prüfungsausschuss bestand aus Prof. Dr. Heinrich Miller (erster Gutachter), Prof. Dr. Gerrit Lohmann (zweiter Gutachter), Prof. Dr. Heinrich Villinger, Prof. Dr. Tilo von Dobeneck, Dr. Ute Merkel und Rouven Brune

Abstract

Atmospheric circulation pattern highly influence the concentrations of ice core constituents by affecting their source strength, transport path and deposition. In 2007 four firn cores were drilled in the Ekströmisen catchment area (ECA), covering a time interval of 50 years. The ECA is located in the hinterland of the German wintering station Neumayer that is characterized by very high accumulation rates. The objective of this study is to connect records of ice core constituents with atmospheric circulation pattern on regional and synoptic scale.

Continuous flow analysis (CFA) was used to quantify concentrations of firn core constituents and discrete samples were taken that were analyzed using ion chromatography (IC). Spatial gradients of mineral dust, sea salt, sulphate and nitrate showed that sea salt concentrations are closely connected to the cyclones approaching from the southern ocean. Mineral dust particles have their source in Patagonia and are then transported in the upper troposphere to the Antarctic plateau, where they subside. From the Antarctic plateau they are transported to the ECA by katabatic winds. Sea salt particles are closely connected to local atmospheric processes as cyclone activity. Sulphate in coastal Antarctica depends on the presence of sea ice and the solar cycle. Nitrate concentrations are uniformly distributed within the ECA, indicating that nitrate concentrations are independent of local conditions.

To investigate the atmospheric circulation pattern connected to events in firn core constituents monthly NCEP-NCAR reanalysis data where used to calculate composite maps. The results showed that on the southern hemispheric scale, concentrations of mineral dust and sea salt mainly depend on the conditions in the source region and that a strong source supports high concentrations of mineral dust and sea salt.

In conclusion, the knowledge of the prevailing local changes in wind and the accompanying changes in concentrations of firn core constituents can be used to investigate changes in local winds and topography in a region were atmospheric measurements are sparse. On the southern hemispheric scale, concentration of firn core constituents can help to better understand the climate in the source region. The method presented in this study provides a robust analysis method for ice core records that gives the opportunity to compare ice core data with atmospheric models.

Zusammenfassung

Durch ihren Einfluss auf Quellstärke, Transport und Deposition von Spurenstoffen stehen atmosphärische Strömungen im engen Zusammenhang zu Spurenstoffkonzentrationen, die in Eisbohrkernen gemessen werden. Das Hinterland der Neumayerstation, in dieser Arbeit als Ekströmisen catchment area (ECA) bezeichnet, ist bekannt für sehr hohe Schneeakkumulationsraten. Im Jahr 2007 wurden dort vier Firnbohrkerne gebohrt, die einen Zeitraum von 50 Jahren abdecken. Das Ziel dieser Arbeit ist es, die Zusammenhänge von atmosphärischen Zirkulationsmustern und Spurenstoffen in Eisbohrkernen auf regionaler und südhemisphärischer Skala zu untersuchen.
Die Eisbohrkerne wurden mit Hilfe von kontinuierlicher Durchflussanalyse (CFA) und Ionenchromatografie (IC) auf Spurenstoffe untersucht. Anhand von räumlichen Gradienten und der saisonalen Verteilung wird gezeigt dass Meersalzkonzentrationen im Eis vor allem von Zyklonen aus dem Südpolarmeer beeinflusst werden. Mineralstaubpartikel haben ihre Quelle in Patagonien. Von dort werden sie über die obere Tropsphäre zum antarktischen Plateau transportiert, wo sie zum Boden abgesenkt werden. Mit katabatischen Winden werden sie von dort weiter in die ECA eingetragen. Sulfatkonzentrationen hängen hauptsächlich von der Quellstärke und dem Sonnenzyklus ab. Nitratkonzentration sind gleichmäßig in der ECA verteilt und somit unabhängig von lokalen Einflüssen.
Aus monatlichen Reanalysedaten (NCEP-NCAR) in denen stabile Isotope im Sauerstoff und Mineralstaub- und Meersalzkonzentrationen einen Grenzwert überschreiten werden Mittelwerte berechnet mit dem Ziel die atmosphärischen Strömungsmuster zu finden welche für hohe Konzentrationen wichtig sind. Für alle untersuchten Spurenstoffe zeigt sich, dass auf der südhemisphärischen Skala die Quellstärke der entscheidende Faktor ist im Vergleich zu Transport und Deposition.
Zusammenfassend kann anhand der lokalen Unterschiede gezeigt werden, dass Spurenstoffe genutzt werden können um lokale Topograhie und Winde in Gegenden zu rekonstuieren in denen es nur wenige atmosphärische Messungen gibt. Zudem kann auf der synoptischen Skala die Quellstärke anhand der Spurenstoffkonzentrationen im Eis rekonstruiert werden. Mit der vorgestellten Methode ist es möglich, eine stabile Analyse durchzuführen um Spurenstoffkonzentrationen im Eis mit atmosphärischen Modellen zu vergleichen und dadurch Klimaveränderungen besser zu verstehen.

Contents

1 Introduction

Aerosols deposited in Antarctica and Greenland provide a unique archive for climate reconstructions. Aerosol constituents and air bubbles are archived in the large ice sheets making it possible to study the climate of at least the last 800,000 years (e.g. EPICA-Community-Members, 2004). Aerosol constituents in ice cores are especially interesting regarding local climate conditions because they are mostly influenced by those, even though some global patterns play a role in source conditions and transport. All of these however depend on the respective ice core constituents and its source. For example, mineral dust concentrations depend mostly on the conditions in the source region (Albani et al., 2012). Therefore, mineral dust concentrations measured in ice cores can give good estimates about the temperatures and humidity in the mineral dust source region (McConnell et al., 2007; Mahowald et al., 2010). The topography in Antarctica can not only influence the accumulation but also the wind near the surface. A ridge orthogonal to the main wind direction can force an air mass to rise in order to pass it. On the other hand, a large temperature gradient along a sloping ridge can force katabatic wind (King and Turner, 1997). This study will show that mineral dust concentrations are also connected to katabatic winds approaching from the Antarctic plateau. The nitrate source is mostly in the stratosphere (Wagenbach et al., 1998b), but it will be shown that part of the nitrate measured in Antarctic ice cores can be explained by re-emission and transport by katabatic wind from the Antarctic plateau.

Sea salt particles have shorter transport paths and thus have the potential to represent the cyclonic activity in Antarctica (Korhonen et al., 2010). Cyclonic storms in Antarctica have a high frequency and can be very intense. Since they have such a great temporal variability it is important to study them on a long time scale Simmonds et al. (2003). This is especially true for the coastal

regions, because the Antarctic plateau forces most low pressure systems to proceed along the Antarctic coastline. The presence of the open ocean or sea ice can strengthen or weaken a low pressure system. This is then also reflected in the wind velocities on the ice sheet. Sea ice plays a large role in the heat exchange between ocean and atmosphere. This leads to a larger or smaller temperature gradient that then leads to pressure differences and thus stronger or weaker winds (King and Turner, 1997). It will be shown that the sea ice extend and sulphate concentrations in ice cores are connected.

The importance of ice cores located along coastal areas came into focus during the last years due to the fact that they have a great capability of studying the relationship of atmospheric processes and ice core constituents. The Ekströmisen catchment area (ECA) located in coastal Dronning Maud Land (figure 1) is one potential high-accumulation location of a drillsite for the ice core array covering the past 2000 years (2k array) planned in the framework of IPICS (International partnership in ice core science, `www.pages-igbp.org/ipics`) with the potential to reach back into the end of the last glacial stage (Drews et al., 2013). Four firn cores have been drilled in 2007 with the goal to find a good drill location to fulfill the requirement for the 2000 year goal of IPICS, which is to build up a network of high resolution ice cores in Antarctica, Greenland and the glaciers in lower latitudes to study the relationship of atmospheric processes and ice cores in detail. For this a good knowledge has to be gained about how aerosol constituents are emitted into the atmosphere, how they are transported and deposited and how they influence the ice itself. Only if all of these processes are understood it is possible to understand past climate and by this gain knowledge about the recent climate change.

The ECA has the big advantage of the closeness of the German wintering station Neumayer, where aerosols and meteorology have been observed since 1983. In addition to that, on the Antarctic plateau at Kohnen Station, an

intense survey has been conducted during the drill phase of the EPICA (European Partnership for ice coring in Antarctica) Dronning Maud Land ice core (EDML).

The objectives of this study are:

1. Analyzing firn cores from a very high accumulation region in coastal Antarctica on ice core constituents. The very high accumulation rates are needed to achieve a monthly resolution in the firn cores.

2. Use the time series above to investigate the regional variability of different ice core constituents and their possible connection to local atmospheric processes.

3. Investigate the seasonal variability of the ice core constituents and study the influence of local factors.

To quantify ice core constituents, continuous flow analysis (CFA) was used, a method that provides a fast and precise quantification of ice core constituents. During the measurements discrete samples have been taken that were analyzed using ion chromatography (IC). With the IC it was possible to study a variety of ice core constituents, that was needed for several reasons: First, some of the species were used to highly improve the dating of the cores that was originally provided by Fernandoy et al. (2010) to an error of $\pm$ 1 year. Second, those species mostly impacted by atmospheric processes were chosen. Different species also have different sources, transport paths and deposition pattern. By comparing the species it was identified how time series and seasonal and local variability of them can be interpreted in terms of changing atmospheric circulation pattern.

The second part of this thesis will enlarge the scale from local weather to southern hemisphere weather. Clearly, the synoptic disturbances are a part

of the global circulation system in the southern hemisphere. In winter, cyclones have their source mostly in the central south Atlantic with a frequency of ~10 low pressure systems per month. In summer, the frequency is lower with ~5 low pressure systems per month and the source is shifted to the Argentinian coast (Turner and Pendlebury, 2004). In the past, low pressure systems in Antarctica have been analyzed by using reanalysis data from the National Centers for Environmental Prediction-National Center for Atmospheric Research (NCEP-NCAR). Simmonds et al. (2003) used an automatic cyclone tracking system to study the characteristics of cyclones in the southern hemisphere. In this work, the connection of concentrations of mineral dust and sea salt concentrations as well as stable water isotopes will be investigated by using only events of high concentrations from the four firn cores from the ECA. Events are then compared to the NCEP-NCAR reanalysis data with the attempt to find climatic conditions that are significant for high concentrations or (in case of stable water isotopes) high temperatures. This will confirm the hypotheses made in the first part of this thesis that mineral dust concentrations are mostly determined by their source in Patagonia while sea salt concentrations are closely connected to local processes, especially the cyclonic activity. Furthermore, this analysis will show that it is possible to use ice core data as a proxy for synoptic disturbances. Even though the analysis will not get that far this already gives an outlook of the possibility to use ice core data in climate models. This will improve them highly by providing data in a region where meteorological observations are only rare.

1.1 Area of Investigation

The Ekströmisen catchment area (ECA) located in coastal Dronning Maud Land (figure 1) is characterized by two topographic ridges, Sörasen in the west (690 m a.s.l.) and Halvfarryggen in the east (654 m a.s.l., Wesche et al., 2009). Glaciological conditions are well known on Halvfaryggen. Snow accumulation rates range from 500 to 1200 kg*m^{-2}*a^{-1} (Fernandoy et al., 2010), providing perfect sites to analyze impurity concentrations in seasonal resolution. Ground penetrating radar and airborne radio echo sounding studies have been used to investigate the temporal and spatial variability of accumulation rates. The three dimensional structure of isochrones and bedrock topography reveal regional highly variable accumulation rates with a decreasing trend from east to west over Halvfarryggen (Drews et al., 2013). The wind regime in the ECA is mostly determined by the high activity of cyclones and the resulting high wind velocities (König-Langlo et al., 1998; Schlosser et al., 2008). Katabatic winds mostly occur during high pressure events (König-Langlo and Loose, 2007).

In 2007, four firn cores were drilled in the ECA (B38, B39, FB0702 and FB0704). Stable water isotopes (δ^{18}O, figure 2) determined on discrete samples provide a reference chronology (Fernandoy et al., 2010). Results from this study also showed that the spatial variability of accumulation rates is linked to the wind regime and the moisture transport. Further it was found that FB0702 is probably influenced by snowdrift from higher altitudes, which was demonstrated by relatively low values of δ^{18}O. A summary of the characteristics of the cores is given in Table 1.

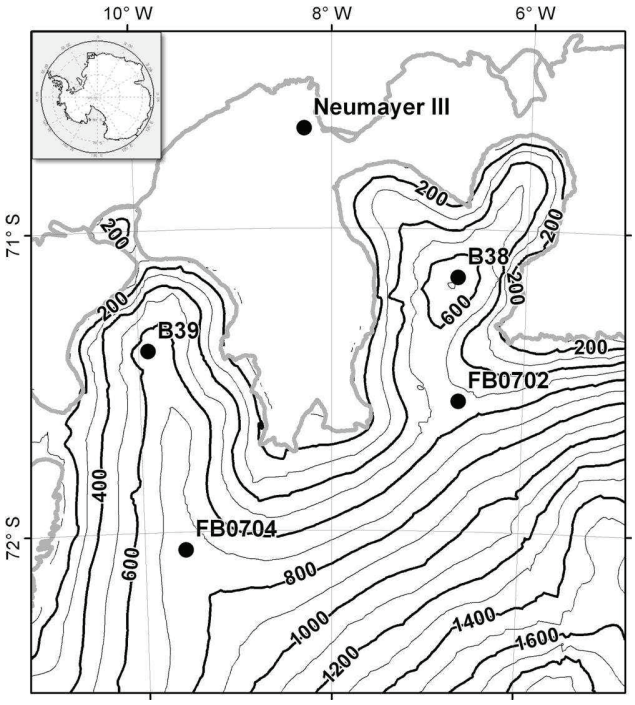

Figure 1: *Overview of Ekströmisen catchment area and the four drilling sites of the ice cores discussed in this study and the location of the German wintering station Neumayer III. Thick gray lines indicate the grounding line and shelf ice edge (Map courtesy C. Wesche).*

1.2 Neumayer Station

The four firn cores B38, B39, FB0702 and FB0704 analyzed in this study were all drilled in the hinterland of Neumayer Station (70°S, 8°W, Figure 1). This proximity has the big advantage that the aerosols deposited in the ice sheet in the ECA can be compared to measurements from the air chemistry observatory and the meteorological observatory.

The aerosol record at Neumayer Station has been obtained since 1983, making it one of the longest continuous aerosol records in Antarctica (Weller et al., 2011). The observatory is located $\sim$ 1.5 km south of Neumayer Station. Wind measurements control the sampling. If the wind direction is from Neumayer Station, the sampling is interrupted. Thus, at this location clean air measurements are verified. Additionally, northerly winds are most unlikely. The

Table 1: *Characteristics of the four firn cores analyzed in this study. Accumulation rates and dating are according to (Fernandoy et al., 2010).*

	B38	B39	FB0702	FB0704
Position (lon)	-6.7°	-9.9°	-6.67°	-9.56°
Position (lat)	-71.16°	-71.4°	-71.57°	-72.06°
Core length (m)	84	78.5	43	36
Age (AD)	1960-2007	1935-2007	1959-2007	1962-2007
mean annual accumulation rate ($kg*m^{-2}*a^{-1}$)	1229	747	520	483
Altitude (m.a.s.l.)	690	654	540	760

air is sampled using an actively ventilated inlet stack placed 8 m above the snow (Weller et al., 2011). Aerosols are collected on filter combinations and quantified using ion chromatography. Samples have an integration time of 7-14 days. In this study, the aerosol record from Neumayer Station is used for comparison to the firn core data with respect to seasonality and concentrations of ice core constituents, e.g. nitrate. This highly improves the quality of the dating of the firn cores, making the comparison to atmospheric circulation patterns possible.

The meteorological observatory was installed in 1981 (König-Langlo et al., 1998). Standard synoptic monitoring is performed, including air temperature, pressure, wind direction and speed, humidity, radiation (long wave and short wave) and visual observations. Surface measurements are stored every 3 hours and a radiosonde is launched once a day measuring vertical profiles of air temperature, wind, air pressure and humidity. By comparing firn core data to these locally measured meteorological data it can be obtained if for example, amongst other a certain wind direction is present when aerosol constituents in the firn cores show very high or very low concentrations. Figure 3 shows the mean seasonal cycle of air pressure and temperature at Neumayer Station (adapted from König-Langlo et al. (1998), but extended to the time

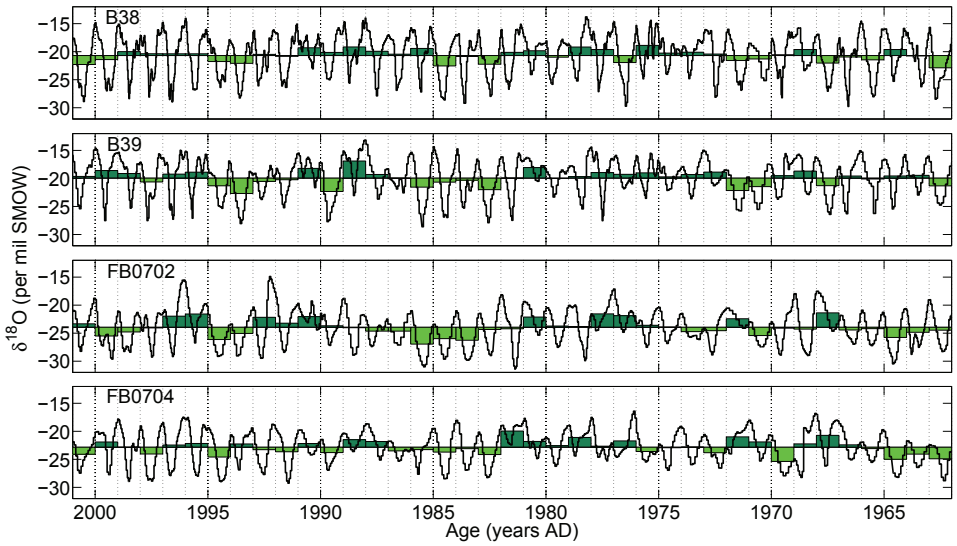

Figure 2: *Profiles of $\delta^{18}O$ from the four firn cores. Dark green boxes are yearly averages that are higher than the mean, light green boxes yearly averages lower than the mean.*

period 1981-2006). The seasonality of air pressure and air temperature has not changed compared to the shorter time period used in König-Langlo et al. (1998). The air pressure is generally low which can be explained by the proximity to the Antarctic vortex (King and Turner, 1997). The seasonal cycle follows a half-year cycle with a minimum in January/ December and June. This semiannual cycle is caused by the movement of the circumpolar trough (van Loon, 1984). The air temperature has a pronounced seasonal cycle and is lowest in Antarctic winter (June, July, August).

The wind is shown in figure 4. Figure 4a shows the frequency distribution of wind direction and wind speed in percent. The black arrows indicate the two wind directions with the highest frequencies. Figure 4b is a contour plot with the month of the year on the x-axis and the wind direction on the y-axis. Colours represent the wind speed as given in the colourbar beneath. Both figures clearly show that easterlies are the most frequent winds at Neumayer Station. They are connected to the eastward moving low pressure systems

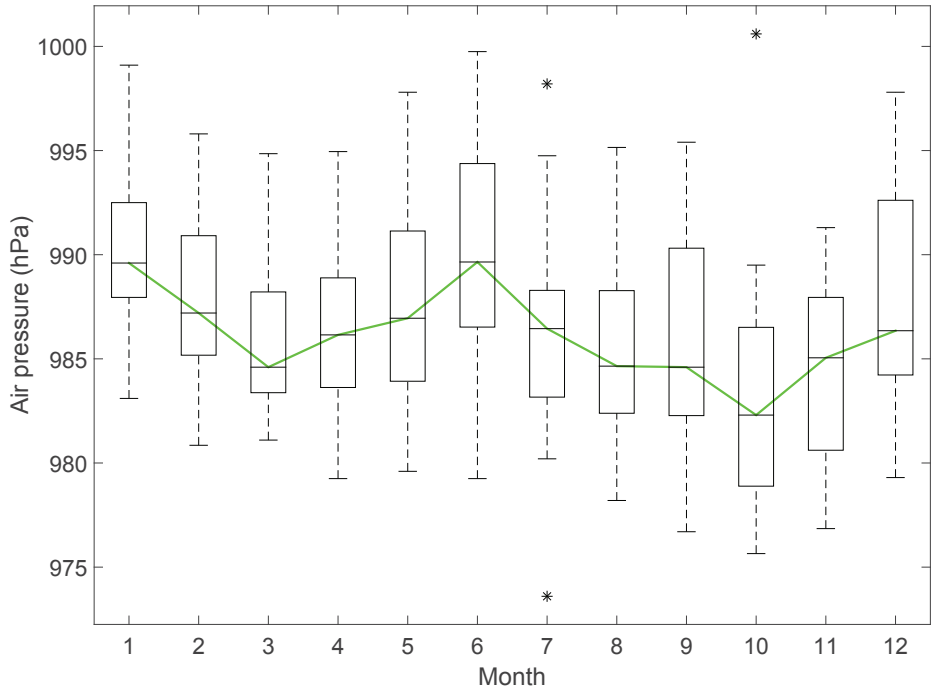

(a)

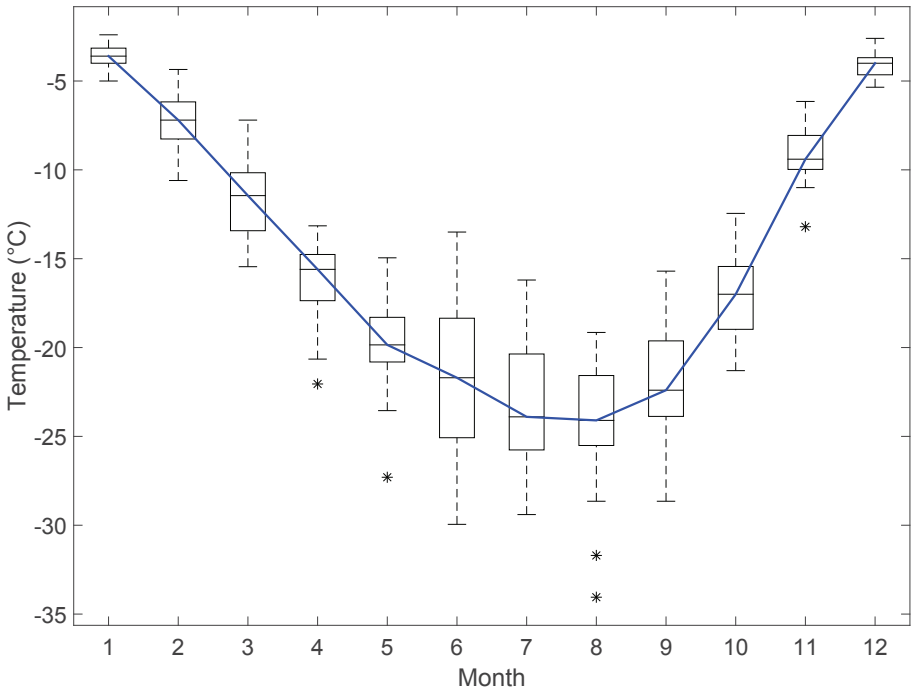

(b)

Figure 3: *Monthly averaged 3a air pressure in hPa and 3b air temperature in °C (modified after König-Langlo et al. (1998), data available at* `doi:10.1594/PANGAEA.759434`*)*

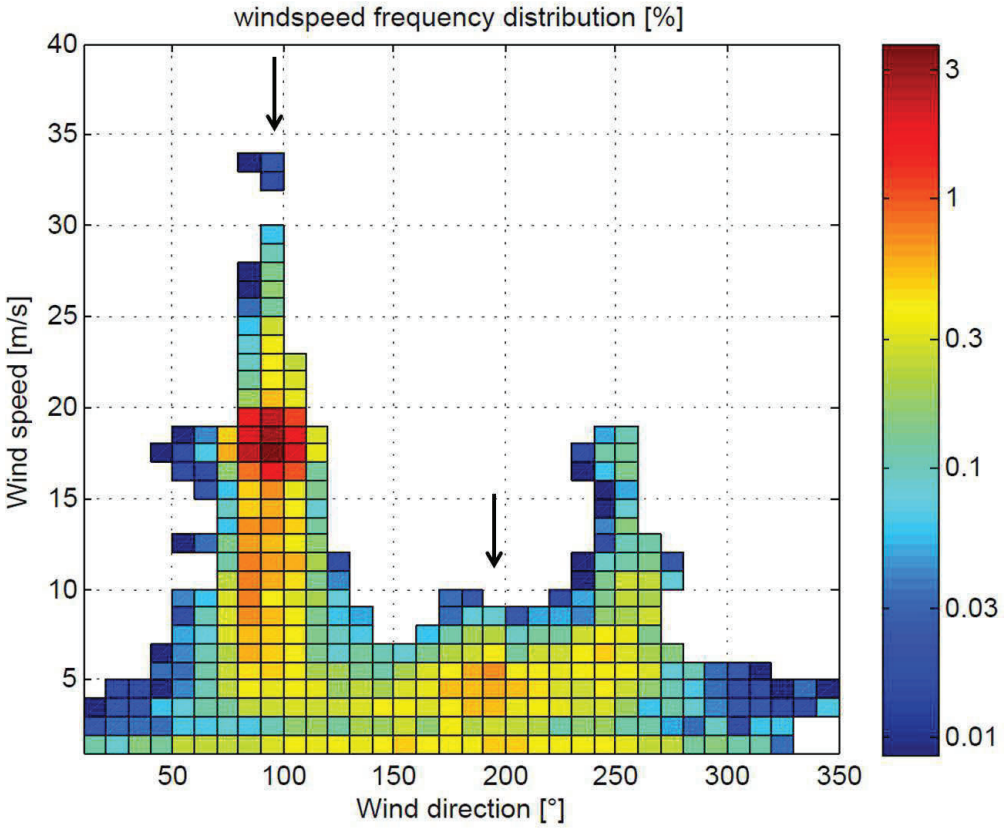

(a)

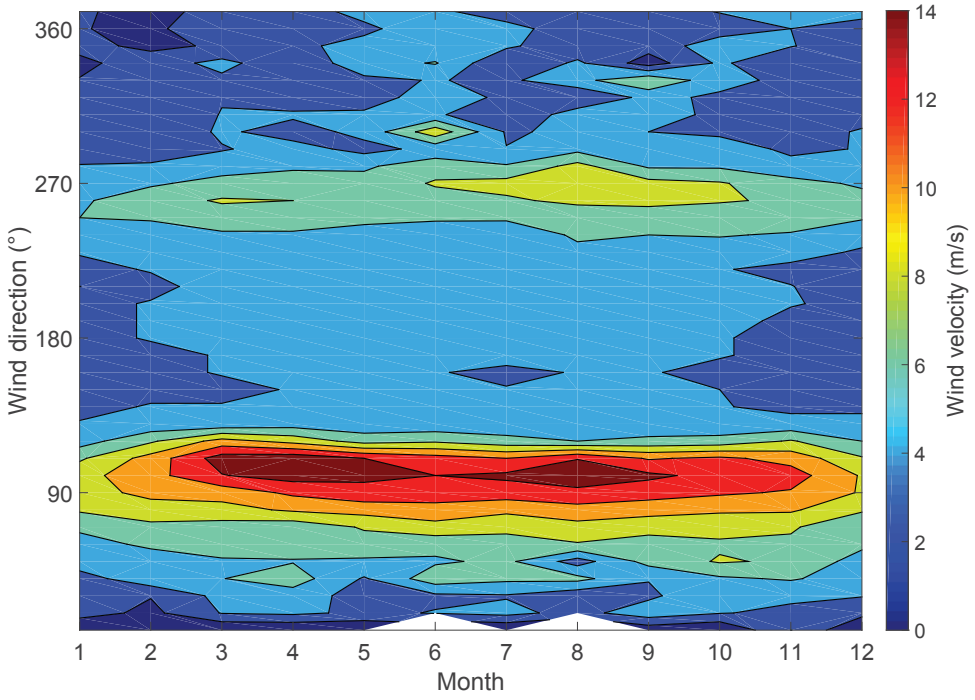

(b)

Figure 4: *4a frequency distribution of wind direction and wind speed in percent and 4b monthly averages wind speed contours (modified after König-Langlo et al. (1998), data available at* `doi:10.1594/PANGAEA.759434`*)*

with wind velocities of 13 m/s. The connection to low pressure systems is also visible in the semiannual cycle the easterlies follow, similar to the semiannual cycle of the air pressure at Neumayer Station. The second maximum in the frequency diagram is a southerly wind. These winds usually have low wind velocities around 5 m/s and are associated with katabatic winds (König-Langlo et al., 1998).

1.3 Aerosol constituents: Source-Transport-Deposition

To investigate the relationship of atmospheric circulation patterns and aerosol constituents in ice cores the focus of this study is on the processes that directly connect concentrations of ice core constituents and atmospheric circulation processes: emission, transport and deposition of aerosol constituents. Aerosol components considered in this study are mineral dust, sea salt, nitrate, sulphate and stable water isotopes.

1.3.1 Mineral dust

The mineral dust entrainment at the source is generally highly related to wind speed and aridity: Higher wind velocities enlarge the emission of mineral dust particles into the atmosphere (Hobbs, 2000). The availability of mineral dust particles on the surface depends on aridity, plant growth and size distribution of mineral dust particles. A wet surface produces less mineral dust particles because it is hard, while a dry surface is more dynamic, enlarges friction and hence mineral dust emission (Reynolds et al., 2007). Mineral dust is emitted by saltation (Figure 5): Larger particles fall on the ground and by this, smaller particles are lifted up. Strong winds transport the mineral dust particles into the high atmosphere (Harrison et al., 2001).
Model simulations (Li et al., 2008) show that South America (Patagonia) is the main source for mineral dust in the plateau region of Dronning Maud Land

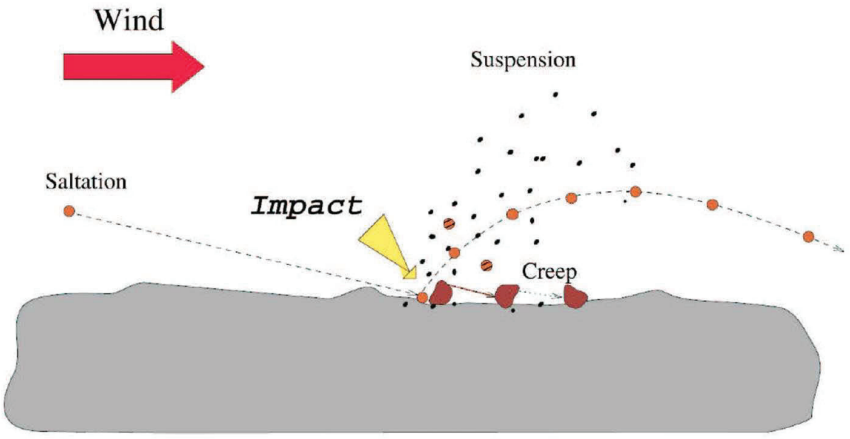

Figure 5: *Saltation of mineral dust in to the atmosphere. Large particles fall on the ground and by this smaller particles are elevated and blown away by wind (figure from Koopmann (2006)).*

in present-day climate, with contributions from Australia and local Antarctic sources. As evidenced by TOMS (Total Ozone Mapping Spectrometer) satellite measurements (Prospero et al., 2002), the dust source in Patagonia shows a large seasonal variability with a maximum between September and January (Albani et al., 2012). In Patagonia, the typical situation for dust uptake is a low pressure system situated above Patagonia or the Falkland Islands. When a cold front of an eastward moving depression arrives from the south Pacific Ocean, it passes the Andes and by this looses a lot of moisture. These dryer air masses meet the warm and humid air over the Argentinian plains. This creates instability and a squall line of supercell thunderstroms. (Goudie and Middleton, 2006). The mineral dust particles are elevated high enough by turbulent processes in the atmospheric boundary layer to enable a transport over very long distances (Johnson et al., 2011; Harrison et al., 2001). Particles from South America are most likely transported below 400 hPa (Krinner et al., 2010) and have an atmospheric residence time of some days to weeks (Petit and Delmonte, 2009; Li et al., 2010). Deposition can be either wet or dry, but as the ECA is an area with very high accumulation rates dry deposition is

unlikely.

1.3.2 Sea salt

The main source of sea salt aerosol is still under debate. Sea salt aerosol can be derived from frost flowers, blowing snow over sea ice or from the open ocean (Wolff et al., 2003; Kaleschke et al., 2004; Wagenbach et al., 1998a; Yang et al., 2008), or a combination of them (Figure 6). Bubble bursting is one of the processes that transport sea salt particles into the atmosphere. When waves in the ocean break, sea salt particles are accelerated vertically. High wind velocities take these particles up in the atmosphere and by this they are transported by cyclones approaching to coastal Antarctica (Wallace and Hobbs, 2006). Fine layers of brine and frost flowers are located on the surface of freshly formed sea ice, providing another source of sea salt particles. High wind velocities are the critical factor for a successful uptake of sea salt particles into the atmosphere (Wolff et al., 2003). High wind velocities are usually connected to the presence of low pressure systems that also transport the sea salt particles to Antarctica. The atmospheric transit time to the Antarctic plateau has been determined to range from 4 to 7 days (Reijmer et al., 2002). Transport and deposition in Antarctica is related to the cyclonic activity, and the input of sea salt constituents in the ECA preferentially occurs during easterly winds (Weller et al., 2011). Sea salt particles are deposited with the accumulating snow. Snow accumulation also depends on the topography when air masses have to pass a barrier and thus topography and accumulation regime is likely to change the distribution of sea salt particles over a certain region. Kreutz and Mayewski (1999) and Mahalinganathan et al. (2012) found that sea salt concentrations mostly depend on the topography and by this the elevation rather than on the distance to the coast.

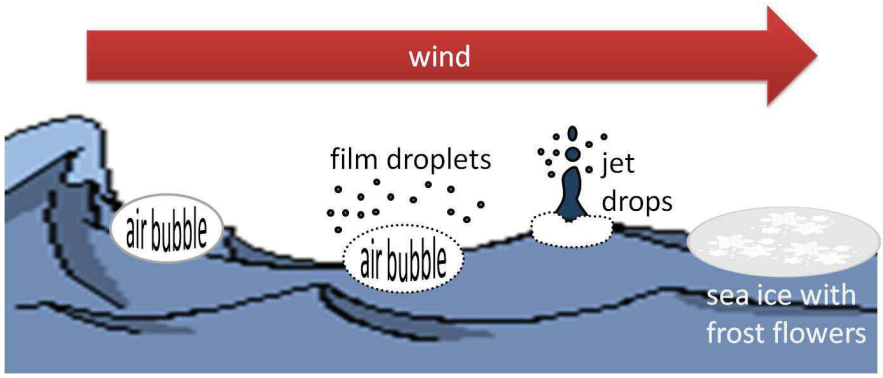

Figure 6: *Possible sources of sea salt particles in coastal Antarctica. Over the open ocean, wave breaking leads to bursting of air bubbles that elevate sea salt particles from the ocean into the atmosphere. Over sea ice, fine layers of brine and frost flowers are formed that provide the sea salt source. Both sources need high wind speeds to take up sea salt particles into the atmosphere (figure modified from Wallace and Hobbs (2006)).*

1.3.3 Sulphate

Sulphur components are mostly obtained by the concentration of non sea salt (nss)-sulphate (SO_4^{2-}) and methane sulfonic acid (MSA). Nss-SO_4^{2-} is calculated using the approach from Wagenbach et al. (1998a):

$$nss - SO_4^{2-} = SO_4^{2-} - k * Na^+ \tag{1}$$

with k the sulphate to sodium ratio. Due to chemical fractionation k was found to be 0.07 from March to October and 0.252 from November to February (Wagenbach et al., 1998a). $Nss - SO_4^{2-}$ in coastal Antarctica is primarily a proxy for biological activity in the ocean, but can also have contributions from the stratosphere, continental aerosol and volcanism (Minikin et al., 1998), while MSA is only derived from biological activity (Legrand and Pasteur, 1998). MSA and $nss - SO_4^{2-}$ are both atmospheric oxidation products of dimethyl sulfide (DMS). DMS itself is emitted by oceanic phytoplancton which is common in brine pockets in the sea ice (Legrand and Pasteur, 1998).

Minikin et al. (1998) as well as Curran et al. (2003) showed that changes in MSA concentrations are mostly related to changes in sea ice. Hezel et al. (2011) used a global chemical transport model to obtain the relationship of sea ice and wind speed with DMS emissions. As already obtained by observations they also found strong regional effects and sea ice as the main influencing factor of DMS emissions. Wind speeds may also play a role, which is however negligible because it is overwhelmed by the seasonal cycle, magnitude, and meridional gradients of the sea water DMS concentrations. Accordingly, in coastal areas sulfuric component are mostly used as proxies for sea ice and biological activity (e.g. Curran et al., 2003). $Nss - SO_4^{2-}$ and MSA are most likely transported by cyclones (Abram et al., 2013) and wet deposited. However, source, transport, and deposition patterns highly depend on the local conditions in the particular area of investigation. Abram et al. (2013) compared multiple studies on the MSA to sea ice relationship and concluded that it can be either positive or negative correlated, depending on the location of the MSA sampling. For Dronning Maud Land, Abram et al. (2008) found a negative correlation between MSA concentrations and sea ice. However, this results may be equivocal because Weller et al. (2011) also performed correlation analysis and found a positive correlation between MSA concentrations and sea ice. Due to the absence of light in the polar night, the sulfuric components have a maximum in the Antarctic summer.

1.3.4 Nitrate

For nitrate, the source budget is not well defined. It is suggested that sedimentation from polar stratospheric clouds is a major source (Wagenbach et al., 1998b) while continental sources like biomass burning are probably insignificant for Antarctica. However, the observed seasonal maximum of atmospheric nitrate in November (Wagenbach et al., 1998b) cannot be explained by strato-

spheric nitrate input. Also post-depositional losses to the atmosphere for example related to photolysis during summer (Röthlisberger et al., 2002a; Jacobi and Hilker, 2007) alter the nitrate concentration in the firn in low accumulation areas significantly and can contribute to elevated atmospheric nitrate levels in the boundary layer (Wagenbach et al., 1998b). The long-term loss of nitrate from the snow pack linked to photolytic processes at the snow surface observed in the interior of the Antarctic ice sheet (Röthlisberger et al., 2002a) can most likely be neglected in the ECA due to high snow accumulation rates. However, fast nitrate loss from fresh snow has been reported (Neubauer and Heumann, 1988) and is also reflected in the geographical distribution of nitrate concentrations in surface snow (Bertler et al., 2005).

1.3.5 Stable water isotopes

In glaciological studies, δ^{18}O is mostly used as a proxy for atmospheric temperatures (e.g. Dansgaard, 1964). The ocean water contains heavier and lighter molecules of hydrogen (^1H, ^2H, ^3H) and oxygen (^{16}O, ^{18}O, ^{19}O). When water evaporates from the ocean, lighter molecules evaporate at first due to the lower vapor pressure, enriching the water vapor in the atmosphere with lighter molecules that then contains more lighter molecules than the ocean water. At condensation, the process is contrary. At first, heavier molecules condensate and by this, the water vapor in the atmosphere gets even lighter. The process of evaporation and condensation also depends on the temperature, which is why the water vapor gets lighter when the air packages are transported to the polar regions (figure 7, e.g. Hoefs, 2008).
By measuring the ratio of isotopes in snow and comparing it to a standard (e.g. standard mean ocean water, SMOW), the temperature at the time of the deposition can be obtained. Figure 8 shows the annual variability of δ^{18}O in the ECA, and compared to figure 3b the relationship of temperature and

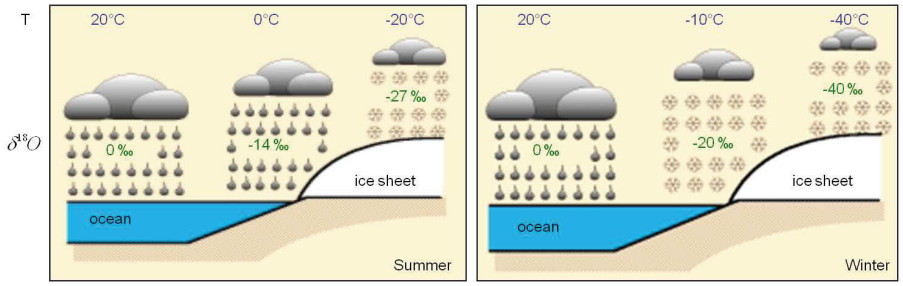

Figure 7: *Principle of isotopic fractionation of stable water isotopes in the atmosphere. Figure from Stauffer (2001).*

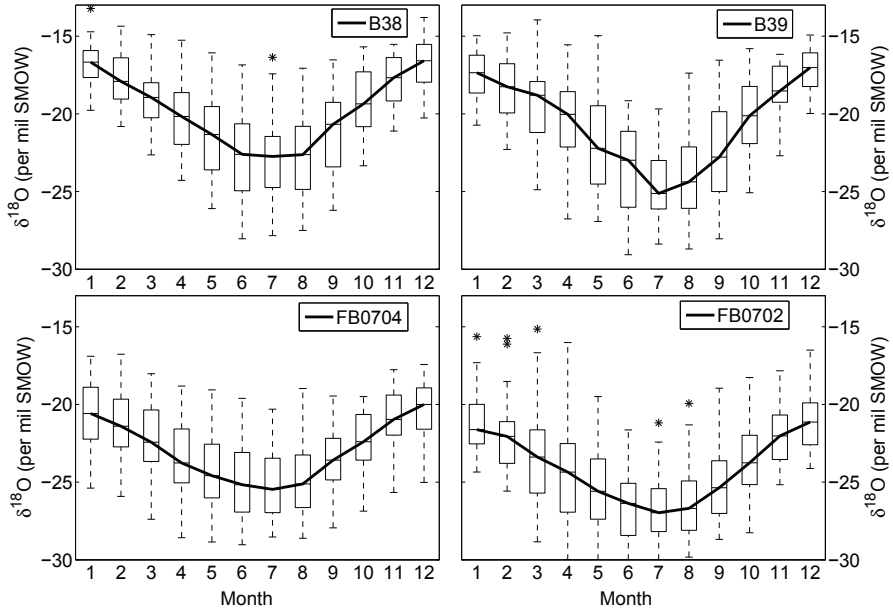

Figure 8: *Monthly stacked $\delta^{18}O$ record in the four firn cores from the ECA. Thick black lines give the median, boxes give 25 and 75% variability. Error bars are calculated as 95% confidence interval. Stars indicate outliers (outliers are defined as values outside the 95% confidence interval).*

δ^{18}O is unambiguous. Since δ^{18}O is bound in the water vapor the transport and deposition of δ^{18}O is mostly conducted by atmospheric circulation in the troposphere and wet deposited to the ice sheet (Masson-Delmotte et al., 2008).

1.4 Reanalysis data

Reanalysis data has been chosen for comparison to ice core data because it represents the most reliable available data at the moment, especially for the southern hemisphere. The reanalysis data will be used in this study to investigate the changes in atmospheric circulation pattern in comparison to ice core constituents. For this, reanalysis data from the National Centers for Environmental Prediction-National Center for Atmospheric Research (NCEP-NCAR) is used. The NCEP-NCAR reanalysis data is not the only data package that is available. The European Centre for Medium-Range Weather Forecasts (ECMWF) reanalysis data (ERA-40) would produce very similar results in this region. Renwick (2004) determined the differences between pressure trends from NCEP-NCAR and ECMWF reanalysis data in the southern hemisphere. The analyses are consistent, but most reliable after 1980.

The basic idea of the NCEP-NCAR reanalysis data is to use both, a forecast system and existing measured data (1957 until present) and perform data assimilation. This provides a useful data set for climate research to compare recent weather anomalies with the long time observations while the analysis system is not changed ("kept in frozen state"). By this, the impact of the current weather anomalies can be investigated in comparison to the long-term mean. Observational data includes radiosondes, data from ships and aircrafts, satellite sounder data and surface land measurements. A full list is given in Kalnay et al. (1996). The observational data has been quality checked and in case of doubt corrected or taken out of the analysis.

The output of the reanalysis data includes for example geopotential height,

atmospheric temperature, humidity, and winds. These output variables differ in their reliability because of their differences in measurement techniques or modeling. For this, Kalnay et al. (1996) gives four different classes for the data: Fields, that are obtained by observations belong to class A and include for example temperature fields at 17 vertical levels. If the data is partially defined by observations, but also influenced by model data the field belongs to class B. This can be for example the relative humidity through the whole atmospheric column. If a fields is classified to class C this indicates that no observations influence the analysis, for example the three dimensional diagnostic fields like the latent heat flux. Fields that belong to class D are climatological values that do not depend on the model (e.g. land-sea mask). Clearly, the analysis is most reliable when the field considered is classified as A, and the interpretation of the data has to be more cautious when using data fields from class B or C. The full list of output parameters and their classification is given in appendix A of Kalnay et al. (1996).

In this study, monthly geopotential height (Z500), meridional wind (V500) and zonal wind (U500), all in 500 hPa height are used. These three belong to class A. Anomalies are calculated for this study, which is the difference between the long-term mean of a field variable (e.g. temperature) and the actual value of the same field variable. This gives the deviation from the long-term means. For example, if the geopotential height anomaly is high this means that in that month the geopotential height was higher than average.

Since the reanalysis data are updated on a regular basis to improve the quality and quantity of the data set, current issues with the reanalysis data are regularly posted on the NCEP-NCAR website (`http://www.esrl.noaa.gov/psd/data/reanalysis/problems.shtml`). However, some issues have already been reported. Kistler et al. (2001) tested the reanalysis data and found some limitations that also have to be considered when interpreting the re-

sults from this study. By comparing the pre-satellite to the satellite era they found that the data is most reliable in the satellite era. For this, trends analyzed with the NCEP-NCAR reanalysis set should always be quality controlled by comparing the pre-satellite (1948-1979) to the satellite era (1980-present). The comparison to in-situ observations shows this most clearly. Radiosonde measurements are considered to have the highest influence. Hence, regions with a higher data coverage of radiosonde data are more reliable than those with less observations. This is especially important when studying the Antarctic region or comparing the northern to the southern hemisphere. Because of the higher density of observations the data from the southern hemisphere is less reliable than the data from the northern hemisphere. This is especially true for data polewards of 40° S. Marshall (2002) compared monthly mean NCEP-NCAR geopotential heights to corresponding radiosonde data from four Antarctic research stations (Mawson, Davis, Casey and Halley). For the 500 hPa geopotential height the difference was less than 0.2 m and decreases after 1980 (Kistler et al., 2001). For this, monthly means of the reanalysis data are robust in general, but the difference between pre-satellite and satellite era has to be taken into account when using this data set in monthly resolution as conducted in this study.

2 Methods

2.1 Continuous flow analysis

Impurity concentrations in all four firn cores (section 1.1) were quantified using a continuous flow analysis system (CFA, Kaufmann et al., 2008) at the University of Berne. With this technique, the firn is melted continuously and the clean inner part is automatically separated from the possibly contaminated outer part. This is realized using a specially designed melthead. The melthead consists of two squares as described in Bigler et al. (2011) with radial grooves to allow for steady melt water transport (figure 9). For this study, a small aluminum plate was inserted into the center of the melthead to increase the flow resistance and thus to ensure a stable sample flow while melting the porous firn. Note that this method allows for essentially contamination-free sampling of glacier ice below the bubble close-off. However, contamination of the sample stream by particles entering the open pore space of the core in frozen state during transport and core processing and by a limited wicking effect of melt water into the open pore space during the melt process cannot entirely be ruled out (see discussion of the particulate dust concentration). The meltspeed was decreased with increasing depth and density from 6.0 cm/min to 3.5 cm/min to provide a constant water flow to the system. For the CFA-analysis, a piece of 34x34 mm^2 was cut out of the middle section of each 1 m firn core section in the cold room facilities at Alfred Wegener Institute in Bremerhaven and shipped to University of Berne. Before the measurements, each piece was prepared by measuring full length and break positions, cleaning the breaks by cutting off about 2 mm of firn and placing them vertically inside a tray. Prior to every meter of firn a cube of frozen ultra pure water was melted. Melting one meter of firn and the ultrapure water cube is here referred to as one run. Before the melting started and

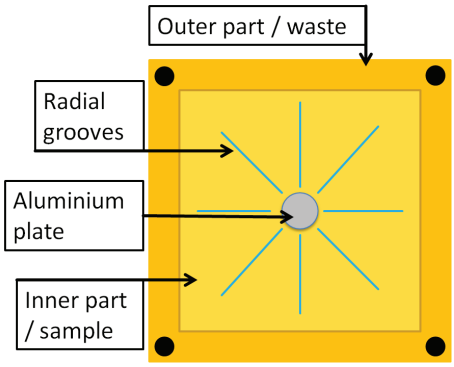

Figure 9: *Melthead for continuous flow analysis as used in this study. Consists of two parts that automatically separate the clean inner part (sample) from the possibly contaminated outer part (waste). Radial grooves allow a steady meltwater transport and the aluminium plate in the center of the melthead increases the flow resistance and is needed for the melting of porous firn cores.*

after it ended a baseline using ultra pure water from a reservoir bottle was recorded for about 3 minutes. Start and end of the run was recorded with a short electronic signal.

The CFA-System including the water flow is shown in Figure 10. The melt water was pumped from the melthead to a debubbler, that ensures a bubble-free water flow inside the detection units. The master valve switched at the beginning of each run from the ultra pure water reservoir bottle to the melthead line when both bubble detectors detect bubble-free water.

The CFA system was calibrated every two hours. Standard concentrations, calibration method, and detection limits are given in table 2. During the CFA analysis concentration profiles of calcium, sodium, nitrate, ammonium, hydrogen peroxide, mineral dust and in addition conductivity and pH were quantified. A Picarro instrument (Gupta et al., 2009) was added to the existing system to determine oxygen and hydrogen isotopic ratios (δ^{18}O, δD). From the CFA analysis only concentration profiles of calcium (Ca^{2+}), particulate mineral dust and nitrate (NO_3^-) will be discussed. For dating purposes pH and concentration profiles of hydrogen peroxide (H_2O_2) were used.

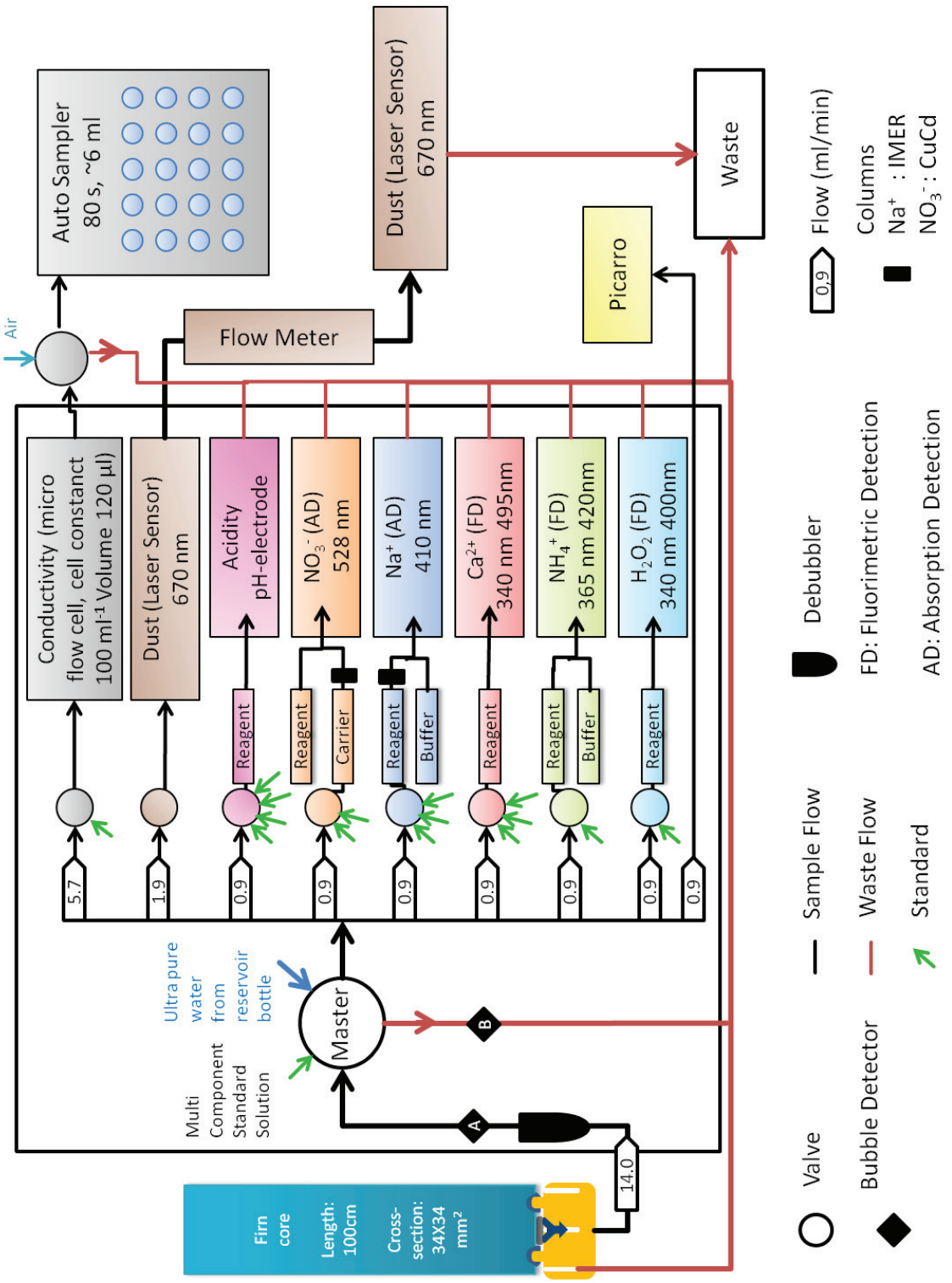

Figure 10: *Schematic overview of the CFA-system used in this study*

Ca^{2+} concentrations are quantified by a fluorimetric method in a flow-through cell containing a fluorescent spectrometer and a LED (λ = 340 nm) that is protected from daylight. The instrument has an error of less than 1% with a detection limit of 0.1 ppb (Röthlisberger et al., 2000a).

The mineral dust concentration was quantified using a dust particle sensor (Klotz GmbH, Bad Liebenzell, Germany) where the size of the insoluble particles was determined by a laser beam (λ = 670nm) in 32 size bins (1 μm - 10 μm). Thus, the size distribution and the total number of insoluble particles can be quantified at the same time. The sensor is described in detail by Ruth et al. (2002). Due to the detection limit of this method only particle sizes bigger than 1μm were taken into account. The laser sensor is very stable and does not need frequent calibration. A methodological comparison of mineral dust measurements using the laser sensor, coulter counter, ion chromatography (IC), inductively coupled plasma mass spectrometer (ICP-MS) and proton induced x-ray emission (PIXE) all showed high correlation with the coulter counter measurements, which itself had a correlation of 1 with the laser dust particle sensor (Ruth et al., 2008). During the measurements a second laser sensor from Alfred Wegener Institute was added to the CFA system. The comparison of the two sensors (figure 11) shows that they do not differ in their seasonality but in the quantity of mineral dust particles. For this study, the data from the Bern Sensor is used.

For the NO_3^--measurements, a reagent and a carrier was added to the sample flow, reducing NO_3^- to nitrite (NO_2^-) in a copperized cadmium column. NO_2^- was detected in an absorption spectrometer with an LED (λ = 528 nm). The instrument was calibrated every two hours. Additionally, the column was changed after 50 hours of measurement time. The detection limit is 1 ppb with an error less than 5%. All analysis units are placed in temperature controlled modules minimizing baseline drift and signal noise. More details on

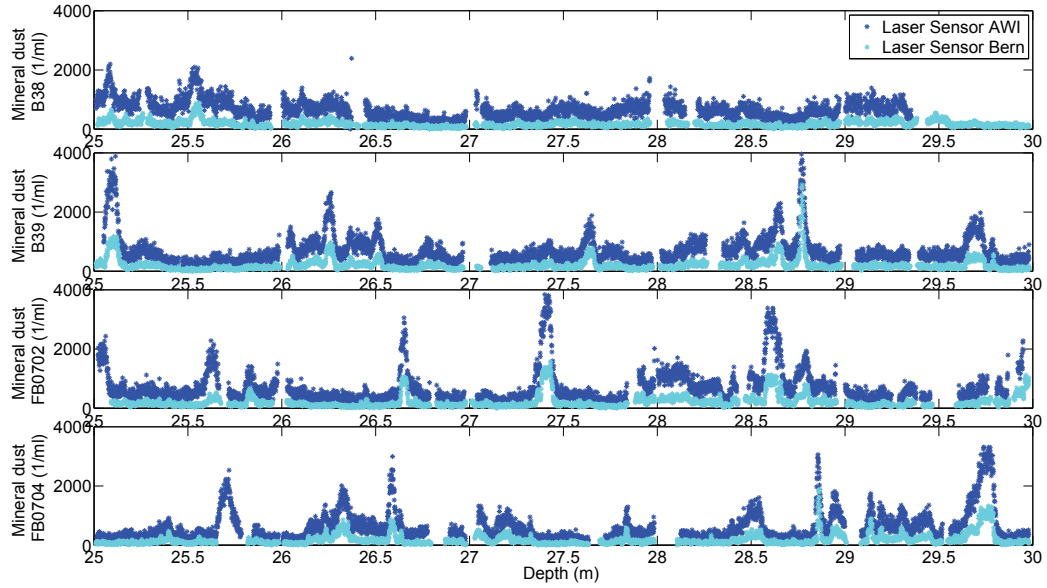

Figure 11: *Comparison of the two dust laser sensors used during the measurements for this study. AWI laser Sensor data in dark blue, Bern laser sensor data in cyan.*

Table 2: *Standard concentrations, detection method (AD: Absorption detection, FD: Fluorescence detection), calibration method, detection limit and error for the CFA-measurements. A full description of measurement technique is given in Kaufmann et al. (2008) and Röthlisberger et al. (2000a).*

Species	Standard concentration	Detection method	Calibration method	Detection limit	Error
NO_3^-	66 ng/g 33 ng/g	AD	linear	1ppb	<5%
Na^+	507 ng/g 255 ng/g 128 ng/g	AD	exponential	0.5 ppb	<5%
Ca^{2+}	160 ng/g 65 ng/g 33 ng/g	FD	linear	0.1 ppb	<1%
NH_4^+	16 ng/g	FD	linear	0.1 ppb	<5%
H_2O_2	18 ng/g	FD	linear	0.1 ppb	<1%

the detection methods are given by Röthlisberger et al. (2000a) and Kaufmann et al. (2008).

Sodium was detected by using the enzyme activity of o-nitrophenyl-β-D- galactopyranoside that itself depends on the sodium concentration. In the measurement aperture this is realized using a reaction column (Immobilized enzyme reactor, IMER). After the reaction column, ammonia solution is added to the flow to achieve maximal absorption. The detector itself is an absorption spectrometer with an LED lamp in a flow through cell. A photosensor module is used for light detection. Sodium measurements have a detection limit of 0.5 ppb and an error of less than 5%. Hydrogen peroxide and ammonium are both detected using a fluorescence detection. For H_2O_2 a reagent and for NH_4^+ a buffer and a reagent were added to the melt water. This is carried trough a mirrored micro flow cell containing a photosensor module and an orthogonal mounted LED light source. H_2O_2 has a detection limit of 0.1 ppb and an error of less than 1. NH_4^+ has a detection limit of 0.1 ppb and an error of less than 5%. In addition to the continuous analysis, an automatic sampler was added to the CFA-system. This gave the opportunity to quantify more proxies than possible using the CFA-System, but with the disadvantage of a lower temporal resolution. The automatic sampler was added at the end of the conductivity line. Again, a valve was used to separate the flow of ultra pure water from the sample. The automatic sampler filled each sample vial with an amount of $\sim$6 ml.

2.2 Data processing and dating

During data processing the following steps were performed: Breaks were eliminated, the ionic concentrations were calculated from the slopes of the nearest calibration run, and a depth assignment was derived from continuous monitoring of the meltspeed. A comparison between continuous and discrete

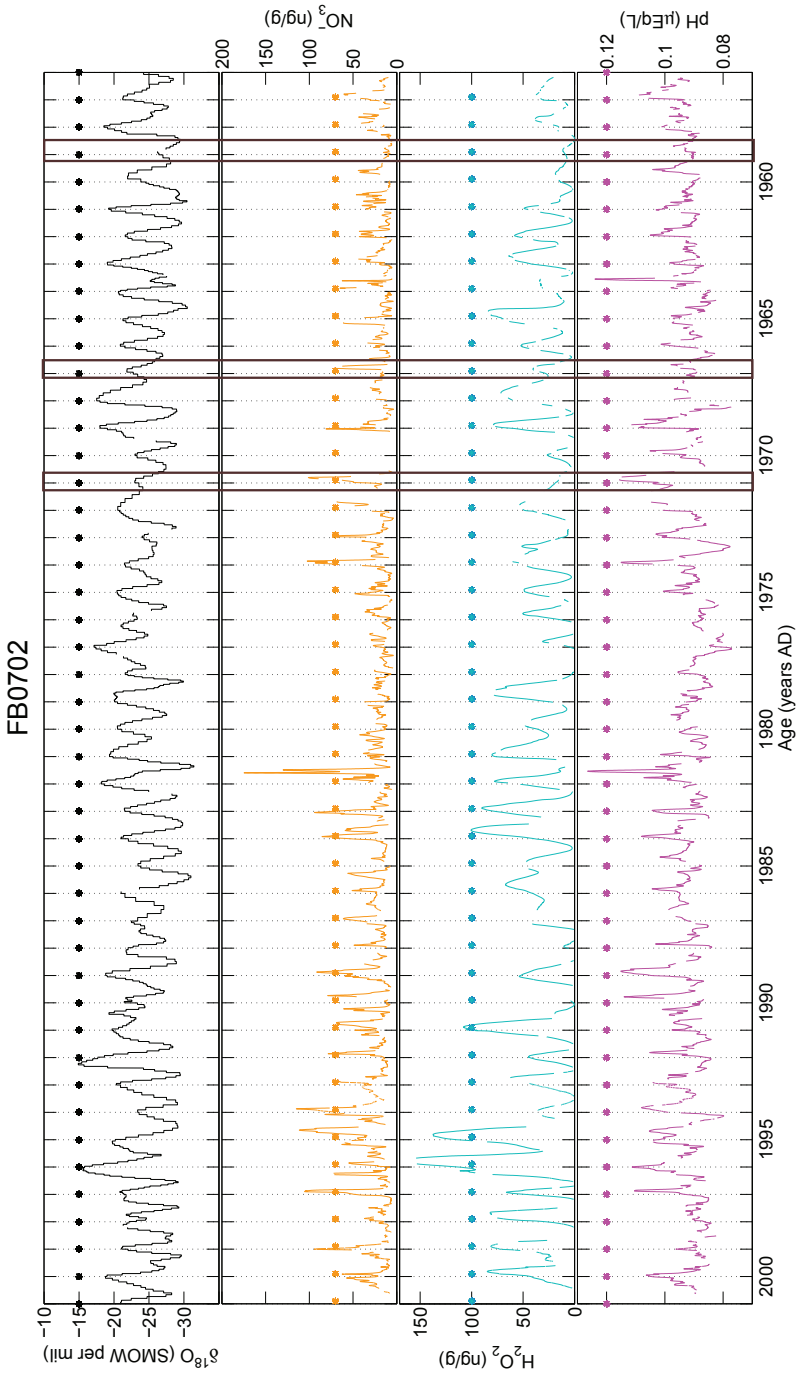

Figure 12: *Dating of the firn core FB0702. For the dating, concentration profiles of $\delta^{18}O$, NO_3^-, H_2O_2 and pH values were used. Stars mark the season when the respective proxy should have its maximum according to literature. Boxes mark the time when additional years have been inserted in core FB0702 (see text).*

records of δ^{18}O from the depth assignments of CFA and the existing data set of Fernandoy et al. (2010) showed a nearly perfect match. The time series of δ^{18}O is shown in figure 2.

The dating of the cores according to Fernandoy et al. (2010) was improved using concentration profiles of NO_3^-, H_2O_2, pH-profiles and δ^{18}O-profiles (figure 12 shows FB0702 as an example). NO_3^- and H_2O_2 show highest concentrations in November (Wagenbach et al., 1998b; Riedel et al., 2000), δ^{18}O and pH highest values in summer (Dansgaard et al., 1985), where the pH seasonality is most likely related to the strong biogenic $H_2SO_4^{2-}$ input in coastal Antarctic aerosol during summer (Minikin et al., 1998). Even though, both H_2O_2-concentration and pH can be influenced by postdepositional and postcoring processes, the seasonal variability is clearly visible and can be used for dating purposes. The δ^{18}O maximum is taken as the beginning of January. When δ^{18}O was ambiguous, and the other proxies indicated a different position of the summer maximum, the mark for the beginning of the year was shifted. The depth interval between two yearly markers was interpolated linearly, assuming a constant accumulation rate throughout the year. The shifting never exceeded 2 cm, but led to a better agreement of the maxima of NO_3^-- concentrations, pH and H_2O_2-concentrations. In core FB0702 smaller peaks of $\delta^{18}O$ occurred together with peaks in NO_3^- and H_2O_2 during the years 1961, 1969 and 1971 in the old dating (boxes in figure 12). Here, an additional year was inserted and the rest of the data set was processed as described above.

Finally, Tritium concentrations (Fernandoy et al., 2010) and the air temperature record from Neumayer Station (König-Langlo et al., 1998) were used to validate that the adjustment using NO_3^- and H_2O_2 concentrations did not impair the dating. The improvement of the dating resulted in a reduced uncertainty to ± 1 year for all four cores.

2.3 Ion chromatography

The discrete samples taken during the CFA campaign were frozen immediately, transported in frozen state to the Alfred Wegener Institute in Bremerhaven and analyzed using Ion Chromatography (IC), an established method to quantify water soluble ionic components (sodium, ammonium, potassium, magnesium, calcium, fluoride, MSA, bromide, sulphate, nitrate, e.g. Fischer et al., 2007b).

The depth assignment of the samples has been conducted by equally distributing the samples over the core length, which was usually 1 m. If for example the run (1 m of melted firn) contained 20 samples, this resulted in one sample every 5 cm. Breaks were eliminated according to the break positions in the CFA dataset. The concentration profiles of Na^+, Ca^{2+} and NO_3^- quantified by IC and CFA were compared over the whole length of the cores. An example is given for NO_3^- in figure 13, and similar results were obtained for Na^+ and Ca^{2+} (appendix A). Ammonium was also quantified by both methods, but was discarded due to contamination in the IC measurements.

To test the quality of the depth assignment, the time series were compared using Pearson's correlation rank test (on the logarithmic data sets due to logarithmic distribution, see 4.1), once using monthly means and to eliminate eventually occurring seasonal influences using bagmeans. The correlations are all strong for monthly and bagmeans ($r \geq 0.8$, $p \leq 0.001$) except for the NO_3^- bagmeans in FB0704 ($r \equiv 0.7$, $p \leq 0.001$). This moderate correlation might be due to the large data gaps in the upper part of the firn core. Even though the bagmeans have slightly higher correlations, the correlation for seasonal resolution is also strong and thus the depth assignment for IC measurements is of good quality.

In order to get a measure for the differences between the two detection methods, the means and standard deviations on the same data sets as above were

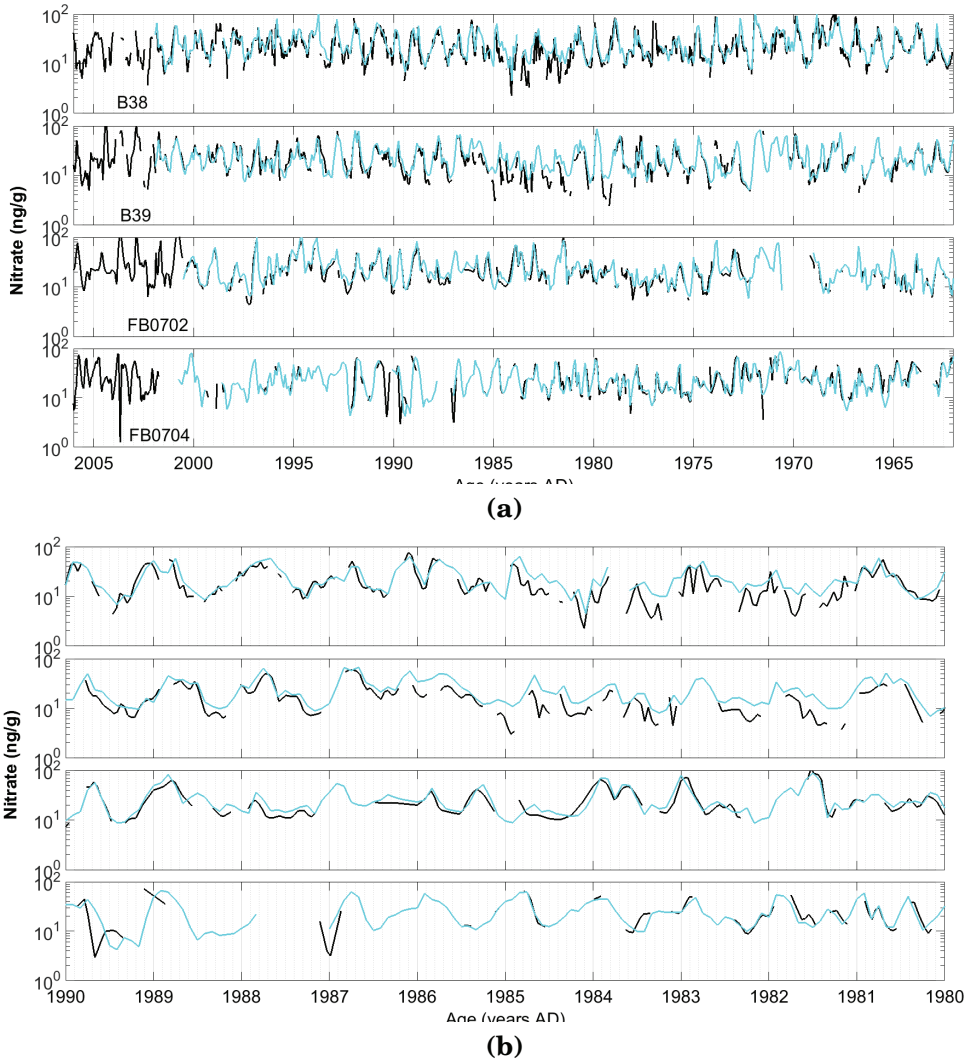

Figure 13: *Comparison of nitrate concentrations quantified by CFA (cyan line) and IC (black line). 13a shows the full record, 13b the time series from 1980 to 1990.*

calculated and CFA concentration means were subtracted from IC concentration means. The differences were then 'calculated back' from logarithm to 'normal' concentrations and are in the range of the detection limits. They are also in the same range between 1 and 1.6 ng/g in the three ionic species despite their varying mean concentrations. Thus the differences are due to the differences in the detection methods rather than to an incorrect depth assumption of IC data. In conclusion, the control of depth assignment and

eliminated breaks showed good agreements in the data sets. but due to the, compared to CFA depth assignment, more rough method the concentration profiles quantified by IC measurements have an uncertainty of $\sim$ 5 cm. When assuming an average accumulation rate of 1 m of snow per year this leads to a dating error of $\sim$16 days relative to concentration profiles quantified by CFA. In addition to the discrete samples filled using the CFA, the first 6 m were cut manually to quantify major ions using IC. In the first 6 m, the firn was not dense enough to use CFA and had more breaks than below 6 m. For this, the cores were prepared as discrete samples in a clean room environment (clean bench class 100). About 5 mm from the outer part of each core section was removed with a pre-cleaned ceramic knife. One sample was taken every 5 cm. This was filled in a glass beaker that was sealed and transported in a frozen state to the IC laboratory, where the samples were melted and analyzed.
For B38 and FB0704, the upper 6 m were taken from the same cores. For FB0702 and B39 two 6 m cores that were drilled right beside FB0702 and B39 were used (cores FB0701 and FB0703).

2.4 Sea salt proxy

Ca^{2+} and Na^{+} in ice cores are mainly originating from mineral dust and sea salt. In coastal areas like the ECA the aerosol input is strongly influenced by very high sea salt input by the marine environment. In contrast to the plateau region, we can safely assume, that in this area Ca^{2+} is mainly sea salt derived (Röthlisberger et al., 2002b; Weller et al., 2008). Figure 14 shows 1m averaged calcium versus sodium concentrations in the four cores quantified by CFA (Fig. 14a) and IC (Fig. 14b). The 1m averages were chosen to eliminate influences from seasonal variability. In the background, the monthly data from all cores is plotted in pale gray. A line has been added showing the sea salt (ss)-Na^{+}/ ss-Ca^{2+}-ratio for marine aerosols as derived by Röthlisberger

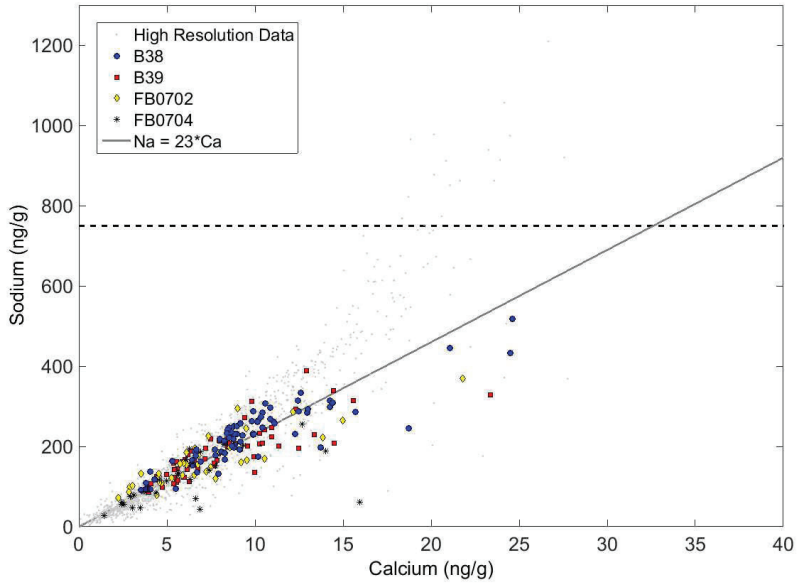

(a)

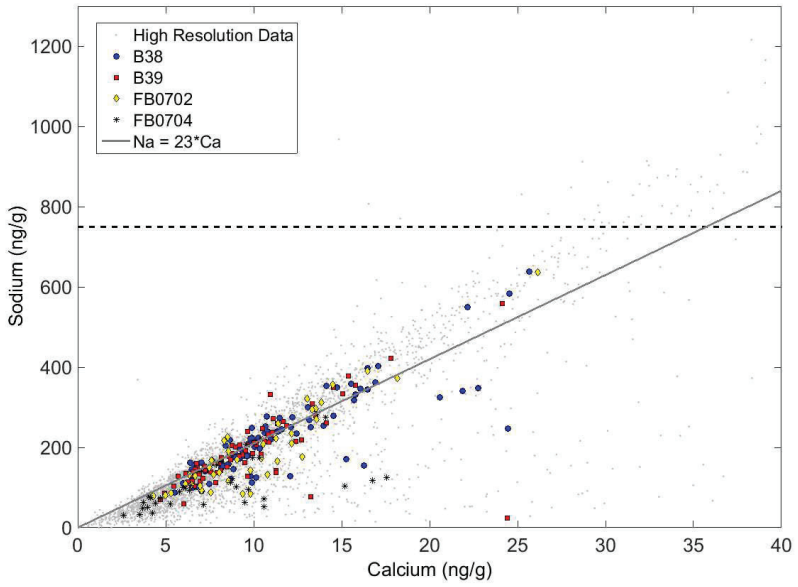

(b)

Figure 14: *Sodium concentration versus calcium concentration using 14a CFA and 14b IC in B38 (blue dots), B39 (red squares), FB0702 (yellow diamonds) and FB0704 (black asterisks). Pale gray points in the background show the monthly resolution data (see text). Solid gray line is the sodium concentration calculated from calcium.*

et al. (2002b):

$$ss - Na^{+} = Na^{+}/Ca^{2+} * ss - Ca^{2+} \quad (2)$$

with the (Na^{+}/Ca^{2+}) = 23 that was derived by Bigler et al. (2006).
It is clearly visible that Ca^{2+} concentrations barely rise above 30 ng/g, while in 6% of the total length of analyzed material, Na^{+} concentrations are above 750 ng/g, which is the upper concentration limit of the detection method used. Only during data processing, after the CFA was terminated it was found that the upper detection limit was too low because of the unexpected very high concentrations of Na^{+}. Thus, Na^{+} concentrations above this limit cannot be considered reliable. Data points below that line have an additional contribution from mineral dust,or may be subject to sea salt input from sea ice, which is depleted in Na by 10-15% (Bigler et al., 2006). Data points above 750 ng/g are more likely influenced by analysis artifacts. Even below the highest standard the quantification of Na^{+} seems to be biased to higher concentrations possibly because already below 750 ng/g the calibration curve is relatively flat leading to a high uncertainty. In comparison the IC measurements have a much more linear relationship showing that the slope in the CFA data is actually a measurement error rather than due to a real effect. Overall, figure 14 clearly illustrates that the majority of the Ca^{2+} and Na^{+} data follow the marine Ca^{2+}/Na^{+} ratio. Hence, Ca^{2+} is mainly of seasalt origin in the ECA. Thus, in this study we will use the Ca^{2+} concentration as a proxy for sea salt input to ECA.

2.5 Contamination of mineral dust

Figure 15 shows the concentration profile of mineral dust particles with diameters larger than 1 μm. Due to the overall very low dust concentrations in the ECA, the risk of contamination of solid particles is very high, especially in

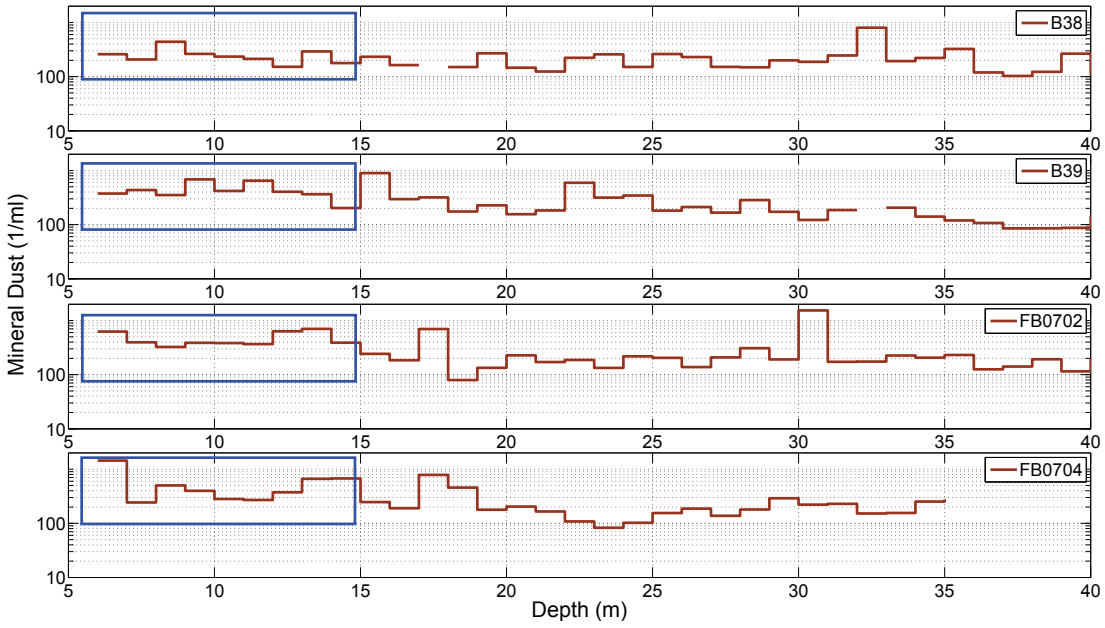

Figure 15: *Mineral dust records between 5 and 15 m for the four firn cores. The probably contaminated part (see text) is marked with a blue rectangle.*

the uppermost part of the firn cores, where the firn has a high porosity. If the increase in the concentration is due to contamination in the open firn during core processing, the onset of the increase should occur at a similar depth in all cores. If the increase reflects a real atmospheric signal, it should occur in the same year. In all cores an increase in mineral dust particle concentration was found in the upper 15 m. The upper 40 m of the firn cores are shown in figure 15. It is most likely that the higher level in mineral dust concentration is due to contamination rather than a real dust concentration increase in the firn and for further discussion (only for the mineral dust time series) only the core sections covering the time before 1990 is used, which is the start of the common time period in the four cores.

3 Local changes in ice core constituents

Local effects on aerosol impurity concentrations are determined by analyzing the spatial and temporal variability of the four cores in the ECA. Concentrations of firn core constituents from the firn cores quantified by continuous flow analysis (CFA) and ion chromatography (IC) are presented. The CFA data covers the time interval from 1962 until 2002. Since the temporal resolution of the data set changes with increasing depth, a running mean with 1000 data points per year was calculated. For the presentation of the IC-results a different resolution of 25 data points per year was chosen due to the overall lower resolution. The time series is extended until 2006 because the samples from the upper 6 m that could not be analyzed using CFA are included in the data sets.

3.1 Time series

An overview of the time series of the concentration records of ice core constituents is given in Fig. 16 - Fig. 21. Since the sea salt proxies are so much alike, for sea salt two proxies were chosen (Ca^{2+} quantified by CFA and Na^{+} quantified by IC). Sulphate is represented by $nss - SO_4^{2-}$ and MSA. All time series not shown in this section are shown in appendix B. The high number of data gaps in the IC data is due to the lower resolution of the IC data and the fact that in cases of breaks or other contamination the whole sample had to be deleted.

An event of high mineral dust concentration can be observed around 1970 in all cores (Fig. 16), however only weakly pronounced in core FB0704. The two southern cores show a peak around 1986/87.

In the sea salt record (Ca^{2+} and Na^{+}, figure 17 and 18), concentrations are higher in the years 1975-1977 in all four cores. The increase occurs slightly

earlier in the northern cores than in the southern cores. Seasonal variations are visible with the maximum concentration in Antarctic winter (June, July, August), except for Na^+ concentrations in FB0704 where the time series have a large number of data gaps. The time series from Na^+ mostly show the same characteristics as the Ca^{2+} time series. The Na^+ time series also shows that the maximum concentrations were in fact overestimated using CFA, since the IC time series do not exceed this threshold and the limit of 750 ng/g for Na^+ quantified by CFA was chosen properly. The time series from cores B39 and FB0702 both have a negative anomaly in Na^+ concentrations between 2006 and 2002 that is not visible in the two other cores.

The time series of $nss - SO_4^{2-}$ and MSA concentrations (figure 19-20) show a clear seasonal cycle with a maximum in Antarctic summer (December, January, February), except for FB0704 where the time series have many data gaps. According to Castellano et al. (2005), two volcanic eruptions occurred during the time period, one in 1964 (Agung) and one in 1992 (Pinatubo). However, these are not present in the $nss - SO_4^{2-}$ time series from ECA. Kaufmann et al. (2010) found a volcanic contribution of 8% in the total $nss - SO_4^{2-}$ flux (1000 year average) in the EDML core on the Antarctic plateau. For the coastal locations this contribution is even lower due to the closer distance to the coast and the resulting very high sea salt concentrations.

Nitrate concentration records (Fig. 21) are higher between 1969 and 1971 in the cores B38, B39 and FB0704. In core FB0702 concentrations are higher in 1971, but due to a data gap it cannot be distinguished whether the maximum is also present in the previous two years or not. A pronounced seasonal cycle shows a maximum in late spring and early summer.

Even though the concentration records show some events, none of them has a trend in the common time interval.

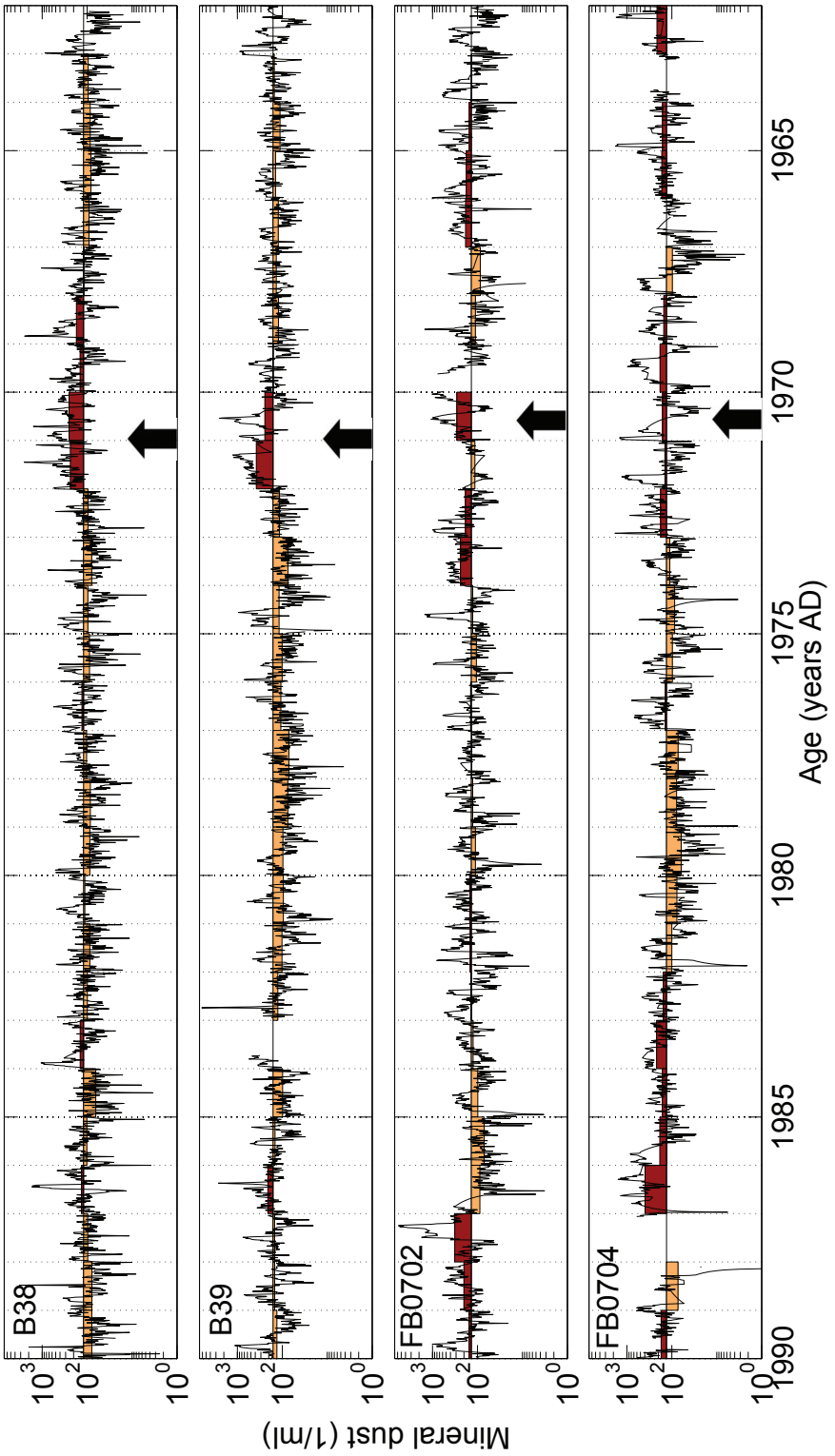

Figure 16: *Mineral dust time series including all particles with a diameter larger than 1 μm. Black lines indicate high resolution with 1000 data points every year, bars are yearly mean values. No yearly mean value was calculated if more than 30% of the data was missing. Vertical dashed lines indicate the beginning of the year, arrows indicate a common maximum in all four cores within the dating uncertainty of ±1 year (see text).*

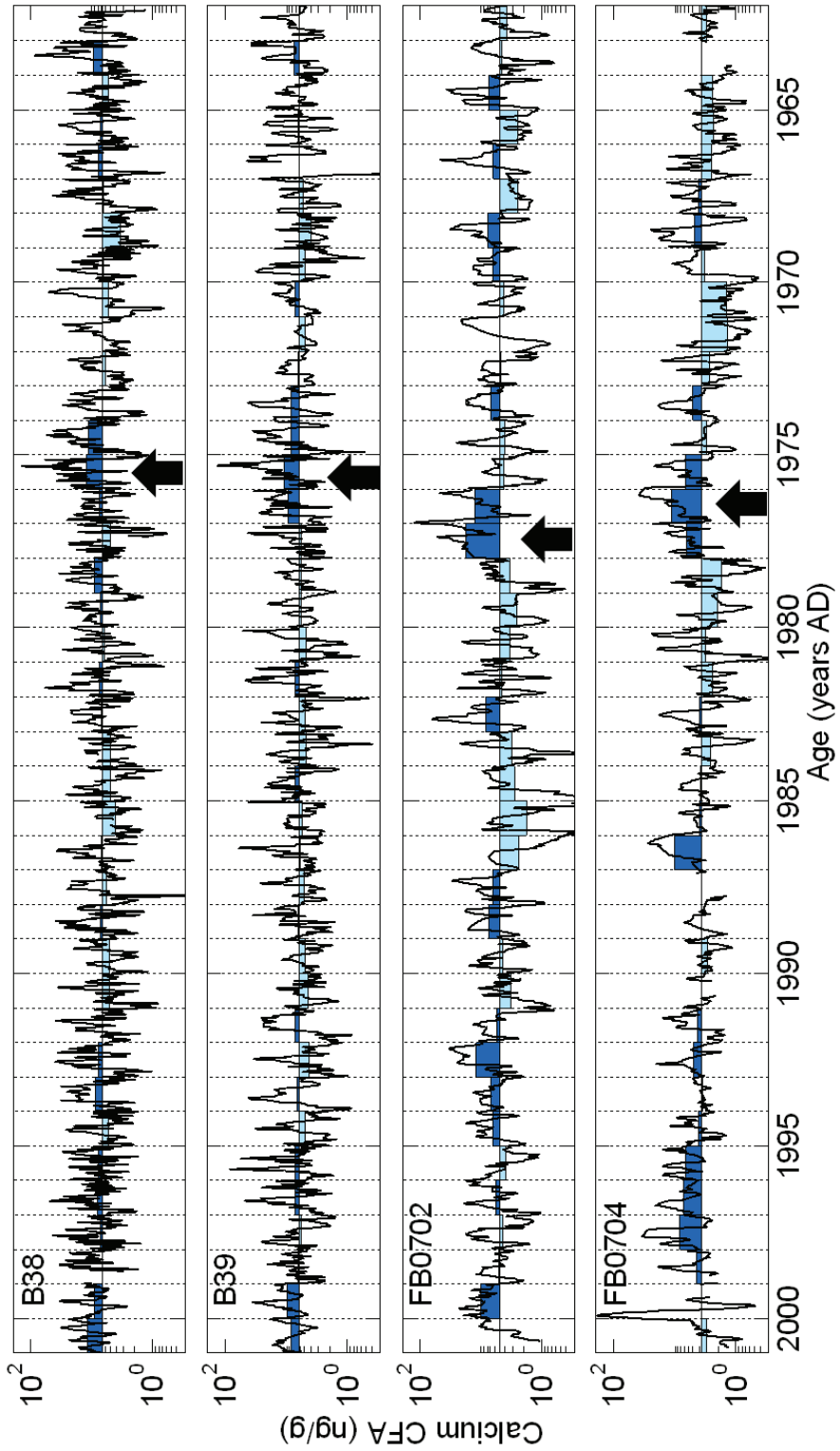

Figure 17: *Ca^{2+} time series from CFA. Black lines indicate high resolution with 1000 data points every year, bars are yearly mean values. No yearly mean value was calculated if more than 30% of the data was missing. Vertical dashed lines indicate the beginning of the year, arrows indicate a common maximum in all four cores within the dating uncertainty of ± 1 year (see text).*

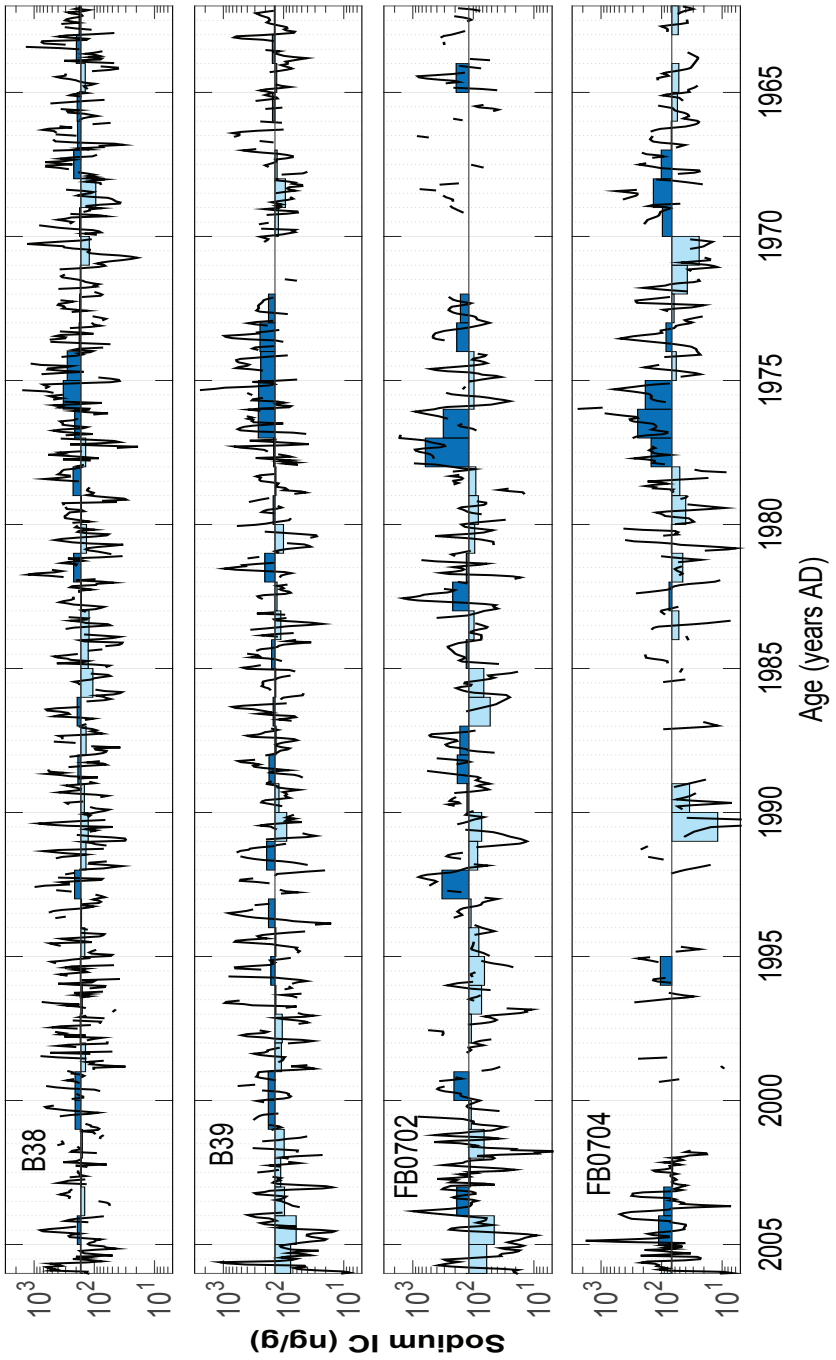

Figure 18: *Sodium time series from the IC. Black lines indicate time series with 25 data points per year, bars are yearly mean values. No yearly mean value was calculated if more than 30% of the data was missing. Vertical dashed lines indicate the beginning of the year, arrows indicate a common maximum in all four cores within the dating uncertainty of ±1 year (see text).*

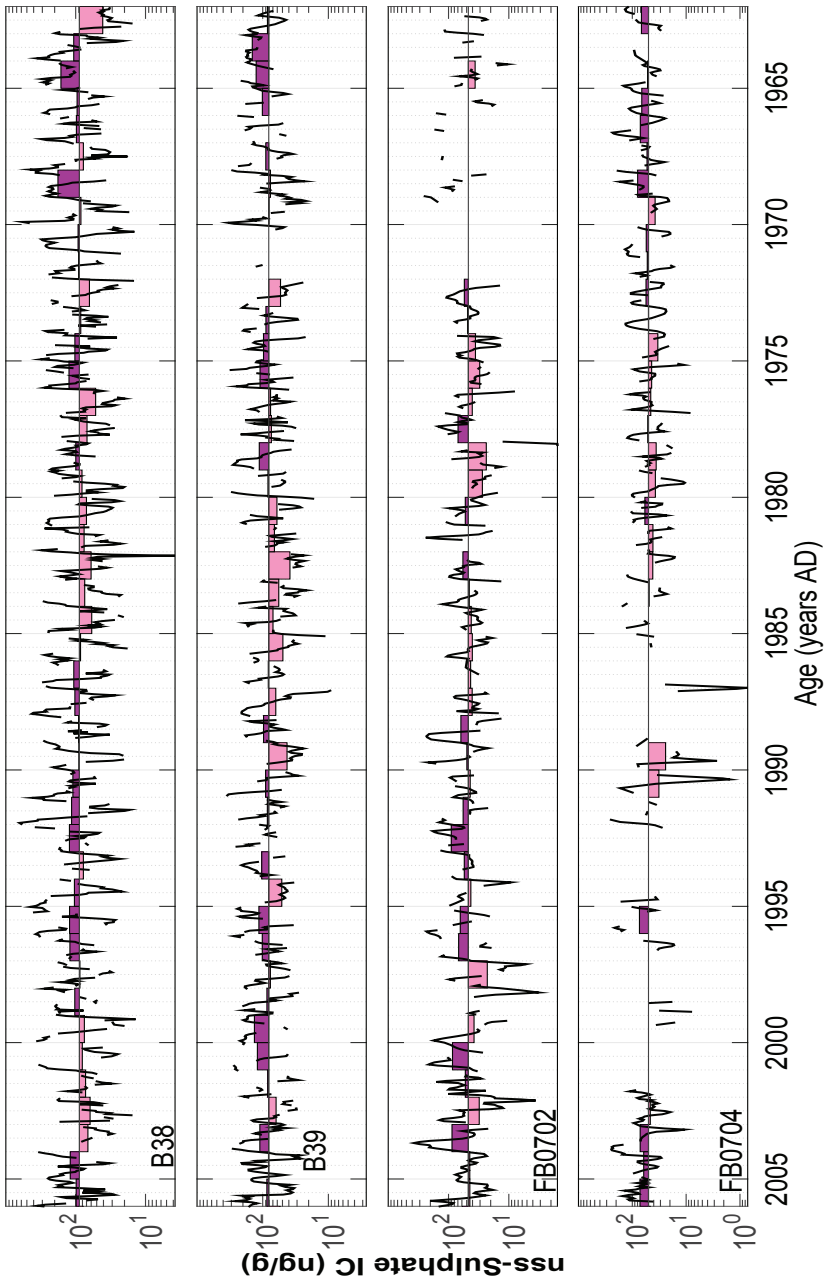

Figure 19: *As figure 18 but for nss-sulphate time series from the IC measurements.*

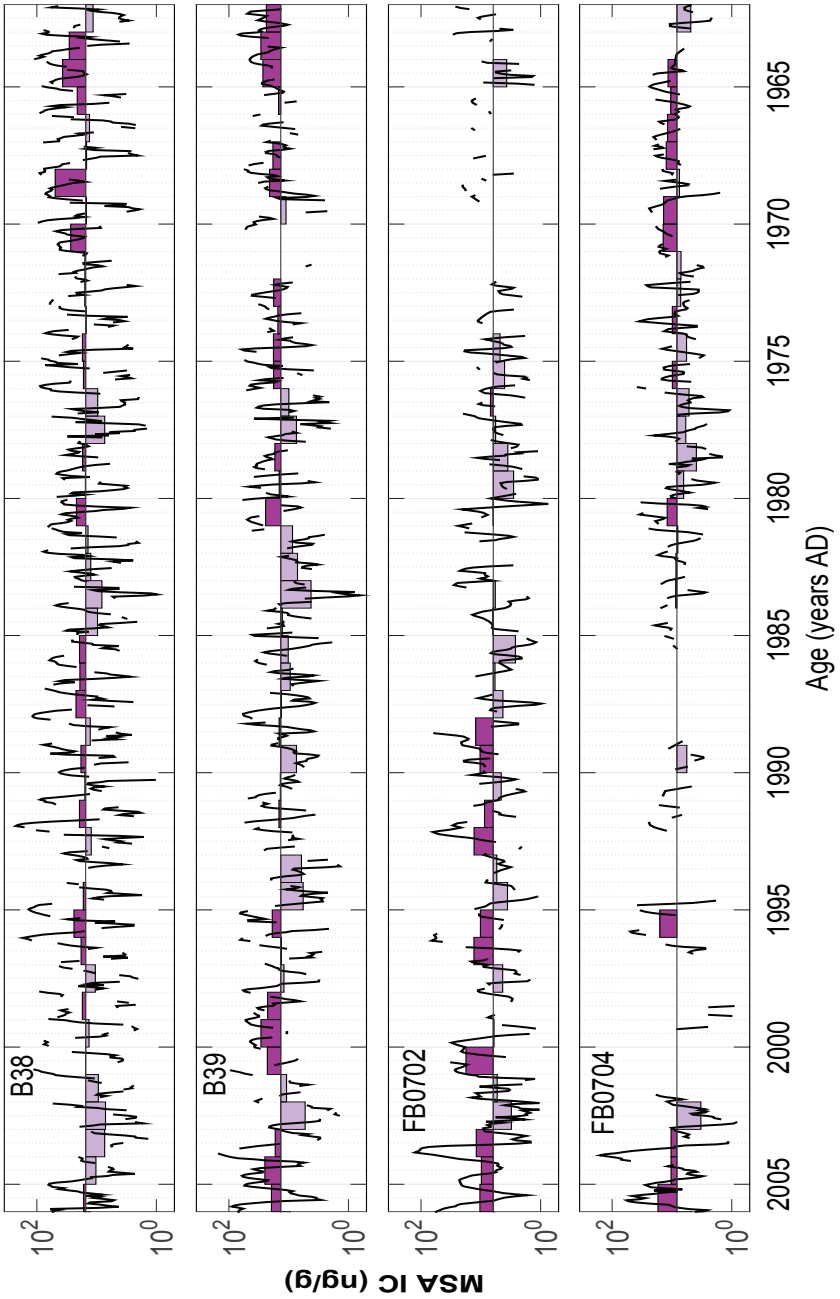

Figure 20: *Same as figure 16 but for MSA from IC.*

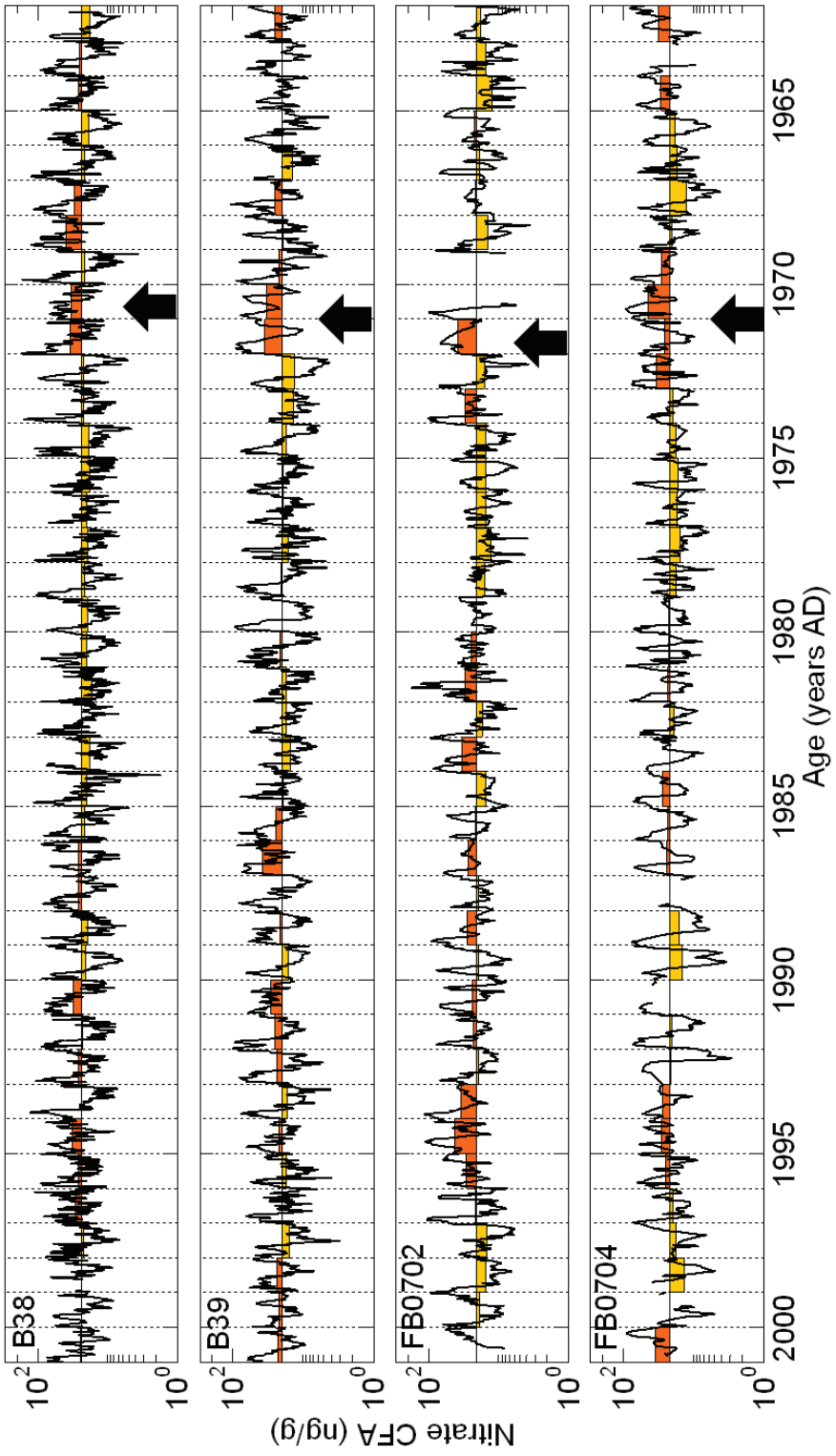

Figure 21: *As figure 17 but for but for nitrate concentrations from CFA.*

3.2 Data distribution and local gradients

For a further evaluation of the time series data, they are tested for distribution, their mean and standard deviation as well as their confidence intervals. The test for normal distribution is important to investigate if a further statistical analysis is suitable or if the data sets have to be treated so that a parametric analysis is possible. The data sets of each species and firn core are plotted in a histogram (figure 23-33, left sites) and additionally the data sets were tested for a normal distribution (figure 23-33, right sites). Colored dots represent the data sets while the black lines show the calculated normal distribution. Figure 22 shows the nitrate data sets without any calculations. Clearly, the data sets do not follow a normal distribution. The time series already show that most of the data have a logarithmic distribution. Thus, the logarithm of the data sets was taken and this treated data has been used for all the following analyses. Here the data for calcium (figure 25), sodium (IC, figure 27), nitrate (figure 33), mineral dust (figure 23), MSA (IC, figure 31) and nss-sulphate (IC, figure 29) are shown. As clearly visible in the figures, the time series have a lognormal distribution. In the following all calculations will be done using the logarithm of the values. Below the figures, tables are inserted giving the mean, median, confidence intervals and standard deviations of each species concentration (left site table) and flux (right site table). Those values have been calculated using the logarithm of the data and then calculated back to original values by using the exponent. Using the logarithmic data sets works here as a tool to use parametric statistical methods rather than going for less reliable nonparametric methods.

To estimate the influence of accumulation on the concentrations of ice core constituents the total deposition flux J_{ice} was calculated as described by Fischer et al. (2007b)

$$J_{ice} = C_{ice} * A \tag{3}$$

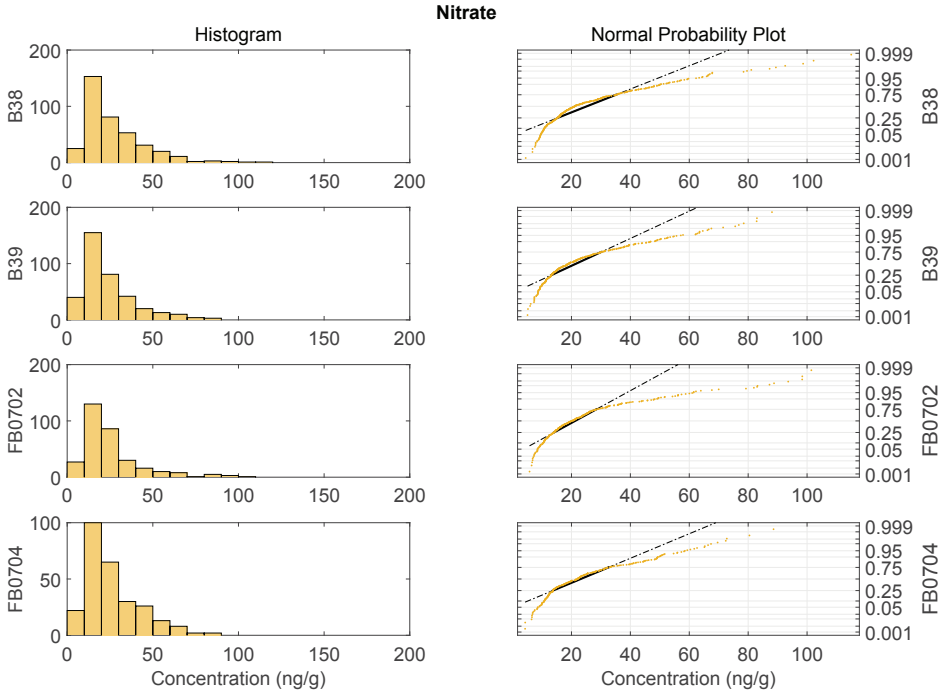

Figure 22: *Histogram (left) and normal probability plot (right) of nitrate concentrations from the four cores from ECA. Colored dots represent the data sets while the black lines show the calculated normal distribution.*

with the average concentration in the firn or ice C_{ice} and the accumulation rate A. It is assumed that changes in the overlaps and gradients over the ECA that differ from the concentration gradients are an indicator of dry deposition. Thus mean, median, confidence intervals and standard deviation were also determined for the time series of the fluxes. The results are shown in the tables below the data distribution plots (right site). The distribution of fluxes has been investigated and showed a logarithmic distribution as well. Thus the fluxes had been treated in the same way as concentrations, but in yearly resolution.

For a comparison of the spatial variability of concentration and fluxes multiple statistical tools are available. One way is the analysis of variance (von Storch and Zwiers, 2002, ANOVA, e.g.). It is a simple and fast way to compare the means from multiple data sets. Combined with a Tukey-test (Hsu, 1996, e.g.) the data sets that differ from each other can be determined. The

second approach is to look at the confidence intervals (Wilks, 1995, e.g.). They define the range of the mean with a given probability. In this study the 95% confidence intervals were used for the comparison of the spatial variability because of their closer connection to the original data sets. Also, calculating and comparing confidence intervals does not have to fulfill the requirements as they are needed for an ANOVA (e.g. independency of the data sets). However, ANOVA was also performed on the concentration records and led to the same results. The figures below the tables show the confidence intervals of the firn core data together with the normal probability density function (PDF) of a gaussian distribution that was calculated using

$$y = f(x(\mu,\sigma)) = \frac{1}{\sigma * \sqrt{2 * \pi}} * \exp \frac{-(x-\mu)^2}{2 * \sigma^2} \tag{4}$$

with μ the mean and σ the standard deviation (Wilks, 1995, e.g.). The confidence intervals are shaded and thus show the intervals where the means of the 4 cores lie. Thus when these do not overlap it is assumed that the means of the respective concentrations are different (as it would be a result of the ANOVA) and that a gradient exists. Naturally the gradient is stronger when the distance between the confidence intervals is higher. When confidence intervals overlap this infers that the means are not significantly different from each other. Confidence intervals are also given in the tables so in cases of close overlaps numbers are available as well. The left sites of the plots show confidence intervals of concentrations while right sites show confidences intervals of the fluxes. By comparing these two the differences in the gradients can be investigated giving an indicator if wet or dry deposition is dominant for the individual ice core constituent. If gradients are the same in concentrations and fluxes wet deposition is assumed. In other cases dry deposition is at least partly present.

Average mineral dust concentrations are very low over the ECA compared to dust concentrations on the plateau (Fischer et al., 2007a), however highest in the southern core on the Halvfarryggen FB0702 (175 part/ml). On Sörasen (B39 and FB0704), the mineral dust concentration does not change substantially from north to south. The confidence intervals overlap in the cores B39, FB0702 and FB0704. B38 does not show a overlap. The dome position of B38 has lower concentrations than the three other core locations. The confidence intervals of mineral dust fluxes have a stepwise overlap. This means: B38 overlaps with B39. B39 overlaps also with FB0702 and FB0702 overlaps with B39 and FB0704. This difference to mineral dust concentration confidence intervals indicates that dust is- at least partly- dry deposited. Although in the high accumulation regime wet deposition of aerosol components appears generally the most important deposition process, it has to be kept in mind that air masses leading to dust transport to the ECA are most likely not connected to moisture transport, hence, snowfall. In conclusion, mineral dust is at least partly dry deposited and has its most important local change on position B38, where concentrations clearly below the concentrations measured in the rest of the ECA.

Proxies for sea salt in the ECA are Na^+ and Ca^{2+}. Concentrations are higher at the core sites located closer to the coast (B38 and B39) and lowest at FB0704. Calcium concentration confidence intervals overlap in the cores B38 and B39. FB0702 and FB0704 do not have any overlap. Sodium confidence intervals have the same overlap of B38 and B39. There is also an overlap of FB0702 and B39, that is not present in the CFA calcium data. Confidence intervals of calcium concentrations overlap only for the cores FB0702 and FB0704. For sodium concentrations they do not overlap at all. Accordingly, we assume that dry deposition is of minor importance as expected in this high accumulation region. Thus, a gradient from the coastal core location to the

inland can be observed, as well as decreasing concentrations from the eastern to the western core locations.

Sulphate (SO_4^{2-} and MSA) show a north-south gradient decreasing from coast to inland, but no substantial east-west gradient. Concentrations are highest at core locations B38 and B39. B38 and B39 as well as FB0702 and FB0704 overlap, however this overlap is more pronounced for $nss - SO_4^{2-}$. The fluxes from the two sulphate components have the same gradients as the average concentrations. There is also an overlap for $nss - SO_4^{2-}$ and MSA fluxes in cores FB0702 and FB0704. For B38 and B39 however, the overlap observed in concentrations is not present in the fluxes any more. Even though little changes are observed between fluxes and concentrations these are not unambiguous and since the gradients themselves do not change wet deposition is most likely for sulphur components.

Nitrate concentrations are on average 21.4 ng/g and do not show any substantial gradient over the whole region of the ECA. Nitrate fluxes vary spatially in comparison to the concentration, they are highest at position B38 (27.2 ng/m^2*a) and lower at B39 (16.2 ng/m^2*a) and the southern sites (10.4 ng/m^2*a). Compared to the average accumulation rates at the sites this shows the dependency of nitrate concentrations on accumulation rates.

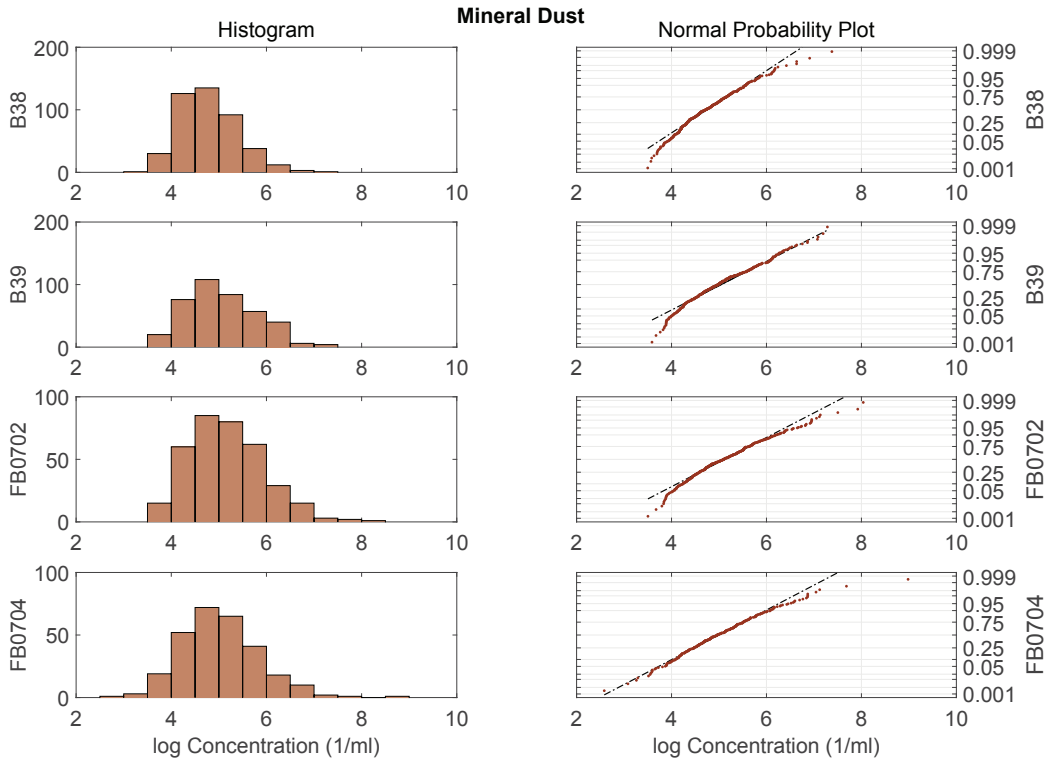

Figure 23: *Histogram (left) and normal probability plot (right)of the logarithm of mineral dust concentrations from the four cores from ECA. Colored dots represent the data sets while the black lines show the calculated normal distribution.*

Table 3: *Basic statistics from mineral dust time series. The values have been calculated using the logarithm of the data and then, for better comparison, been calculated back to original values using the exponent*

	concentration				flux			
	B38	B39	FB0702	FB0704	B38	B39	FB0702	FB0704
Mean	118.91	156.07	175.05	151.86	124.99	99.15	70.96	61.63
Median	112.08	145.08	163.66	142.93	124.85	98.07	76.90	67.79
CI	112.42	145.39	161.29	137.94	107.54	85.90	57.48	52.15
CI	125.78	167.53	189.99	167.19	145.27	114.45	87.61	72.84
Std	1.82	2.05	2.18	2.28	1.47	1.44	1.70	1.50

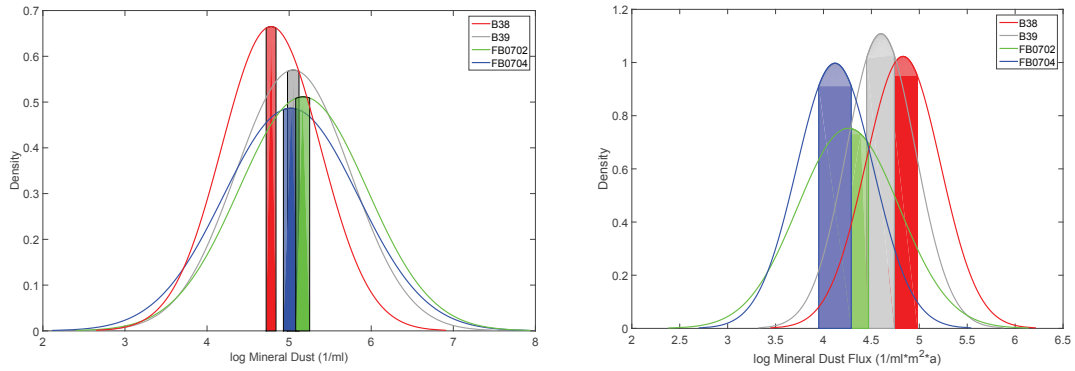

(a) **(b)**

Figure 24: *Comparison of confidence intervals of mineral dust concentrations together with the probability density fuction that was calculated using mean and standard deviation. Figure 24a shows concentrations, figure 24b fluxes.*

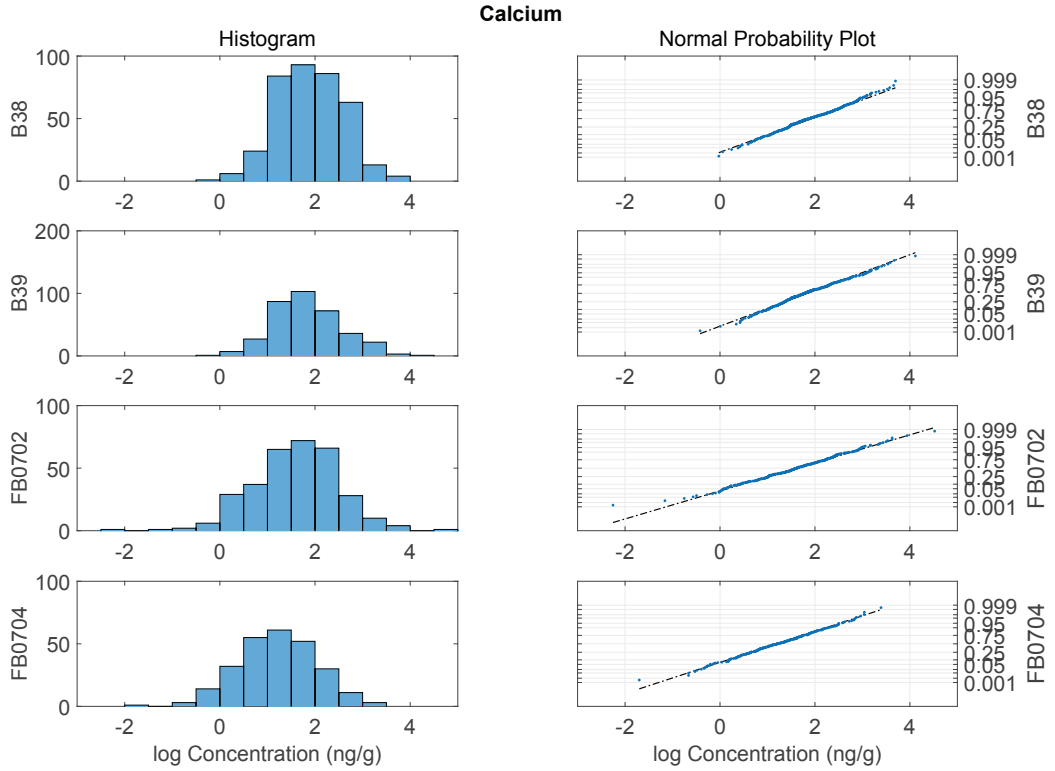

Figure 25: *as 23 but for calcium concentrations.*

Table 4: *As 3 but for calcium concentrations*

	concentration				flux			
	B38	B39	FB0702	FB0704	B38	B39	FB0702	FB0704
Mean	6.73	6.28	4.95	3.37	8.11	4.92	2.51	1.82
Median	6.65	5.98	5.03	3.34	8.42	4.64	2.75	1.67
CI	6.28	5.84	4.48	3.05	6.96	4.31	2.03	1.48
CI	7.22	6.75	5.47	3.72	9.44	5.63	3.10	2.24
Std	1.98	2.02	2.48	2.26	1.59	1.50	1.89	1.81

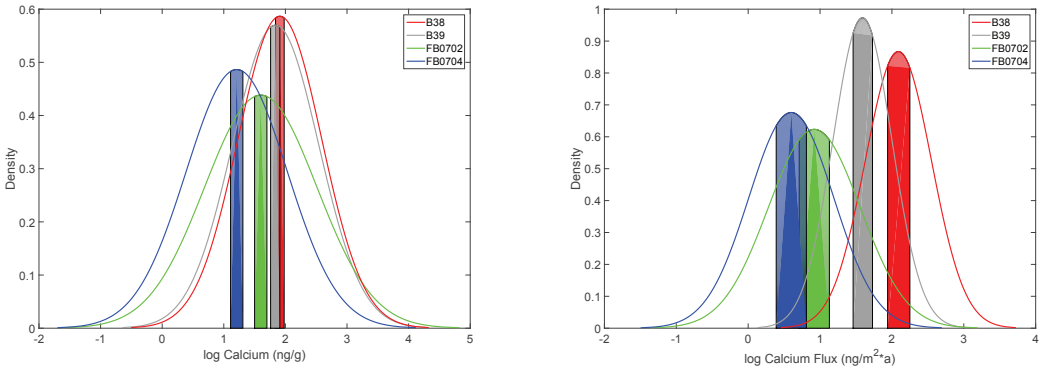

(a) **(b)**

Figure 26: *as 24a and 24b but for calcium concentrations*

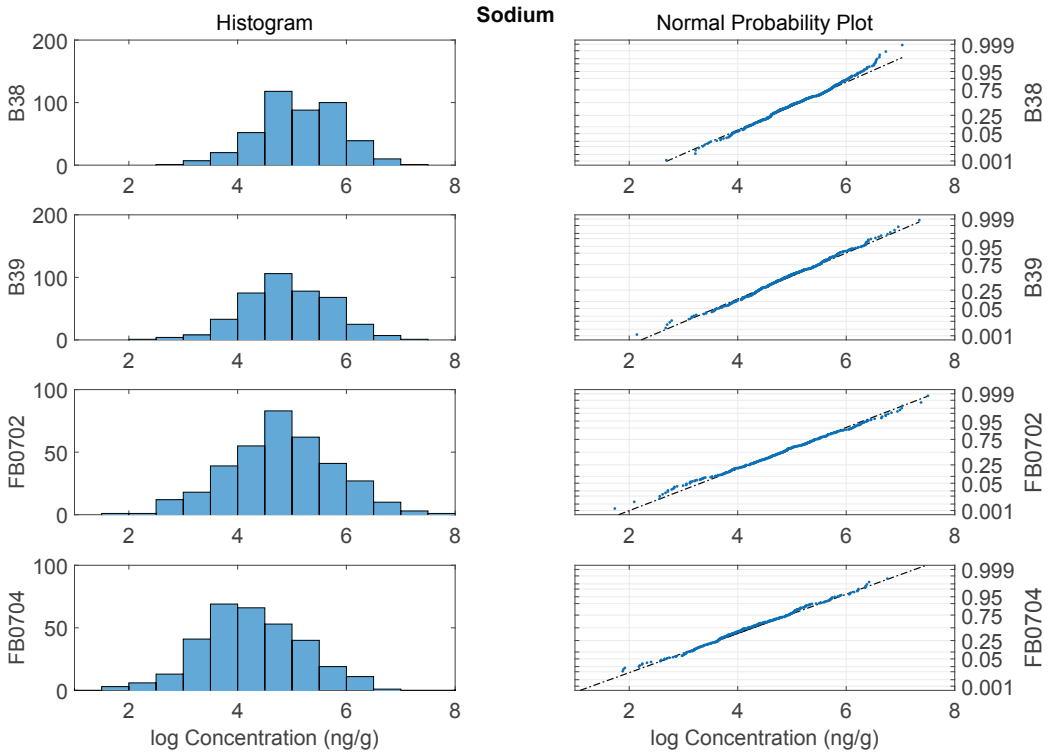

Figure 27: *as 23 but for sodium concentrations quantified by IC.*

Table 5: *same as table 3 but for Sodium IC concentrations.*

	concentration				flux			
	B38	B39	FB0702	FB0704	B38	B39	FB0702	FB0704
Mean	166.96	136.56	122.44	67.30	201.14	120.94	62.08	32.11
Median	164.43	132.54	125.24	66.65	205.70	111.14	56.05	28.57
CI	155.90	126.42	110.52	59.81	173.20	105.54	48.70	22.88
CI	178.81	147.51	135.64	75.73	233.58	138.59	79.13	45.08
Std	2.07	2.21	2.66	2.95	1.59	1.49	1.92	2.19

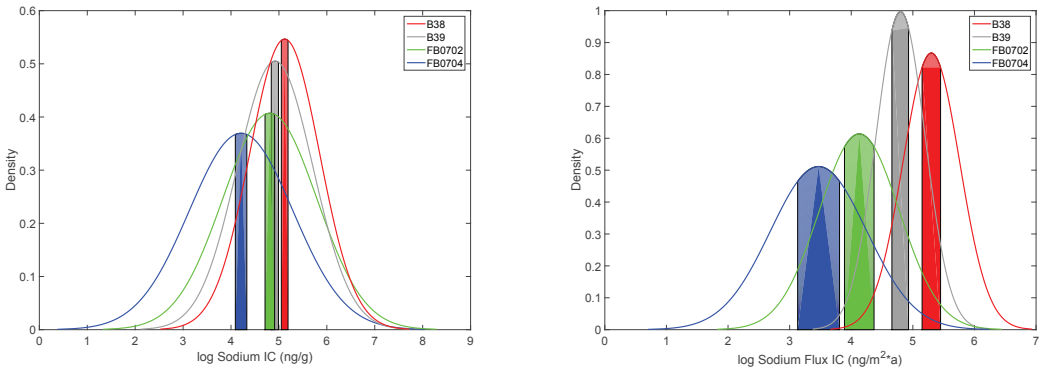

(a) **(b)**

Figure 28: *as 24a and 24b but for sodium concentrations quantified by IC.*

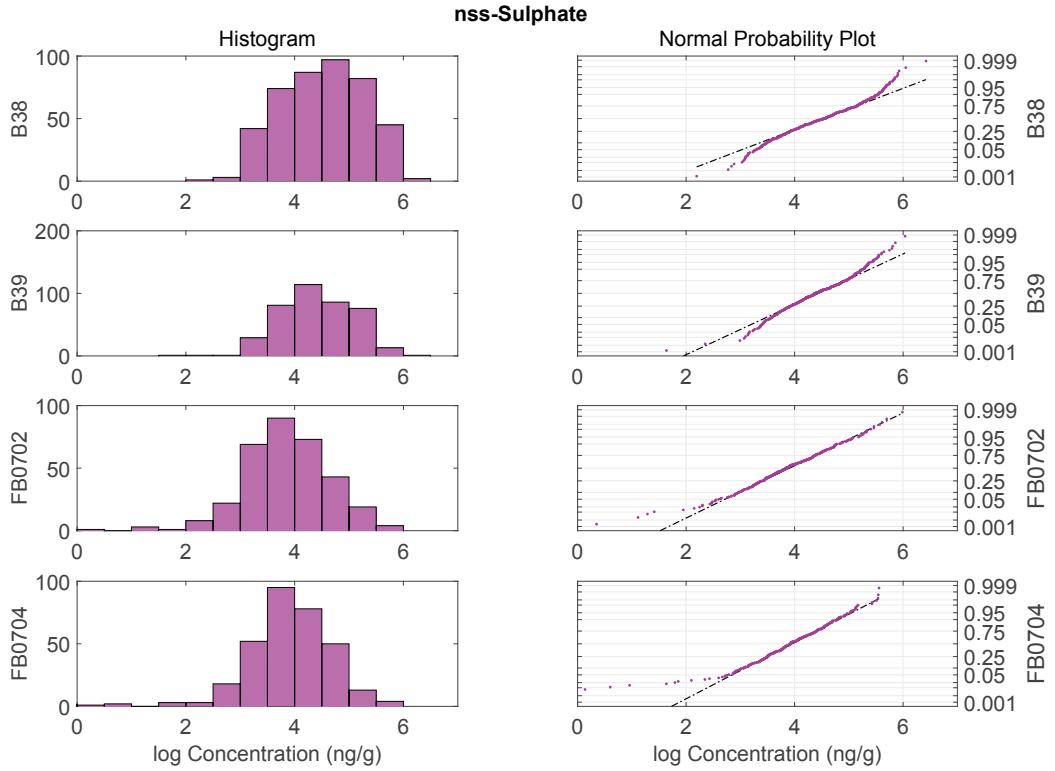

Figure 29: *as 23but for nss-sulphate concentrations quantified by IC.*

Table 6: *same as table 3 but for nss-sufate concentrations.*

	concentration				flux			
	B38	B39	FB0702	FB0704	B38	B39	FB0702	FB0704
Mean	91.29	82.28	47.76	48.64	109.13	66.91	23.08	23.57
Median	95.22	79.94	46.56	50.41	113.83	68.52	21.50	23.79
CI	85.00	77.18	43.93	44.45	95.51	57.56	19.78	19.68
CI	98.05	87.71	51.93	53.23	124.69	77.78	26.93	28.23
Std	2.13	1.92	2.17	2.27	1.51	1.55	1.50	1.52

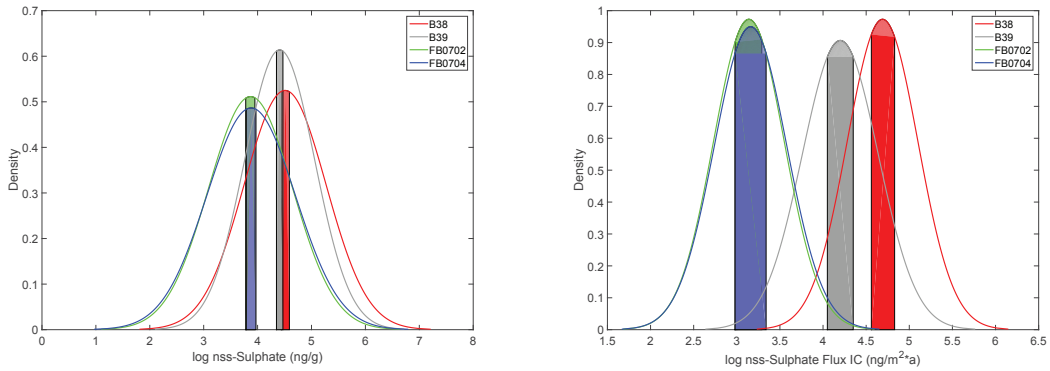

(a) **(b)**

Figure 30: *as 24a and 24b but for nss-sufate concentrations.*

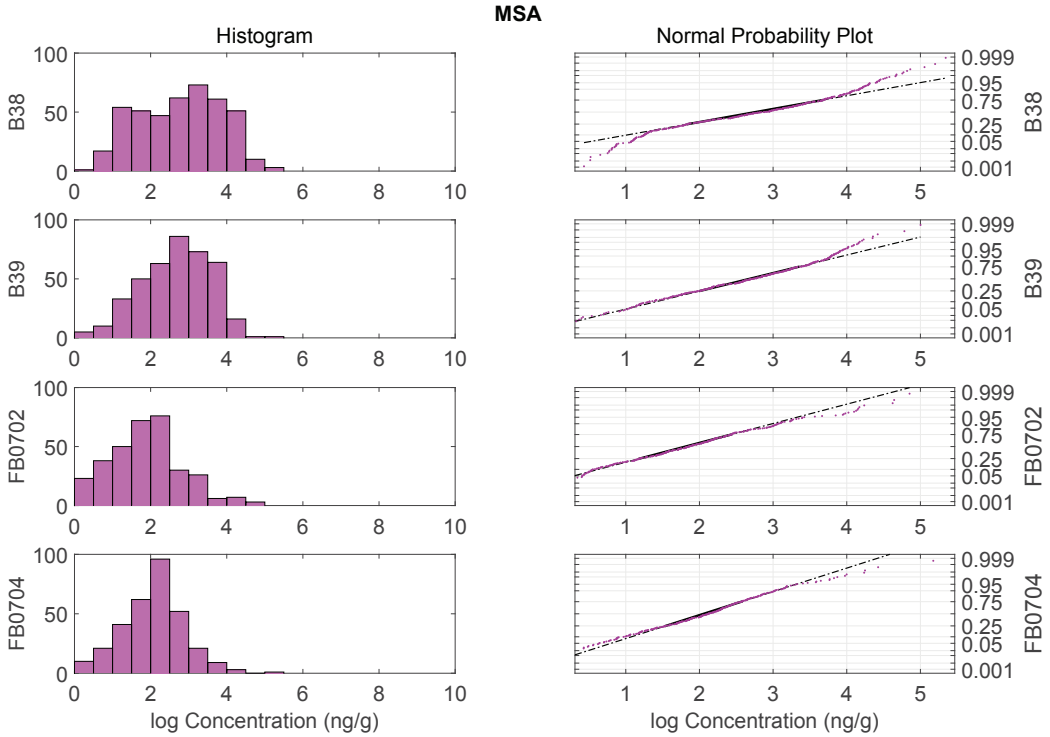

Figure 31: *as 23 but for MSA concentrations.*

Table 7: *same as table 3 but for MSA concentrations.*

	concentration				flux			
	B38	B39	FB0702	FB0704	B38	B39	FB0702	FB0704
Mean	16.01	13.95	6.45	7.88	19.58	11.04	2.96	4.31
Median	17.77	15.24	6.39	8.34	19.45	11.70	2.82	4.10
CI	14.44	12.73	5.82	7.19	17.28	9.28	2.35	3.66
CI	17.75	15.28	7.15	8.63	22.18	13.12	3.72	5.08
Std	2.96	2.55	2.61	2.29	1.46	1.66	1.76	1.45

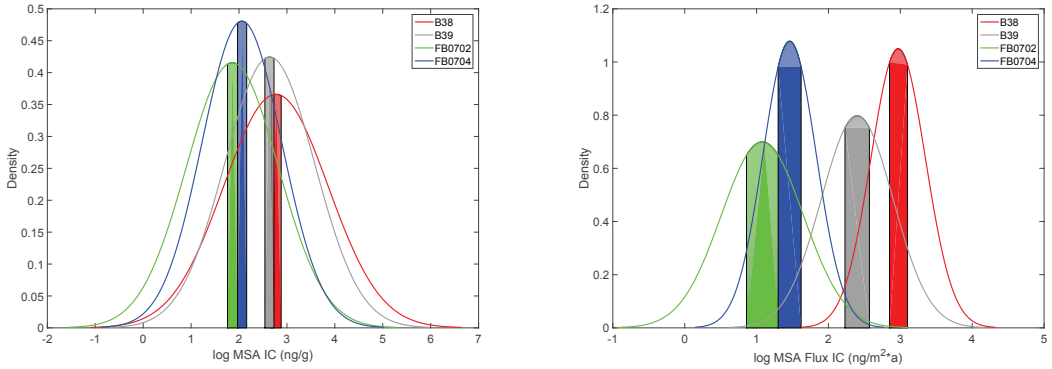

(a) **(b)**

Figure 32: *as 24a and 24b but for MSA concentrations.*

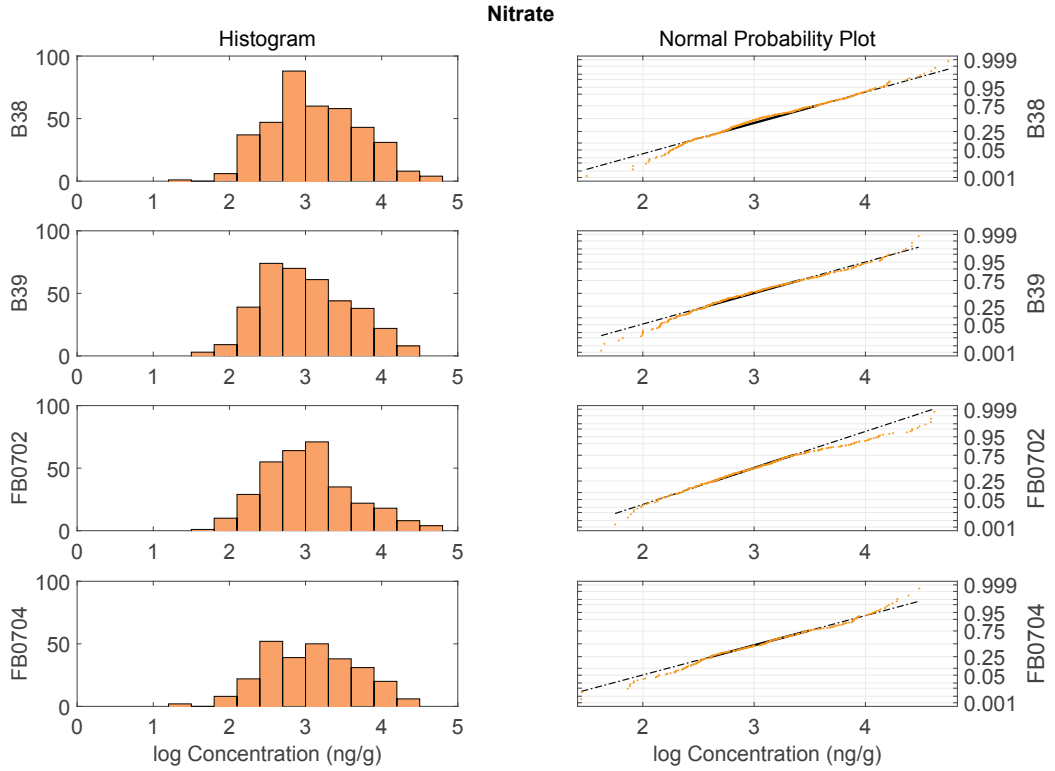

Figure 33: *as 23 but for nitrate concentrations.*

Table 8: *same as table 3 but for nitrate concentrations.*

	concentration				flux			
	B38	B39	FB0702	FB0704	B38	B39	FB0702	FB0704
Mean	22.77	20.26	20.87	21.77	27.22	16.19	10.31	10.49
Median	21.03	19.14	20.02	22.04	26.47	16.67	10.20	10.43
CI	21.48	19.09	19.57	20.27	24.65	14.68	9.27	9.41
CI	24.14	21.51	22.26	23.39	30.05	17.86	11.48	11.68
Std	1.79	1.79	1.79	1.81	1.35	1.35	1.36	1.36

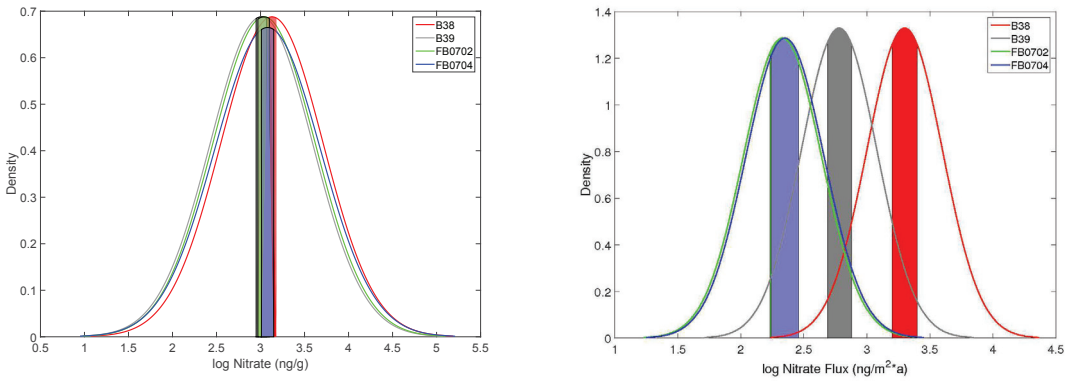

(a) **(b)**

Figure 34: *as 24a and 24b but for nitrate concentrations.*

3.3 Seasonality

The variability of ice core proxies are influenced by atmospheric concentrations (section 1.3), but can also be changed by seasonal variations in the snow accumulation rate. To quantify this effect on aerosol deposition, seasonal accumulation rates derived from an automatic weather station (AWS) on Halvfarryggen very close to core B38, were used here denoted as weighted accumulation.

Figure 35 illustrates how the weighted accumulation is used to obtain the seasonality in a time series. Each color represents one month of the year (1: January to 12: December) and the width of the boxes represent the respective partial of accumulation over one year. Black lines show the calcium concentration from core B38 before (above coloured bar) and after (below coloured bar) using the individual interpolation method. If the data from one year is distributed linearly as in figure 35a, nothing changes in the distribution of the yearly data. However, if a weighted accumulation is used as shown in figure 35b, the time series from the respective year is compressed during the winter and extended during the summer months. Therefore, the higher accumulation rates in summer are taken into account and the seasonal resolution of the data is more precise. Since it is the only place where a weather station is located, the time series from firn core B38 were used to obtain the influence of the weighted accumulation. This was done on three species quantified by CFA (calcium, mineral dust and nitrate) since these have the highest resolution. As shown in figure 36, the seasonality changes only marginally. The sea salt maximum is broader and a narrower minimum evolves during the summer. The mineral dust and nitrate maximum is more confined to late spring and early summer. In summary using weighted or evenly distributed accumulation rates will not effect the results of this study. Additionally, B38 is the only location where an AWS is installed and its seasonality in accumula-

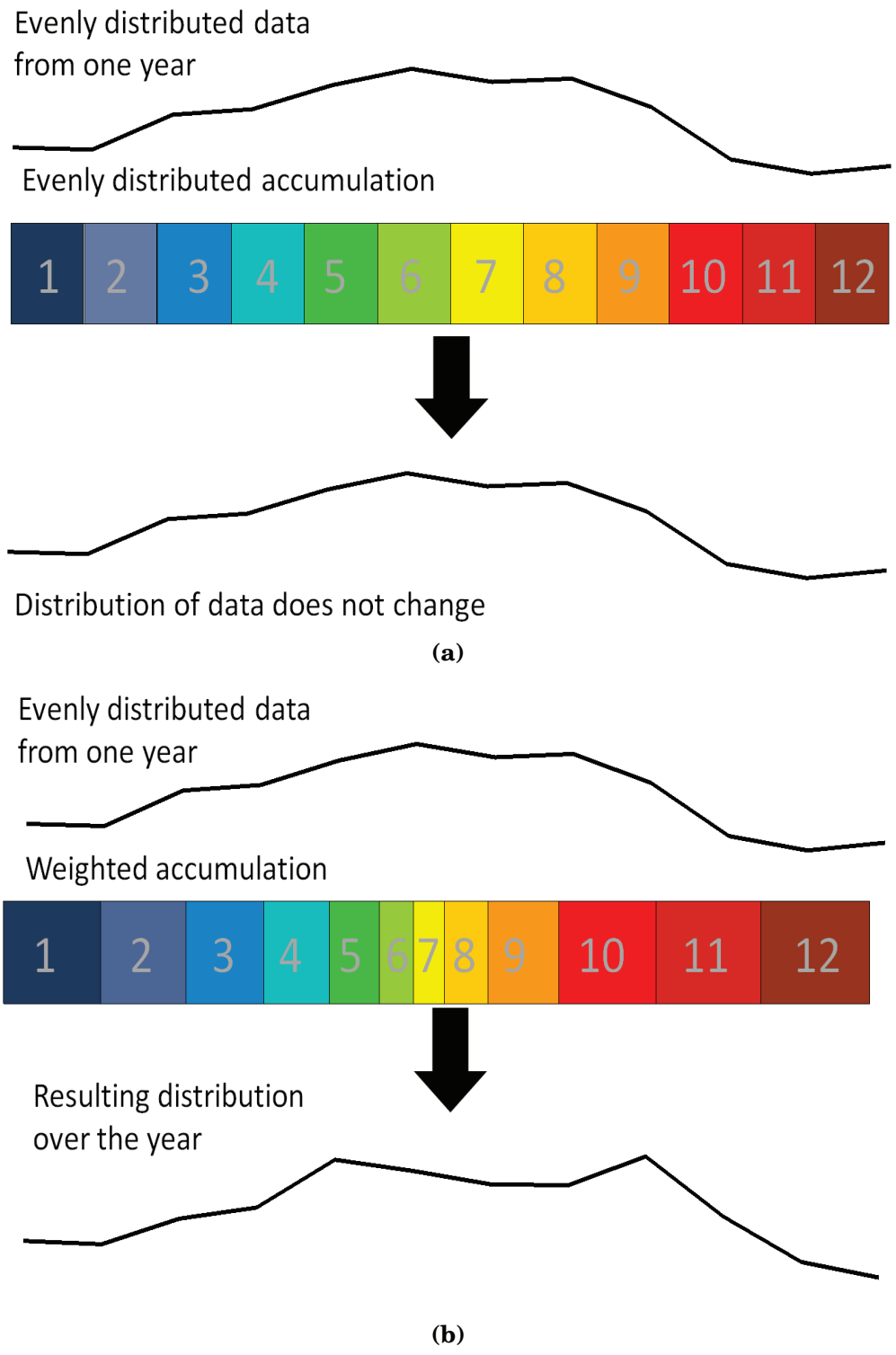

Figure 35: *Principle of the weighted accumulation. Numbers 1-12 denote the months. 35a is the linear interpolation, 35b the interpolation with weighted accumulation rates. The data of one year is taken respectively and distributed over the year as denoted from the weighted accumulation. Black lines show the calcium concentration from core B38 before (above coloured bar) and after (below coloured bar) using the individual interpolation method.*

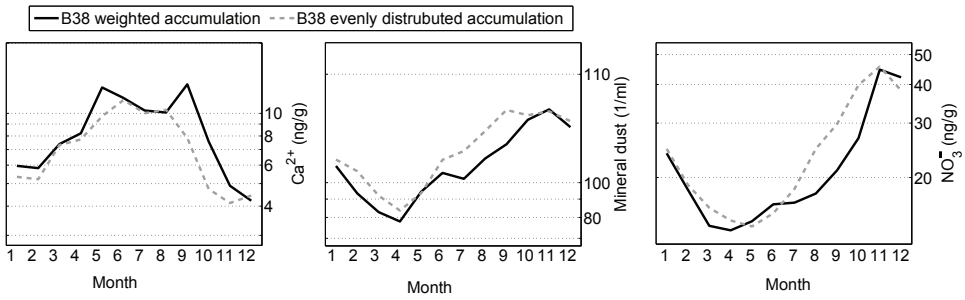

Figure 36: *Seasonal variability of calcium, mineral dust and nitrate in core B38 for constant (dashed line) and seasonally weighted (solid line) accumulation rates.*

tion may not be representative for the other three sites. Therefore, the evenly distributed accumulation is used for further analysis and discussion.

To visualize the seasonality, boxplots are used that are produced from stacked monthly means (figures 37-42). This means that monthly means from all years have been taken and each month has been averaged separately (e.g. Januaries from each year are taken to produce the first box). The boxplots show the median of a respective month (thick black line), the 25 and 75% variability (boxes), error bars with the 95% confidence interval and stars that represent outliers from the confidence interval. As a measure of the annual variability R table 9 gives the percentage deviation of a dataset X (the annual range) from the mean.

$$R = \frac{100}{mean(X)} * \frac{Range(X)}{2} \tag{5}$$

The seasonality of the species quantified by CFA is shown in monthly resolution (blue lines in respective plots). Because of the larger error in the dating the seasonal variability in the IC-datasets is only given for the seasons summer (months December, January, February), autumn (months March, April,

Table 9: *Mean annual variability R calculated from monthly stacked means.*

		B38	B39	FB0702	FB0704
$\delta^{18}O''$	R (%)	17.2	14.3	12.8	11.0
Mineral dust CFA	R (%)	25.6	32.3	25.5	33.6
nss-Ca^{2+} IC	R (%)	27.9	18.2	28.9	39.0
Ca^{2+} CFA	R (%)	60.4	50.2	39.5	21.6
Ca^{2+} IC	R (%)	45.3	33.4	36.9	21.7
Na^{+} IC	R (%)	73.6	52.1	50.4	22.9
Cl^{-}'' IC	R (%)	78.6	57.3	57.2	26.2
Cl/Na IC	R (%)	7.7	7.1	7.9	12.2
K^{+} IC	R (%)	45.9	36.0	32.8	13.2
Mg^{2+} IC	R (%)	72.2	50.0	46.2	20.7
NO_3^{-} CFA	R (%)	69.6	56.8	38.0	40.4
NO_3^{-} IC	R (%)	69.6	56.8	38.0	40.4
MSA IC	R (%)	143.8	71.6	18.9	18.6
nss-SO_4^{2-}''	R (%)	112.0	50.3	24.3	29.4

May), winter (months June, July, August) and spring (months September, October, November, red line in respective plots). As a comparison the respective concentrations that have been quantified in the air chemistry laboratory at Neumayer Station are plotted in gray lines, if available.

For mineral dust records at all sites highest concentrations occur in spring (August - November) and lowest concentrations in summer to fall (Fig. 37). No comparable mineral dust record from Neumayer is available. However, the determination of crustal elements in aerosol filters from Neumayer showed, in contrast to this study, highest concentrations in summer (Weller et al., 2008). A study by Ruth et al. (2008) based on ice samples proved the equivalence of crustal elements and particulate dust as dust tracer in ice cores. However, here aerosol filter analysis is compared with snow sample analysis, where deposition effects could affect the concentrations. Additionally, the crustal element concentration is related to the mass concentration of dust, while here the number concentration is used due to the low overall dust concentration. Both facts might influence the results.

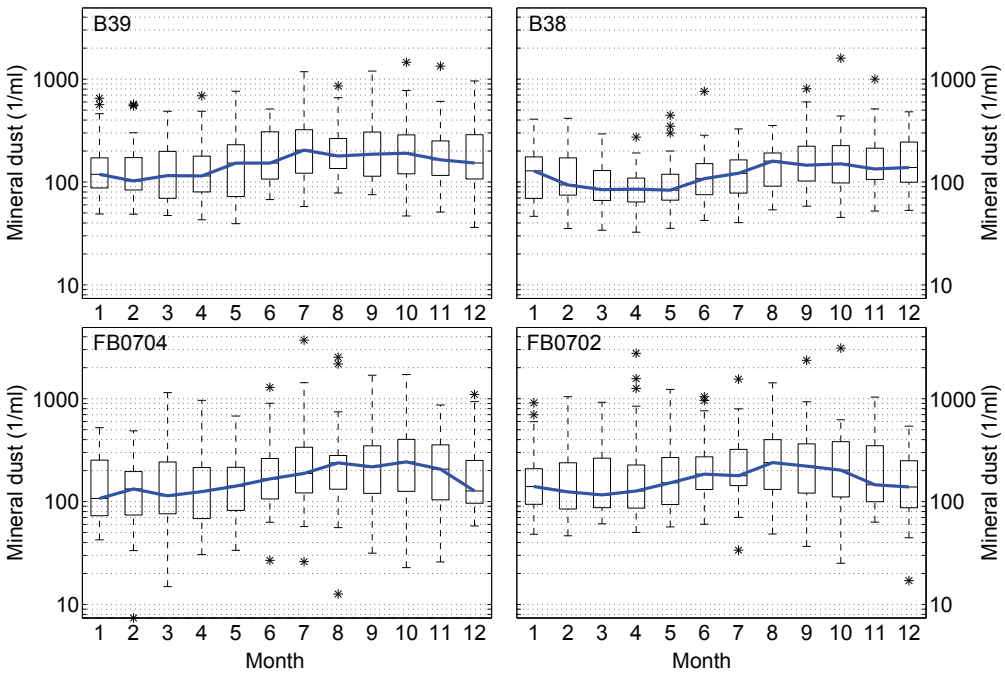

Figure 37: *Monthly stacked mineral dust record: Thick blue lines give the median, boxes give 25 and 75% variability. Error bars are calculated as 95% variability. Stars indicate outliers.*

Besides the overall higher calcium concentrations in the northern cores compared to the southern cores, also the annual variability of the calcium concentration decreases from north to south, and from east to west (R_{B38} = 60.4%, R_{B39} = 50.2%, R_{FB0702} = 39.5%, R_{FB0704} = 21.6%, Fig. 38). All sites show highest calcium concentrations in winter. However, at Halvfarryggen (B38 and FB0702) a broad maximum evolves during the winter months while at Sörasen (B39 and FB0704) the winter maximum is slightly more confined to June/ July. At all sites lowest calcium concentrations occur in October/ November. In core B39 a secondary minimum occurs in February and March. B38, B39 and FB0702 have a similar seasonality as the Ca^{2+}-concentrations measured at Neumayer Station and a correlation analysis confirms this visual impression (r_{B38} = 0.9, r_{B39} = 0.7, r_{FB0702} = 0.8, p <0.01). Only for FB0704, the correlation is lower (r = 0.6, p <0.05). Note that a different seasonality

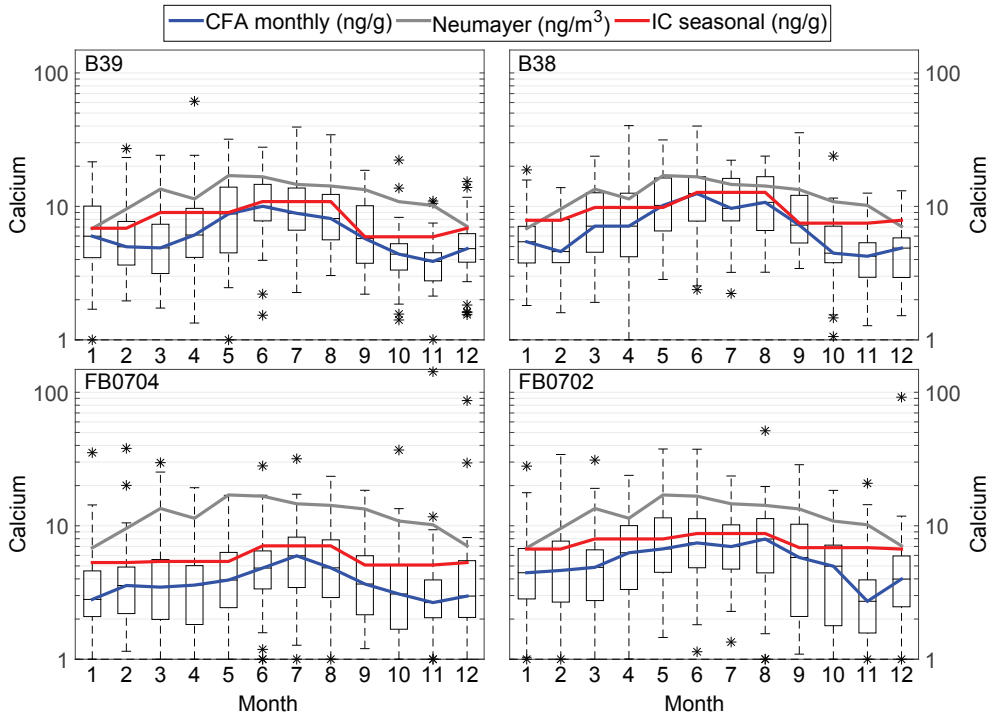

Figure 38: *Monthly stacked calcium record quantified by CFA (boxplots and blue line) as in Fig. 37 and seasonal calcium record quantified by IC (red line). Gray lines represent stacked data from Neumayer Station over the time period (1984-2000).*

in the accumulation rate at the four drill sites may also contribute to those subtle differences in seasonal cycles of chemical components. Na^+ basically show the same seasonality as Ca^{2+} quantified by CFA. The maximum concentrations also occur in the summer months and the concentration is lowest in the spring.

The seasonal cycle of $nss - SO_4^{2-}$ has a maximum in summer, following the seasonality from Neumayer. Since the dating was performed without using $nss - SO_4^{2-}$ this also confirms the quality of the dating. However, in the two southern cores FB0702 and FB0704 the minimum is slightly shifted to an earlier time of the year, while the maximum is still in summer. From coast to inland, the amplitude of the seasonal cycle decreases. This is more distinct in the annual variability of MSA (figure 41 and table 9), where the annual

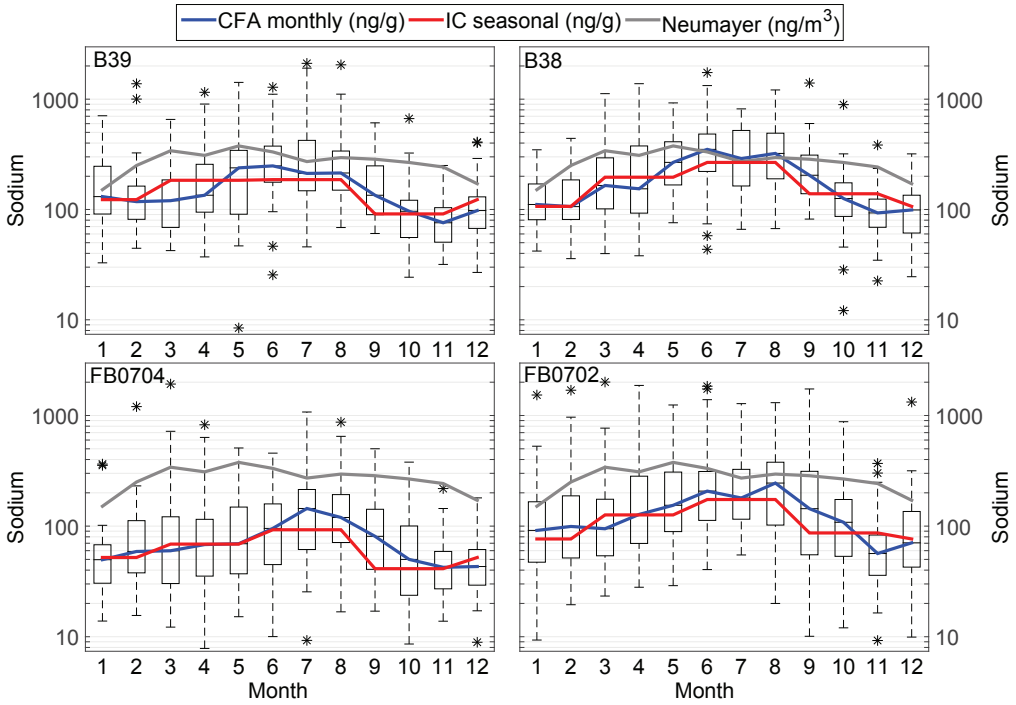

Figure 39: *Same as in figure 38, but for sodium.*

cycle in the two cores located closer to the coast (B38 and B39) is much more distinct than the annual cycle in the two cores located closer to the plateau (FB0702 and FB0704). For MSA, the minimum is distinct in the winter and the maximum distinct in the summer. In both $nss - SO_4^{2-}$ and MSA the seasonal amplitudes at Neumayer Station are much more distinct than the amplitudes from the firn cores.

Nitrate was used for dating purposes, explaining the seasonality with the maximum in spring and the minimum in autumn (figure 42). Therefore, correlation with the seasonality at Neumayer Station is by definition high (r >0.9, p <0.001 for all cores). The annual variability is more pronounced in the northern cores (R_{B38} = 69.6%, R_{B39} = 56.8%, R_{FB0702} = 38.0%, R_{FB0704} = 40.4%). To understand the regional variability of the average concentrations and differences in the seasonality in the four records, different characteristics of the drill sites have to be taken into account. The distance to the source region,

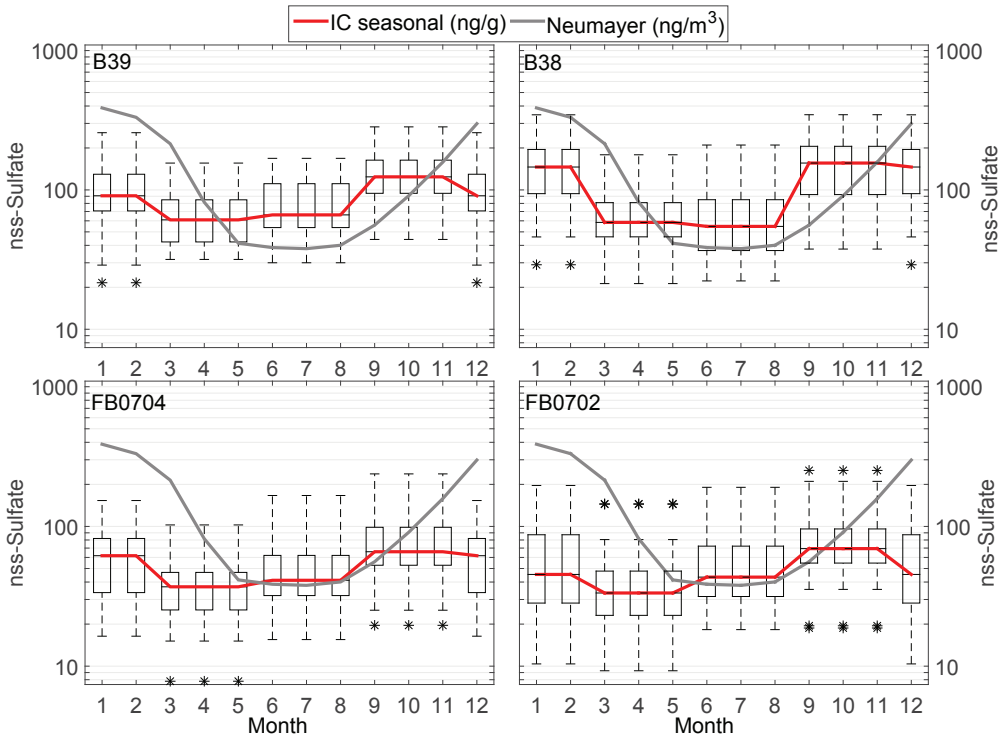

Figure 40: *Same as in figure 38 but for nss-sulphate.*

topography, accumulation rates and local winds are the main factors that are considered to influence the aerosol input (e.g. Bertler et al., 2005).

In this study all drill sites are close to the coast, however the southern cores are ∼70 km further inland. The two northern sites are located on dome positions (B38 and B39), whereas the two southern sites are located on slopes (FB0702 and FB0704). The increase in altitude from the coast to the dome positions is ∼650 m. On Sörasen, the altitude increases to the drill site of FB0704 to 760 m, while on Halvfarryggen the altitude decreases from 690 m to 540 m to the drill site of FB0702, which is located on a saddle (Wesche et al., 2009). Further south the ice surface increases from both drill sites until it reaches the Antarctic plateau at around 2900 m.

In an area with strong winds like the ECA (König-Langlo et al., 1998) the aerosol input is likely to be influenced by drifting snow. Regarding the impact on regional changes Fernandoy et al. (2010) investigated accumulation

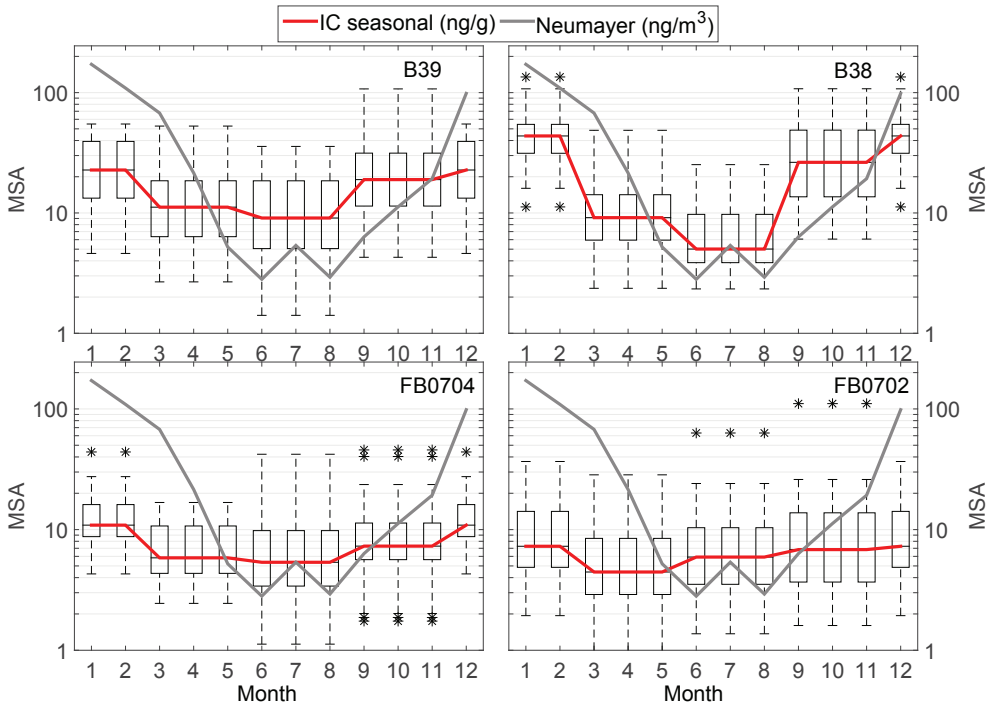

Figure 41: *Same as in figure 38 but for MSA.*

rates of the four cores that are also investigated in this study. FB0702 is the only site that shows a significantly decreasing trend in accumulation rates between 1960 and 2006, which may be due to the location of the core and the prevailing topography that is most likely enhancing wind speeds. By comparison to snowdrift events at Neumayer station they concluded that FB0702 is most probably the only location where snowdrift might occur. Regarding the seasonal variability no significant changes between FB0702 and the other drill sites is observed in this study (section 3.3) and thus it is assumed that the influence of snowdrift can be neglected.

In the following, the aerosol input at the four different sites in the ECA are discussed with respect to distance to source region, topography, accumulation and wind regime.

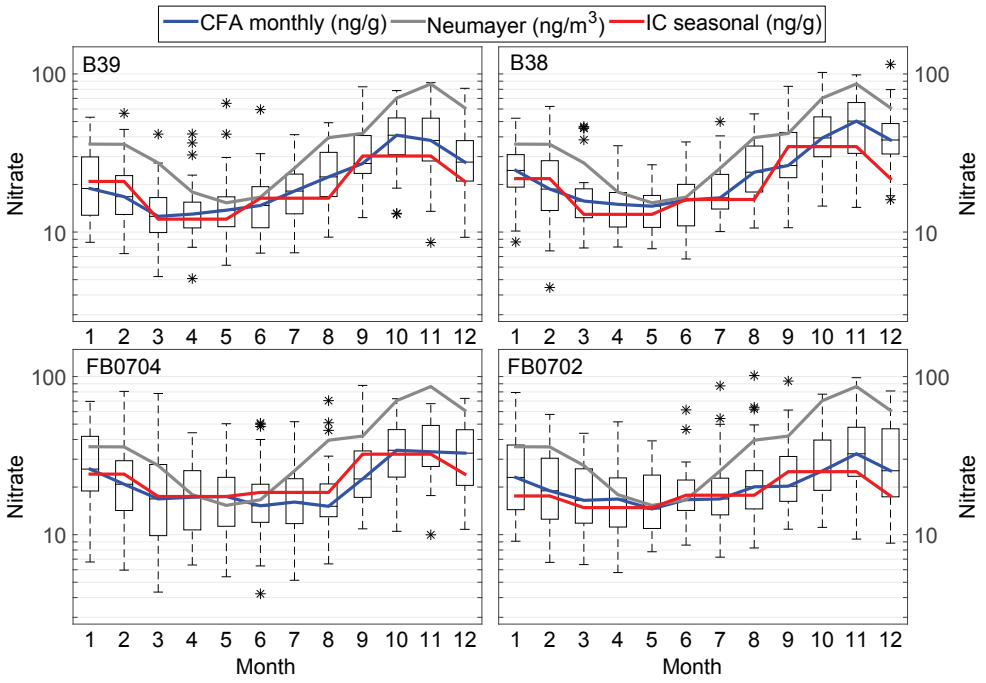

Figure 42: *Same as in figure 38 but for nitrate.*

3.4 Influence of katabatic winds on the mineral dust concentration

Mineral dust concentrations are lowest at B38 and at least partly dry deposited over the ECA. The seasonal cycle is only weakly pronounced with a maximum in Antarctic spring.

The main source region for mineral dust particles for Dronning Maud Land during the 20th century has been determined to be mainly Patagonia (Albani et al., 2012)), the same source as for Berkner Island (Bory et al., 2010) and the Antarctic Peninsula (McConnell et al., 2007). It is assumed that this is also true for the ECA. A higher emission of mineral dust particles in southern South America should therefore result in higher mineral dust concentrations in the ice cores (Mahowald et al., 2010). Based on comparable continuous flow analysis, McConnell et al. (2007)) observed a doubling of mineral dust concentration in a firn core from the Antarctic Peninsula over the 20th century. Since

it is not possible to exclude an increase in mineral dust concentrations due to contamination in CFA measurements in low density firn this observation can neither be confirmed nor rejected.

The dust particles, that arrive on the Antarctic continent have typically a diameter significantly smaller than 5 μm (e.g. Delmonte et al., 2004b) after long-range transport in the upper troposphere (Krinner et al., 2010). This enables particles to be transported over large distances to the Antarctic plateau. The atmospheric pressure system with a high over central Antarctica and a subpolar low pressure trough causes a subsidence over the Antarctic continent (King and Turner, 1997) that also favors the sinking of dust particles (Delmonte et al., 2004a). Together with the near-ground katabatic winds at the slopes of the Antarctic plateau, this presents a possible transport path for dust particles from the inland to the coast and from high to low altitudes. Strong katabatic winds transport dry air masses and aerosols. The katabatic winds develop due to the height differences between Antarctic plateau and coastal regions and the corresponding temperature difference. Since the colder air masses at the plateau are denser than the air masses in the coastal regions, the cold air masses are advected to the coast. The wind velocities thereby depend on the slope of the terrain (Parish and Bromwich, 2007) and the strength of the cyclones in the coastal regions. At Neumayer Station the prevailing wind direction is from the east. However, a second maximum for lower wind speeds occurs from the south due to the katabatic winds (Figure 4, König-Langlo et al. (1998)). These katabatic winds approaching from the Antarctic plateau are not a source for moisture. Thus, two main wind regimes prevail in the ECA: Dry katabatic winds possibly bringing dust particles and cyclonic systems carrying moisture Schlosser et al. (2008)) and sea salt aerosol, and katabatic winds carrying mineral dust particles. However, due to the lower windspeeds of katabatic winds they can only occur during

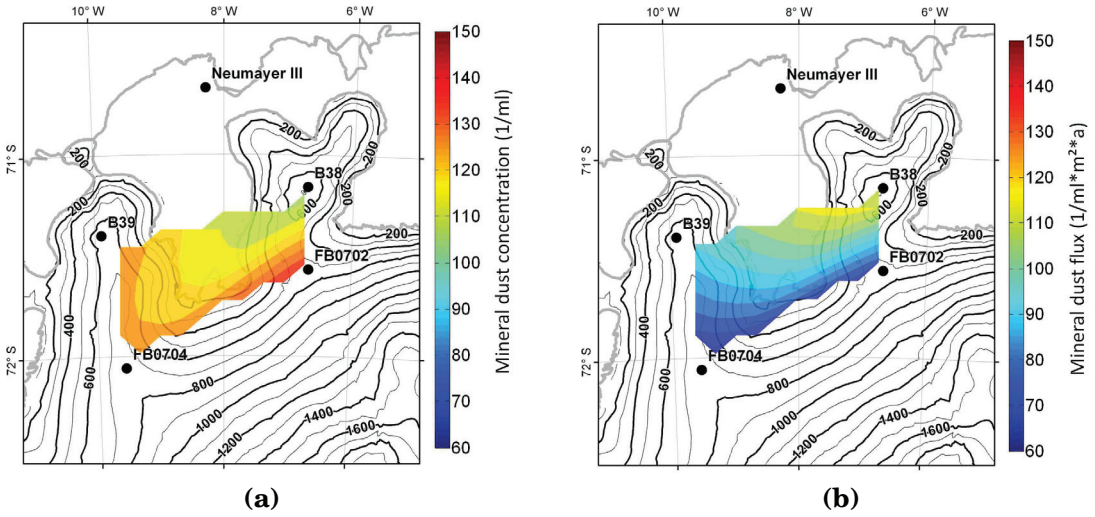

Figure 43: *Mineral dust gradients for 43a mean concentrations (in 1/ml) and 43b mean fluxes (in 1/ml*m^2*a). The contours are calculated using linear interpolation between the core locations. Background map courtesy of C. Wesche.*

low cyclonic activity.

To further estimate the influence of katabatic wind and thereby dry air masses approaching from the Antarctic plateau average mineral dust fluxes are compared to average mineral dust concentrations. To calculate the gradients of the average, values from table 3 are linearly interpolated and then plotted with contours and a map of the ECA in the background to visualize the connection to the topography (figure 43). Since the fluxes are a product of mean concentrations and accumulation rates (section 3.2) the fluxes give an estimate if the specific ice core constituents is more likely wet or dry deposited.

The mineral dust concentration is on average higher closer to the plateau. Especially on Halvfarryggen, a gradient from low concentrations at positions B38 to higher concentrations at position FB0702 is obvious. Fluxes decrease from coast to plateau and thus have an inverse behavior than mineral dust concentrations. Accordingly, mineral dust particles are both wet and dry deposited and the loading of them changes between the core locations within the ECA. In contrast to sea salt, the gradients do not follow the cyclonic pathway, indicating that cyclones only play a minor role for the mineral dust transport

to this region. The seasonal maximum in the mineral dust concentration is not as distinct as for sea salt. The broad maximum in spring is in the same season with the maximum in meridional wind speed at Neumayer Station from the north, which occurs in September (König-Langlo et al., 1998). The secondary maximum of meridional windspeed at Neumayer station occurs in March/April, but is not associated with a secondary maximum in dust concentration in the ECA. This indicates that the local wind field possibly influences the dust input into ECA, however is not the dominating process.

It is also possible that the Kottasmountains in the Heimefrontfjella located about 400 km south of Neumayer Station provide an input from local sources of mineral dust particles to the ECA. Due to the overall low dust concentrations the dust size as an additional evidence for a local source could not be evaluated. Thus this hypothesis can neither be confirmed nor excluded.

As dust is generally dry deposited (Fischer et al., 2007b, e.g.) and B38 is the site with the highest snow accumulation rate, an alternative explanation for the spatial gradient of the dust concentration could be the different snow accumulation rates. The AWS on Halfvarryggen shows a positive net snow accumulation rate on average every 2-3 days. Thus dry deposition at this site is likely to be negligible. However, even with a dominant wet deposition, a huge snow accumulation could dilute the dust concentration, if the air layer above is not replenished with dust. To investigate this possibility two scenarios will be discussed: First, the dust concentration in the snow reflects the dust concentration in the air above. Thus, the spatial gradient is also present in the air and might be explained by a transport of the dust from south through katabatic flow as explained above. Second, the dust concentration in the snow is modulated through dilution of snow without dust supply. A look at the seasonality will explore the latter:

For particulate mineral dust no data from the air chemistry observatory at

Neumayer Station exist that can be directly compared, but tracers for mineral dust such as the monthly concentration of Lanthanum are highest in summer (Weller et al., 2008). However, the maximum at the ECA drill sites occurs earlier during the year between August and December. A modulation of the dust concentration during deposition could account for this mismatch. The minimum of the snow accumulation rate at the AWS occurs in winter (Figure 35), the maximum in spring at a similar time as the seasonal cycle of dust concentration in B38 increases. If the high accumulation in spring diluted the dust concentration in the snow, the maximum in the air would be even more pronounced and this process would not shift the dust concentration maximum to the summer months to explain the mismatch with the aerosol record from Neumayer. Another explanation for the different seasonality in B38 and at Neumayer could be the influence of different air masses with a dust input to Neumayer in summer and to the ECA in late winter/spring. This could support a transport path of dust to the ECA from the South. As snow deposition seems to have no significant influence on seasonal scale (3.3) a strong influence on a regional scale seems unlikely. Thus the conclusion is that the spatial variability is also present in the air concentrations at the four drill sites (the first scenario). Additionally, the mean dust concentration is comparable between B39 and FB0704 despite a difference in snow accumulation rate by a factor of 1.5. A significant influence by the snow accumulation would result in a stronger dust concentration gradient between B39 and FB0704, as is visible in the fluxes (43b). On the other hand the relatively higher dust concentration in B39 compared to B38 could be explained by the Halfvarryggen, that weakens cyclonic winds approaching from the west and thus allows more katabatic wind flow to reach Sörasen. Since dry katabatic winds originate from the plateau do not bring precipitation, accumulation must be related to another process, likely cyclonic activity. In conclusion mineral dust transport

is likely related to the subsidence over and the katabatic outflow of air masses from the interior of the Antarctic ice sheet. However, wet deposition is likely related to cyclonic activity.

3.5 Influence of cyclonic wind and topography on the sea salt concentrations

The sea salt components Ca^{2+} and Na^{+} have two gradients in the local distribution between the cores: One with decreasing concentrations from coast to inland (north to south), and one with decreasing concentrations from east to west (Halvfarryggen to Sörasen, figure 44). The seasonal cycle has a maximum in Antarctic winter. Especially at B38 the seasonal cycle is very similar to the seasonal cycle observed at Neumayer Station.

The north-south gradient in the sea salt concentrations is most likely caused by the increasing distance to the source region. The source of sea salt particles deposited in the ECA can be either sea ice or the open ocean (Hall and Wolff, 1998; Wolff et al., 2003). This can explain the concentration gradient between the northern and southern cores (figure 44a), even if the distance between the core locations is relatively small.

The sea salt gradients observed in this study match the findings from Bertler et al. (2005), who found decreasing sea salt concentrations from coast to inland at multiple coastal sites in Antarctica which was explained by the change in elevation. Mahalinganathan et al. (2012) found that sea salt concentrations in Princess Elisabeth Land (especially for the coastal part) mainly depend on the slope of the surface rather than on the altitude itself. In this study changes in altitude are not as pronounced and not systematically related to sea salt concentrations, however, sea salt decreases along the pathway of cyclonic systems entering the area from the northeast (König-Langlo

et al., 1998).

The sea salt input is also related to the topographic distribution of snow accumulation, which is generally higher on the wind prevailing site of a ridge (Schlosser et al., 2008) due to relief precipitation. This influence of the topography can also be observed in the ECA by the gradient decreasing from east to west. As also known from accumulation studies (Drews et al., 2013), the Halvfarryggen acts as a the barrier forcing higher snow accumulation on its eastern side. Less precipitation and with it sea salt particles are left to precipitate on Sörasen. This is a possible reason for sea salt concentrations being lower on Sörasen than on Halvfarryggen. Since the gradients are also present in the fluxes (figure 44b), a gradient in the mean concentrations due to dilution can be neglected.

Sea salt particles are also used as a proxy for storminess in the source region. Korhonen et al. (2010) found an increase from 1980 to 2000 in modeled sea salt concentrations above the ocean that was linked to higher wind speeds over the Southern Ocean. Even though the strength of the source should be represented in the sea salt concentrations in the firn cores, this increase is not observed in the ECA. Thus, source strength is probably not the dominating factor for the sea salt input to the ECA.

Accumulation rates that are closely connected to the sea salt deposition, as visible in the similarity of the gradients of the sea salt flux and sea salt concentrations (figure 44b). Thus, sea salt particles are most likely wet deposited in the ECA as it was also investigated by Wagenbach et al. (1998a). Because of the dominating wet deposition, the possible impact of unevenly accumulation should be regarded. The seasonality of snow accumulation from an automatic weather station close to the drill site B38 shows a clear summer maximum in snow accumulation. Consequently, it is possible that the seasonality of snow deposition changes within the ECA also influence the seasonality of sea salt

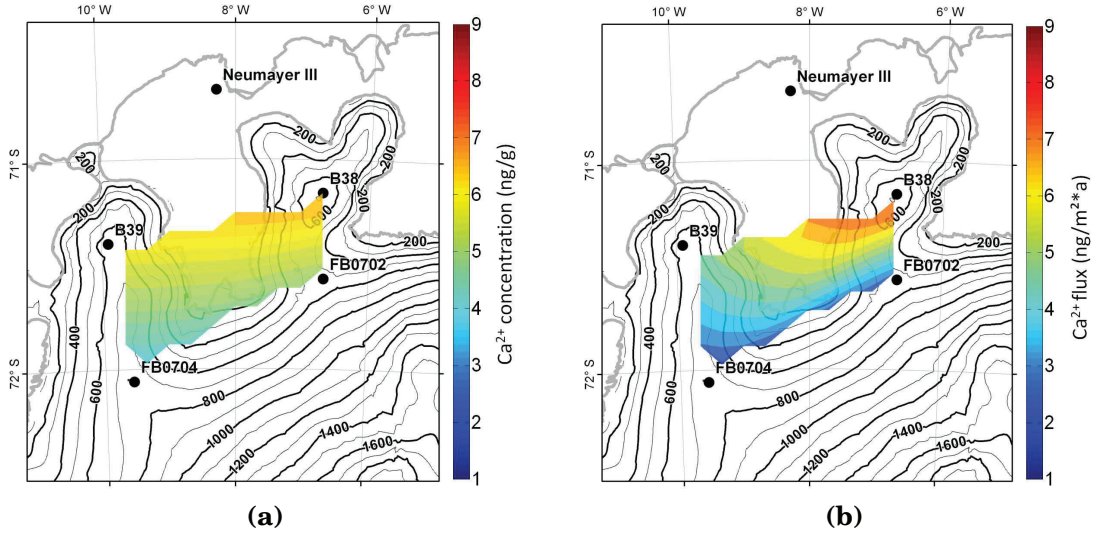

Figure 44: *Calcium gradients for 44a mean concentrations (in ng/g) and 44b mean fluxes (in ng/m²*a). The contours are calculated using linear interpolation between the core locations. Background map courtesy of C. Wesche.*

concentrations. If for example the accumulation would be more evenly distributed at Sörasen this would result in a sharper maximum for the sea salt concentrations than at Halvfarryggen. This means that a broader maximum in concentration can not directly be linked to a broader maximum in aerosol concentration. Thus deposition of sea salt particles throughout the year at one core site compared to another one can also be an implication of different accumulation regimes. As the sea salt records are all very similar in their time series and seasonality changes in the accumulation regime are probably negligible within the ECA.

The lower correlation between Neumayer Station and seasonality of FB0704 might be linked to the furthest distance from the coast regarding the cyclonic tracks, by a change in the wind regime or a change in the seasonal and regional accumulation distribution. This shows that complex processes are involved in the sea salt input because topography has an influence on wind and snow deposition while both influence the topography as well.

In conclusion, local features as distance to the coast and topography and their influence on precipitation brought by cyclonic systems seem to be important

factors influencing the sea salt deposition in the ECA. The similarity between Neumayer Station and seasonality of B38 might be linked to the closest distance from the coast regarding the cyclonic tracks and the fact that both locations are not shadowed by topography upstream of the atmospheric flow, thus receiving a similar sea salt input than Neumayer Station.

3.6 Relationship of sulphate and sea ice extend

Sulphate measurements show a gradient with decreasing concentrations from coast to inland and a clear seasonal cycle that has its maximum in the Antarctic summer. $Nss - SO_4^{2-}$ and MSA in ice cores from Antarctica are mostly originated from biological activity in the sea ice (e.g. Curran et al., 2003). From the meridional gradient (figure 45) and the seasonality (figure 41) it is hypothesized that sulphate concentrations are mainly influenced by the source strength rather than transport or deposition patterns. Compared to $nss - SO_4^{2-}$ concentrations, MSA is only derived from biological activity in the ocean and is not influenced by sea salt fractionation. Since MSA and $nss - SO_4^{2-}$ have the same seasonal cycle and the time series are also much alike, here only MSA will be discussed.

The annual cycle of MSA is linked to the biological activity in the southern ocean and depends on the presence of sunlight (e.g. Abram et al., 2013). Sea ice has its maximum in summer and its minimum in winter. In summer, when sea ice extend is lower, MSA concentrations are highest. This is not only due to the presence of sunlight, but also to the release of micro nutrients (e.g. iron) into the ocean, that enhances the growth of algae and hence the production of DMS, the precursor of sulfuric components (e.g. Minikin et al., 1998).

However, no clear relationship between sea ice and biogenic sulfur emissions could be derived from correlations between sea ice extend and MSA concentrations as tested by Weller et al. (2011). MSA concentrations are decreas-

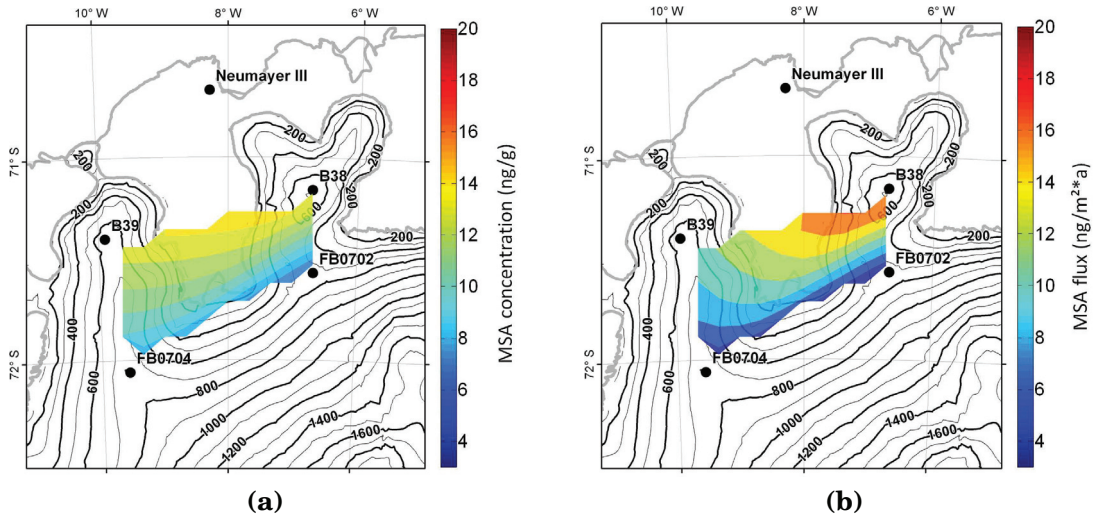

Figure 45: *MSA gradients for 45a mean concentrations (in ng/g) and 45b mean fluxes (in ng/m²*a). The contours are calculated using linear interpolation between the core locations. Background map courtesy of C. Wesche.*

ing from coastal sites to the sites closer to the Antarctic plateau and the fluxes indicate wet deposition of sulphate aerosol, since the gradients of the fluxes do not change substantially compared to MSA concentrations (figure 45a).

The MSA time series shows no trend during the last 60 years. The absence of a trend from present until 1962 was also found by Weller et al. (2011) for the past 25 years in aerosol records from Neumayer Station.

The prevailing meteorological conditions also have a large influence on the concentration of MSA in coastal Antarctica (Abram et al., 2013). Weller et al. (2011) compared surface aerosol concentration of MSA at Neumayer Station and Dumond D'Urville. While Neumayer Station is mostly influenced by cyclones and only weakly by katabatic winds, Dumond D'Urville is a location with strong katabatic winds. The comparison of MSA concentrations from Neumayer Station and Dumond D'Urville shows the dependency of the meteorological conditions because on average, MSA concentrations are higher at Neumayer Station than at Dumond D'Urville, indicating the influence of cyclonic winds transporting MSA from the ocean to Neumayer Station. Similar conditions most probably occur in the ECA. This is also indicated by the gra-

dients in the MSA fluxes (figure 45b) that have a similar gradient as the MSA concentrations. Thus, MSA is wet deposited and closely connected to snow accumulation from cyclones.

When comparing sulphate and sea salt concentrations in ice cores, it is noticeable that on the one hand the two species do have the same source region in the Southern Ocean. On the other hand, they have an inverse seasonality. This difference can be explained by the fact that for biological activity in the ocean the micro nutrients need sunlight which is only present during Antarctic summer, while sea salt particles are present in the brine in the sea ice throughout the year. If the sea salt variability is explained by the presence of cyclonic winds in the deposition area, as described in section 3.5, the difference should be explained by the fact that for sea salt the deposition is more important than source strength and that for sulfur the source strength is most important. From the fluxes it was obtained that sulfur is wet deposited meaning that it also should be connected to cyclonic activity. This influence is visible in the zonal gradient found for the coastal cores. However, the gradient is much stronger for sea salt components than for the MSA. Accordingly, variability in the MSA concentrations is mostly explained by the source strength.

3.7 Independence of nitrate concentrations on source strength and topography

Nitrate is uniformly distributed over the study area and have a distinct seasonal cycle with a maximum in early summer. From this, it is obtained that the location and distance to the coast has no effect on the nitrate input. Considering the lack of a similar spatial gradient (figure 46a) as in sea salt a local marine NO_3^- source appears to be unlikely and nitrate does not seem to be transported by low pressure systems as in the case of sea salt. This is

coherent with the results from (Kreutz and Mayewski, 1999). The seasonal maximum in early summer was used to improve the dating, thus the exact timing of this seasonal peak will not be further discussed. Nitrate is subject to post depositional losses due to outgassing and photolytic reactions in the upper 1.2 - 1.4 m of snow (Weller et al., 2004). Therefore, for the records presented here, the influence of post depositional losses is not exceeding the uppermost year and therefore should be much smaller than in the plateau region, where a quantitative NO_3^-- loss of more than 95% of the initial concentration was observed over many years (Röthlisberger et al., 2000b). Also, the accumulation rate is very high in the ECA, another factor that makes the assumption of post-depositional loss negligible.

While a significant input of nitrate from the stratosphere is found for late winter/spring, the strong spring maximum in nitrate cannot be directly related to stratospheric influx (Wagenbach et al., 1998b). For the coastal station Dumont d'Urville (DDU) the maximum in November/December was explained by snowpack emissions originating from inland Antarctica (Savarino et al., 2007). Also modeling studies have assigned the wide spread spring maximum in NO_3^-- concentrations in Antarctica to post depositional processes (Lee et al., 2014). As the ECA itself is not a major source for re-emitted NO_3^-- due to its high accumulation rates, nitrate aerosol is probably re-emitted in spring over low accumulation areas on the plateau (Röthlisberger et al., 2002a; Neubauer and Heumann, 1988; Bertler et al., 2005) is brought into the ECA by katabatic transport. Wagenbach et al. (1998b) showed that this re-emission can significantly elevate the atmospheric nitrate concentration in the boundary layer. Around the EPICA Dronning Maud Land deep drilling site south east of the ECA nitrate concentrations are much higher than in the ECA (Weller et al., 2004, e.g.). Thus, this area provides a potential source for re-emitted Nitrate. How much the elevated levels inland contribute to the spring snow

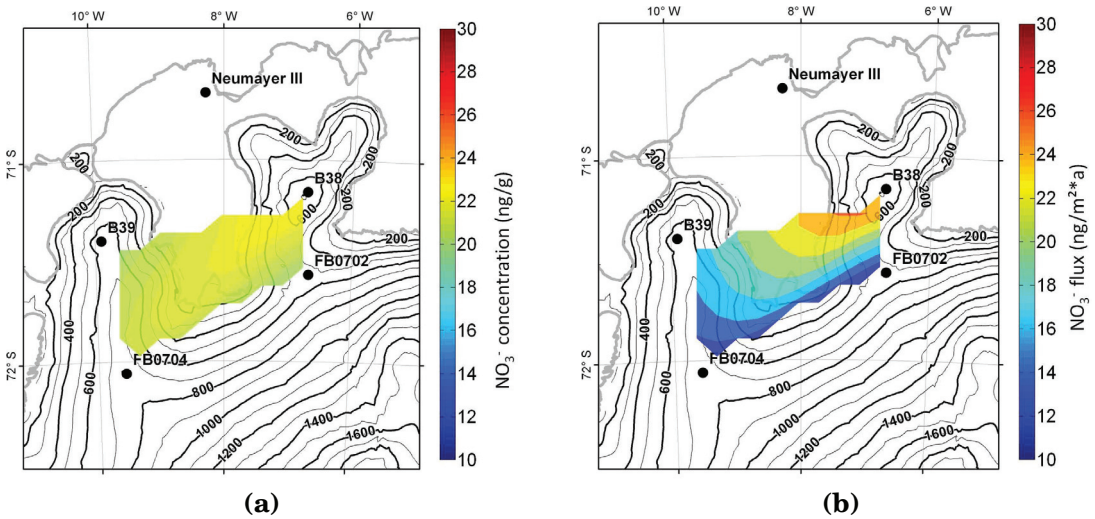

Figure 46: *nitrate gradients for 46a mean concentrations (in ng/g) and 46b mean fluxes (in ng/m²*a). The contours are calculated using linear interpolation between the core locations. Background map courtesy of C. Wesche.*

maximum in nitrate in the ECA cannot be quantified at this stage, but it may provide an explanation for the illusive spring maximum.

4 Variability of ice core constituents related to southern hemisphere atmospheric circulation

In the last section the local influences on ice core constituents was investigated. Now the analysis will be taken one step further by using the four firn cores as an ensemble to study atmospheric circulation pattern on a southern hemisphere scale. Three aerosol constituents were chosen to be used in this analysis: Stable isotopes in water (δ^{18}), Ca^{2+} as a sea salt proxy, and mineral dust. The aerosol concentrations quantified by IC are not used because of their lower temporal resolution compared to concentrations quantified by CFA. The time series are used in monthly resolution.

δ^{18}O, sea salt and mineral dust are proxies that have differences in their source, transport and deposition pattern and for this provide the opportunity to study if these differences are reflected in different atmospheric circulation pattern and if source, transport or emission dominate the concentration profiles.

A well known relationship of atmospheric circulation pattern and ice core constituents can be used in atmospheric circulation models. If for example it is well known that high mineral dust concentrations are connected to dry surfaces in Patagonia, this can be used as a boundary condition for atmospheric circulation models. However, first a method is needed to compare ice core data with atmospheric circulation models. The method described here gives a first approach to solve this issue.

This part of the study is the result of a collaboration. The preparation of the time series as well as the production of the figures are the work of Norel Rimbu (Alfred-Wegener-Institute). The Interpretation of the results and the discussion are the work of the author of this thesis.

4.1 Preparation of the CFA time series

The empirical orthogonal function (EOF) analysis (von Storch and Zwiers, 2002) is used to provide an objective characterization of the dominant modes of the proxy record variability. By this it is possible to understand how the aerosol constituents determined in the firn cores can be used to understand the large scale atmospheric processes that caused the aerosol input in the first place. EOF analysis has been used in the past for statistical analysis of multiple archives, for example sediment cores and ice cores, with the focus on the long-term climate variability (e.g. Jones and Mann, 2004). For example, Rimbu and Lohmann (2010) have shown the relationship of atmospheric circulation patterns and deuterium records in an ice core in central Greenland. Weller et al. (2011) used data from Neumayer Station to establish a relationship to climate variability parameters (e.g. southern oscillation index), but in most cases only very weak correlations were found. The very low correlations may be due to the fact that they used the whole record to calculate the correlations. However, changes in climate do not affect the whole record, but only extreme events in aerosol concentrations.

For this, here an approach is used that only takes the events from a time series with monthly resolution into account to establish a more robust relationship of concentrations of ice core constituents and atmospheric circulation patterns. The first step of the analysis is to calculate the annual cycle of the time series by averaging the concentration values from each month of the year over the entire considered period for all time series (section 3.3). Then the anomalies are calculated relative to these long-term means. The calculated annual cycle is repeated for every year and then subtracted from the original time series to calculate the anomalies. The anomalies are normalized with the corresponding standard deviations (Figure 47). For example, to calculate January anomalies, the value obtained by calculating the annual cycle is sub-

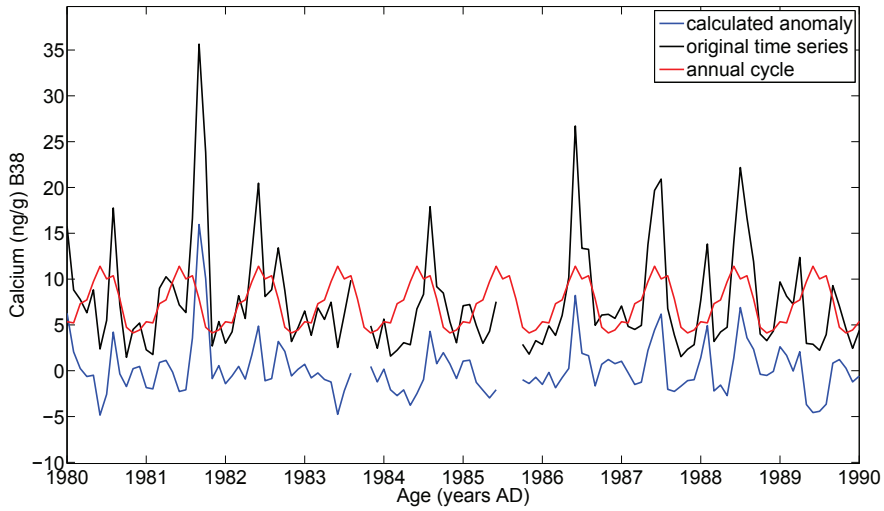

Figure 47: *Example how anomalies are calculated: First, the annual cycle (red line) is calculated from the original time series (black line). The anomalies (blue line) are calculated by subtracting the annual cycle from the original time series.*

tracted from all January values and then normalized by dividing it with the corresponding standard deviation. Anomalies have the same physical dimension and the same physical background as the original data, but normalized data is needed to make the data sets from the four firn cores comparable. Using EOFs give the advantage of capturing the maximum variance of the four ice cores. Also, local gradients are automatically eliminated and thus cannot manipulate the results any more. Regarding that the interest is now taken to the southern hemispheric area, this is an advantage. The definition of Wilks (1995) is used to calculate the EOF. For this, the term EOF refers to the eigenvector of the variance-covariance matrix of the original time series. The first eigenvector points into the direction of the highest common variability of the original time series and for this also describes the correlation of the original time series by the percentage of variability that it represents. The elements of the eigenvector are the EOF loadings, and the principal components (PC) are the new time series that account for the maximum amount of the common variability. These new time series are used for comparison with atmospheric

circulation patterns.

Atmospheric circulation patterns are represented by the NCEP-NCAR reanalysis data base (section 1.4). Only months with high values (PC >0.75) of the time coefficients are taken for the analysis to obtain the dominant patterns of ice core proxy variability. The threshold of 0.75 to define high values of normalized PCs is arbitrary chosen as a compromise between the strength of the proxy anomalies as captured by the corresponding EOF and the number of atmospheric circulation anomaly maps used in the composite analysis. Data covering the time interval from 1962-2006 is used, which is the common period covered by all four records. However, due to a relatively large number of data gaps the analysis of sea salt and mineral dust time series is restricted to the years 1962-1998 and 1962-1990, respectively.

To ensure that events from the original time series are present in the PCs and in the end in the reanalysis data a test was performed (table 10): First, a threshold is defined for the original time series (approximately set to mean + 2*σ, table 3- 8, σ is the standard deviation) and the months that exceed this threshold are written in an array. The same is done for the PCs with the limit of 0.75, which is also used for the actual analysis. Then, these arrays are compared in both directions to find the common dates. In the last step, the percentage of the events from the original time series that coincide with the events from the PC time series are determined. This is calculated for the opposite case as well. As clearly visible in table 10 the data sets match in more than 75 % of the monthly data and thus the PCs clearly represent the original time series.

4.2 Results of EOF Analysis

In this section the EOFs calculated from the original time series will be presented.

The first EOF of the δ^{18}O anomaly time series describes 40% of the vari-

Table 10: *Percentage of months in the original time series that are also present in the PCs (original = PC) and months in the PCs that are also present in the original time series (PC = original). The Limit is set to 0.75 for the EOF time series and to approximately mean + 2*σ, with σ as the standard deviation.*

		B38	B39	FB0702	FB0704	Limit
Calcium	original = PC	89.2	83.8	92.6	81.8	10 (ng/g)
	PC = original	81.3	78.7	90.7	89.3	0.75
Mineral Dust	original = PC	81.0	80.6	93.7	95.3	200 (1/ml)
	PC = original	85.7	76.8	89.3	92.9	0.75
δ^{18}O	original = PC	89.7	88.4	84.6	83.3	-18 (per mil SMOW)
	PC = original	90.2	86.1	98.4	98.4	0.75

ance. The EOF1 loadings are 0.54 (B38), 0.59 (B39), 0.44 (FB0702) and 0.38 (FB0704). The corresponding principal component (PC1, figure 48) shows pronounced interannual to decadal variations and the seasonality observed in the original time series is also reflected in the principal components. For δ^{18}O diffusion within the ice could result in a decreasing annual variability with increasing depth, which would result in a higher impact of monthly mean values from the upper meters in the firn column. Fernandoy et al. (2010) compared δ^{18}O and deuterium records and concluded that post-depositional processes such as diffusion are either acting too slow to influence the δ^{18}O on this high accumulation site and that preferentially the deuterium record is influenced more. Additionally, for the present study the trend of the annual variability was calculated and no trend larger than 0.06 per mil SMOW was found between 2006 and 1962. The seasonal cycle (Figure 8) shows that δ^{18}O is more enriched in summer than in winter. High values (>0.75) of PC1 occur during the whole year: 20% summer (December, January, February), 26% autumn (March, April, May), 28% winter (June, July, August), and 26% spring (September, October, November).

The first EOF of Ca^{2+} anomaly time series describes 37% of the variance and captures an in-phase variability of the four original Ca^{2+} time series. The

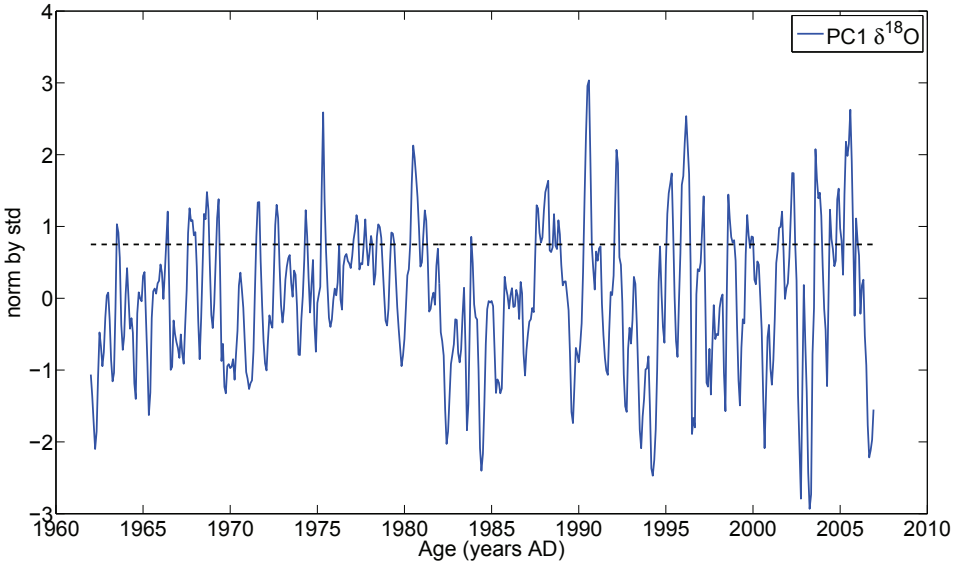

Figure 48: *Principal component time series of the first EOF of $\delta^{18}O$ records (PC1). The horizontal dashed line represents 0.75 standard deviation.*

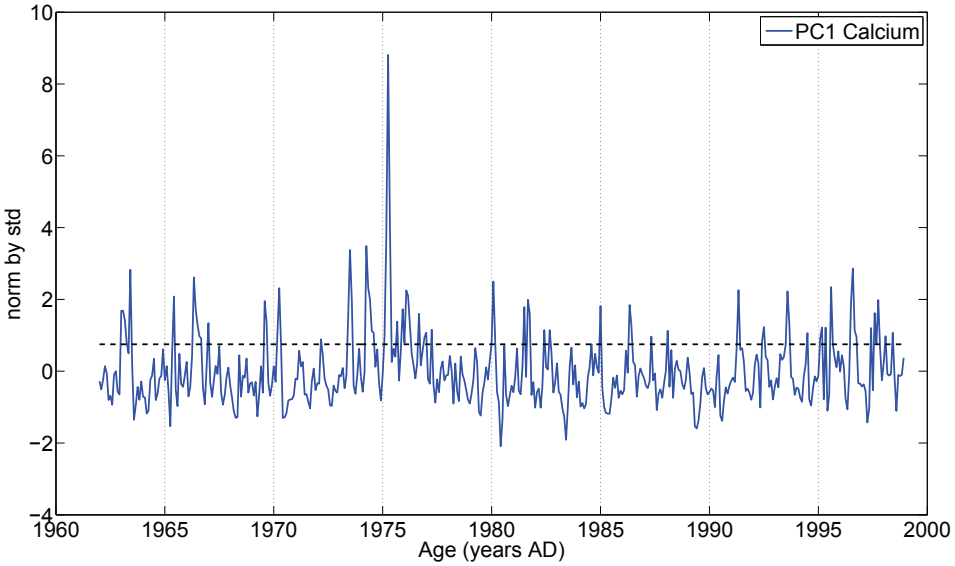

Figure 49: *Same as in Figure 48 but for Ca^{2+} time series.*

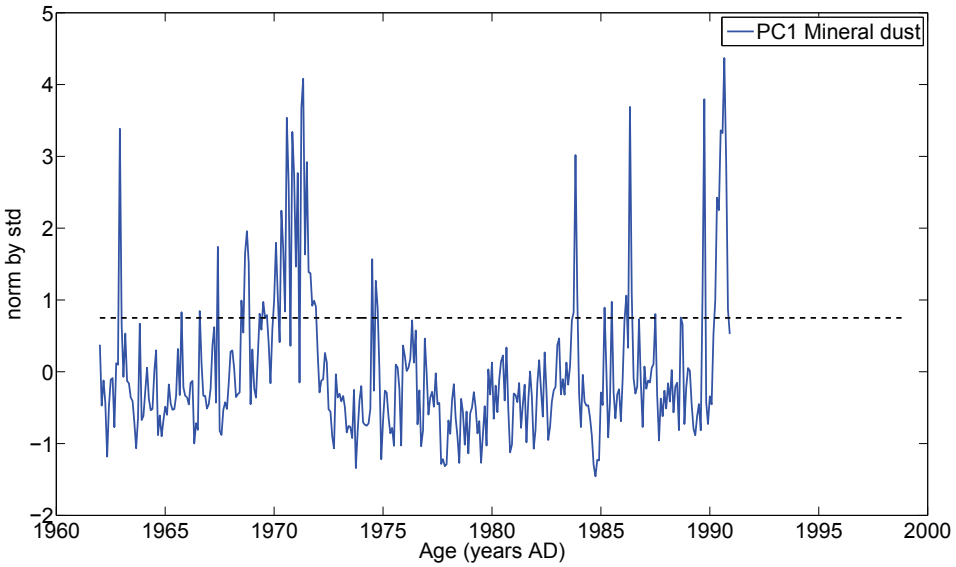

Figure 50: *Same as in Figure 48 but for mineral dust time series.*

EOF1 loadings are 0.63 (B38), 0.67 (B39), 0.11 (FB0702) and 0.36 (FB0704). The corresponding PC1 time series is represented in Figure 49. One large peak in the PC1 time series occurs in ∼1976. Throughout the year (figure 38) higher Ca^{2+}-concentrations are found in winter. Values of PC1 >0.75 are mostly occurring in winter (20% summer, 28% autumn, 35% winter, and 17% spring), which is not significantly more than in the other seasons.

The EOF1 of mineral dust anomaly time series, which describes 36% of the variance, captures also an in-phase variability at the four mineral dust records. The EOF1 loadings are 0.70 (B38), 0.68 (B39), 0.13 (FB0702) and 0.10 (FB0704). The variability of B38 and B39 records dominates EOF1. The corresponding PC1 (Fig. 53a) shows pronounced decadal variations. It indicates a persistent mineral dust event in the region in 1970s which can be identified also in the original mineral dust time series (Fig. 16). Some sharper peaks are visible in 1960, 1984, 1986 and 1990. Mineral dust concentrations are highest in spring (figure 37). 14% of data with high modes of variability are from the summer, 18% from autumn, 32% from winter and 36% from spring. This means that

the mineral dust input is not only lower in summer and autumn, but also less variable during that time of the year.

4.3 Variability of the atmosphere

To investigate the variability of the atmosphere that is connected to high variability in the ice core constituents, NCEP-NCAR reanalysis data is used and atmospheric circulation patterns are calculated using the method described in section 4.1. The NCEP-NCAR reanalysis data can be influenced by differences between satellite and pre-satellite era that are due to the available number of observations (section 1.4). Thus, the robustness of the pattern is tested by comparing two time periods, one from the pre-satellite and one from the satellite era. Results are presented first, then the robustness of the patterns will be tested.

Figure 51 shows the composite of the reanalysis data for the high PCs of δ^{18}O between 1962 and 2006. The most distinct features are a low pressure anomaly over the Weddell Sea and north of that a high pressure anomaly in the east of South America. Strongest wind anomalies occur between these anomalies, enhancing the transport of water vapor to the ECA.

A low pressure anomaly is present in the composite map associated with high PCs of calcium (figure 52) over the Southern Ocean, and two high pressure anomalies, one south of Africa and one over the Antarctic Peninsula. In general, the composite map represents a typical atmospheric wave structure.

In the composite map associated with high PCs of mineral dust (figure 53), a high pressure anomaly is present over the Atlantic Ocean, northwest of the core position and a low pressure anomaly is located over South America. The wave structure is here also apparent, but not as clear as for calcium.

According to the limitations of the NCEP-NCAR reanalysis data set obtained by Kistler et al. (2001) and Marshall (2002), it is predominantly the difference

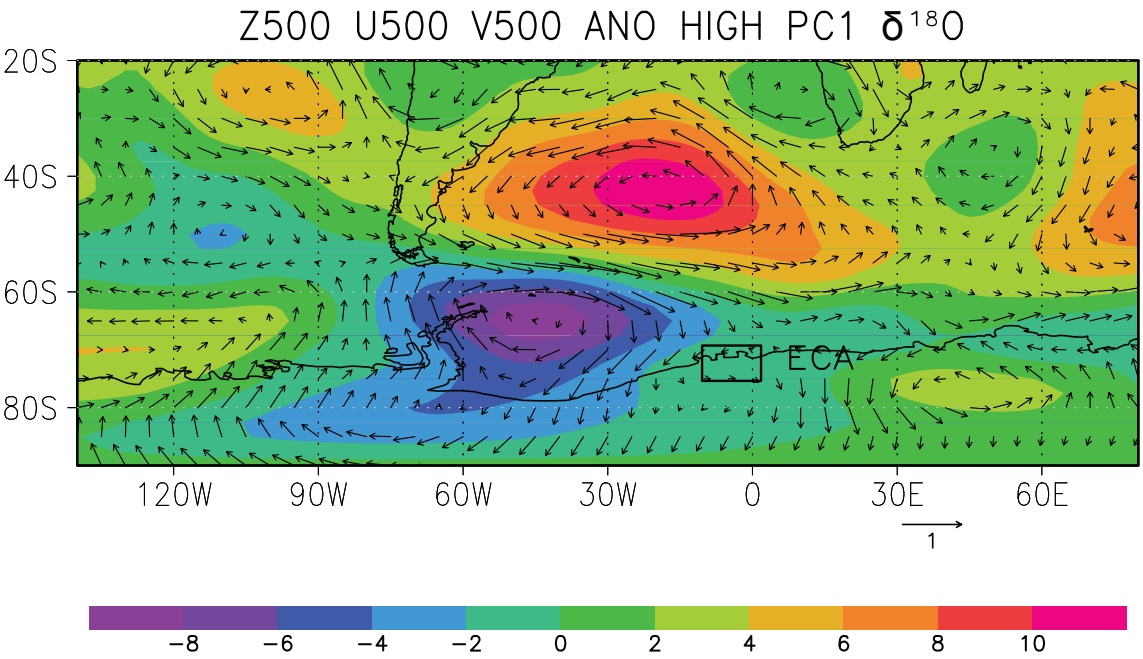

Figure 51: *Composite map of the 500 hPa geopotential height anomalies (color) and wind (arrows) corresponding to the high values (higher than 0.75) of PC1 represented in figure 48. Units m and m/s (figure courtesy of N. Rimbu).*

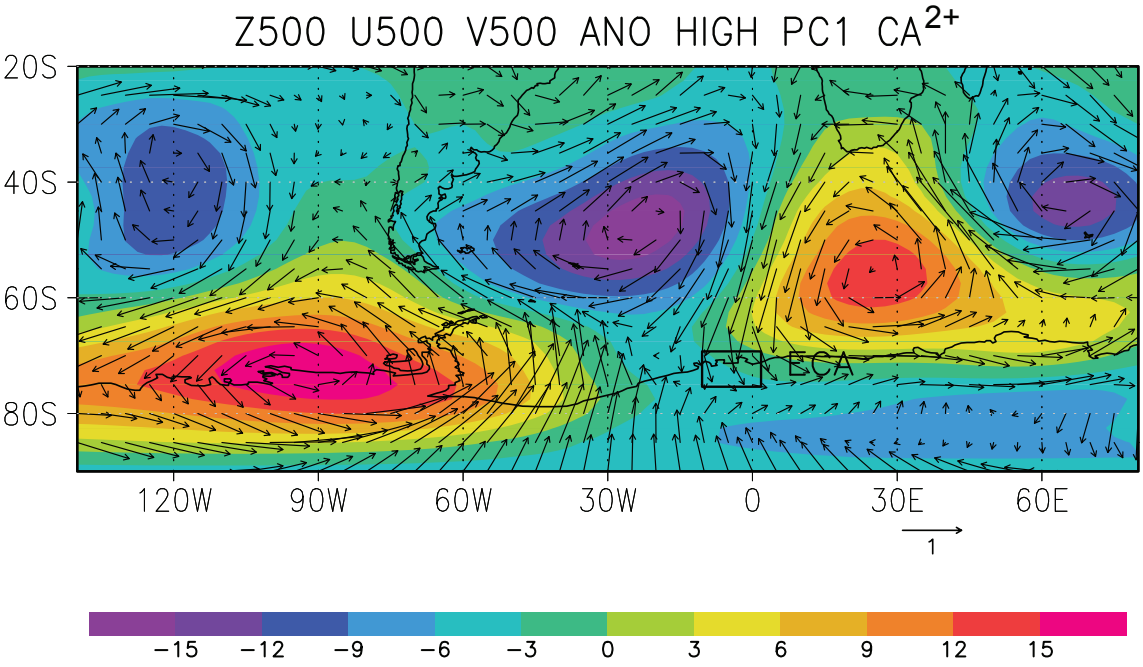

Figure 52: *As in figure 51 but for Ca^{2+} time series and the corresponding PC time series is figure 49 (figure courtesy of N. Rimbu).*

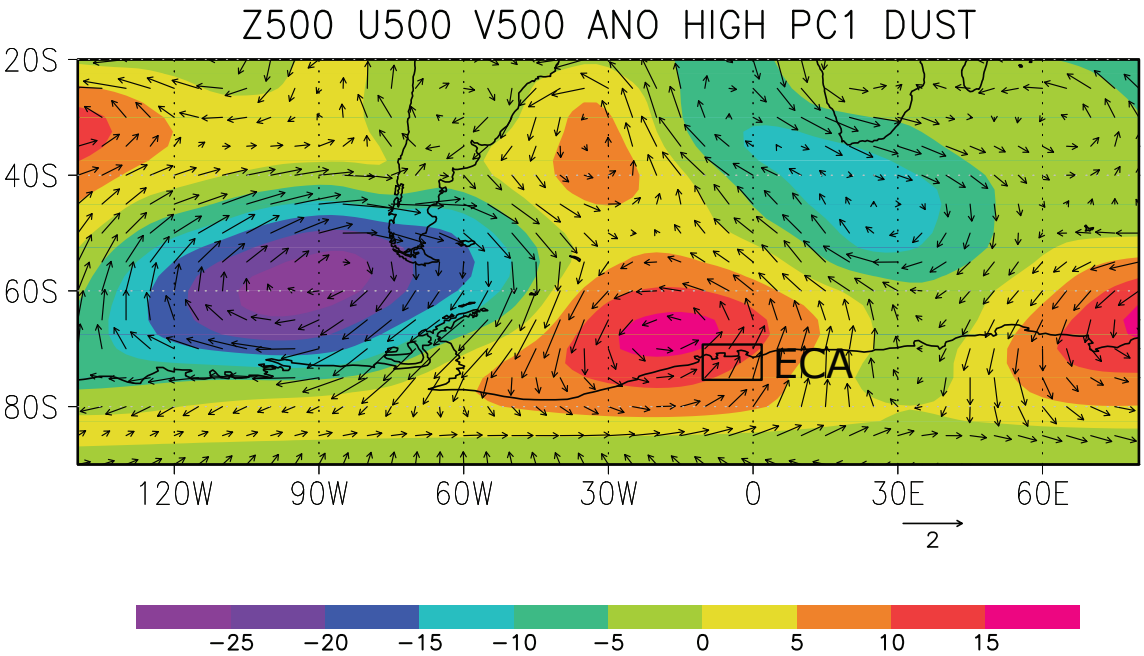

Figure 53: *As in figure 51 but for mineral dust time series and the corresponding PC time series is figure 50 (figure courtesy of N. Rimbu).*

between the satellite and pre-satellite era, where the density of observations changes so that a time slice that covers both time periods can be dominated by the satellite era that infers the robustness of the NCEP-NCAR reanalysis data. To test this limitation the data set is split into two time slices and the results are shown in figure 54 to 56. Note that the resolution is 2.5 x 2.5 degree, and for this small scale features such as the local circulations like katabatic winds that may alter the deposition patterns can not be captured. However, the physical interpretation of the patterns, which is the important part of the analysis is straightforward and a visual interpretation should be adequate to test the robustness of the patterns.

The low pressure anomaly over the Weddell Sea, which is one of the important features in the δ^{18}O associated pattern (figures 51 and 54) is present in both time periods, even thought shifted to the north in the earlier time period. The high pressure anomaly is also present in both time periods and for this, also the higher wind velocities that develop between the high and the low pressure

anomaly are present in both time periods, even though they might be stronger in the later period as can be supposed from the depth of the systems (figure 54b). Considering that 43% of the months with high PCs are within the earlier time period from 1962 to 1984 while 57% are within the later time period, the patterns from the two time periods are a decent reflection of the pattern over the whole time period from 1962 to 2006.

For the atmospheric circulation pattern of high PCs from the Ca^{2+} record, the most important feature within the composite map is the low pressure anomaly over the Southern Ocean (figure 52). This low pressure anomaly is mostly present in the later time period (1982-1999, figure 55b), where also the wave pattern is visible. The later time period represents only 39% of the data while 61% of the months with high PCs of calcium are within the earlier time period (1962-1981, figure 55a). However, there is still an indication of a low pressure anomaly developing above the Southern Ocean within the earlier time period. The patterns for the high mineral dust PC time series are similar in both time periods. 64% of the months with high PCs occur during the first time period (1962-1976, figure 56a) and 36% during the second time period (1977-1990, figure 56b). Both of the time periods show the low pressure anomaly over southern South America and the high pressure anomaly over the ECA is present in both time periods as well. Hence, the influence of the higher density of data during the satellite era does not affect the mineral dust atmospheric circulation pattern.

In conclusion, the comparison of two time periods shows that in principle the analysis is robust. The visual comparison of the two time periods shows that the physical interpretation of the circulation patterns does not change substantially. Some features are not similar for all patterns from one species, especially the comparison of the two time periods considering Ca^{2+}. However, these differences are likely evoked by noisy data rather than differences in

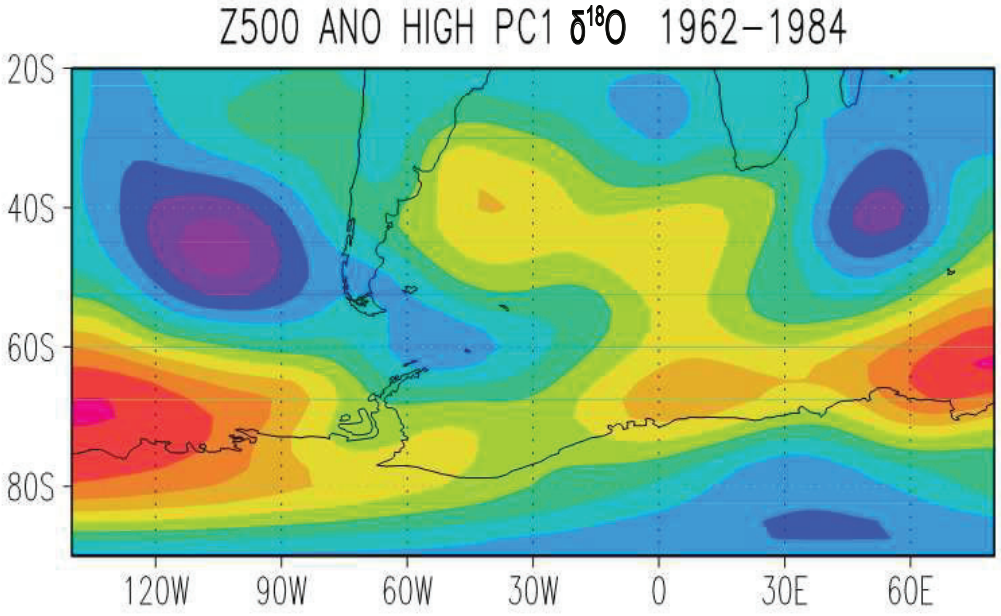

(a)

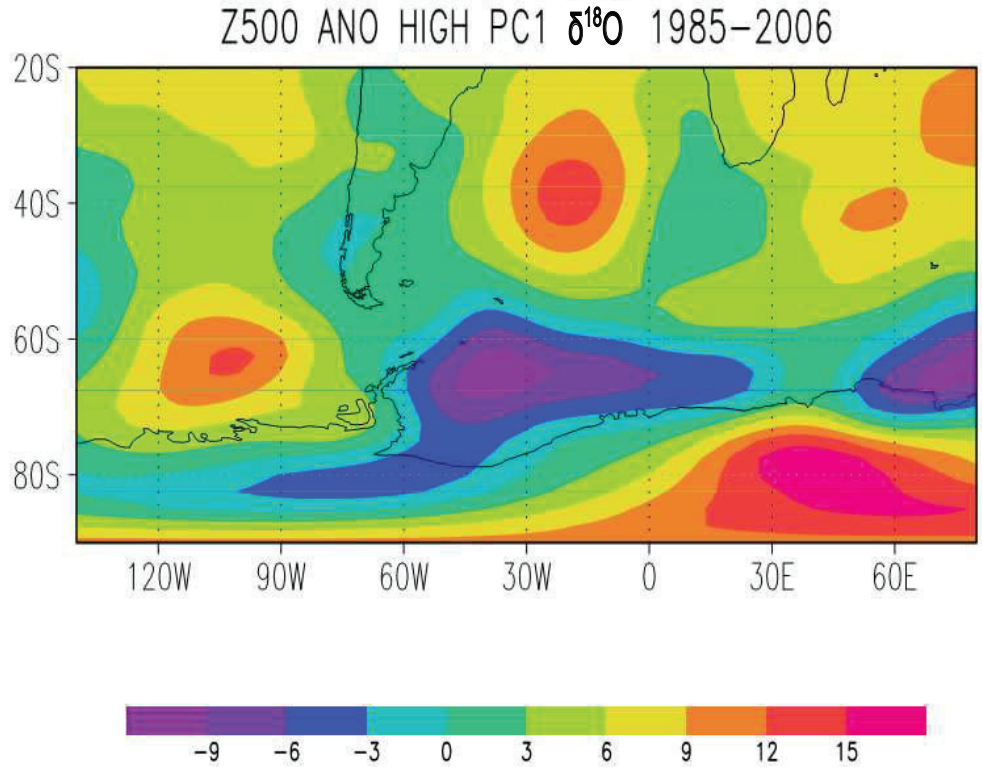

(b)

Figure 54: *Atmospheric circulation pattern associated to high values of the PCs of $\delta^{18}O$ between 54a 1962 and 1984 and 54b 1985 and 2006 (figure courtesy of N. Rimbu).*

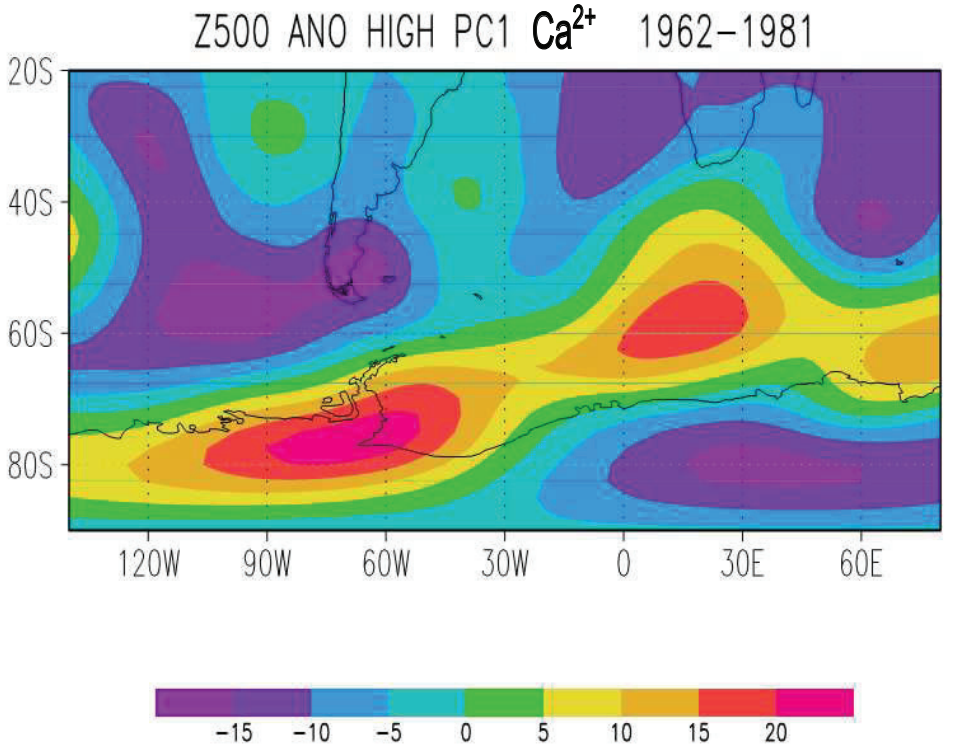

(a)

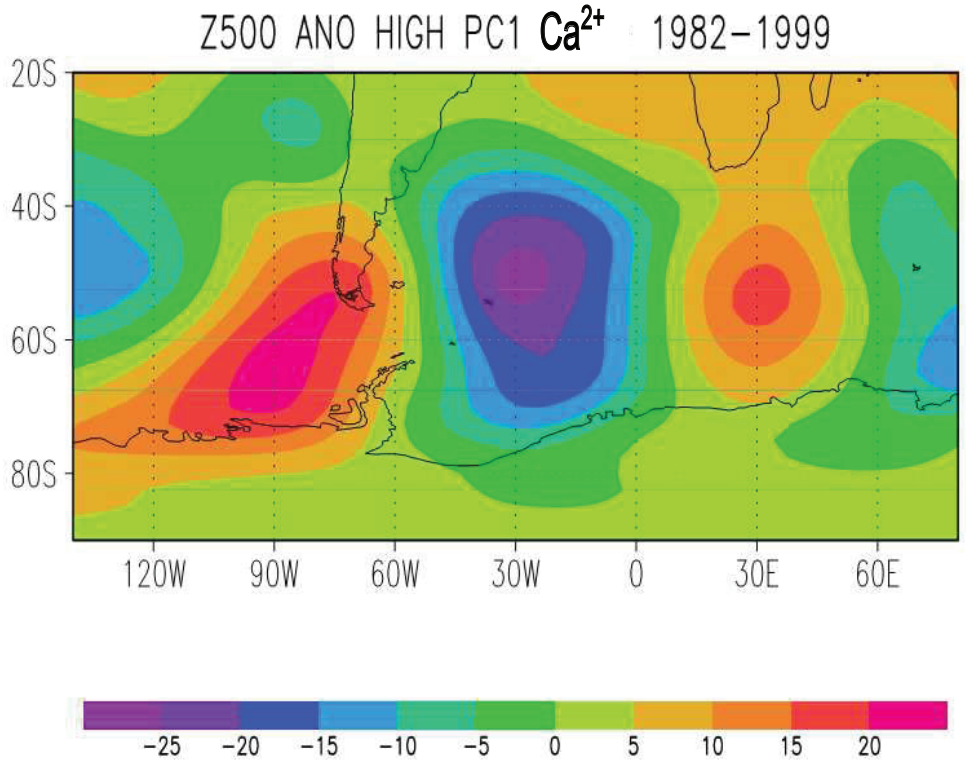

(b)

Figure 55: *Atmospheric circulation pattern associated to high values of the PCs of Ca^{2+} between 55a 1962 and 1981 and 55b 1982 and 1999 (figure courtesy of N. Rimbu).*

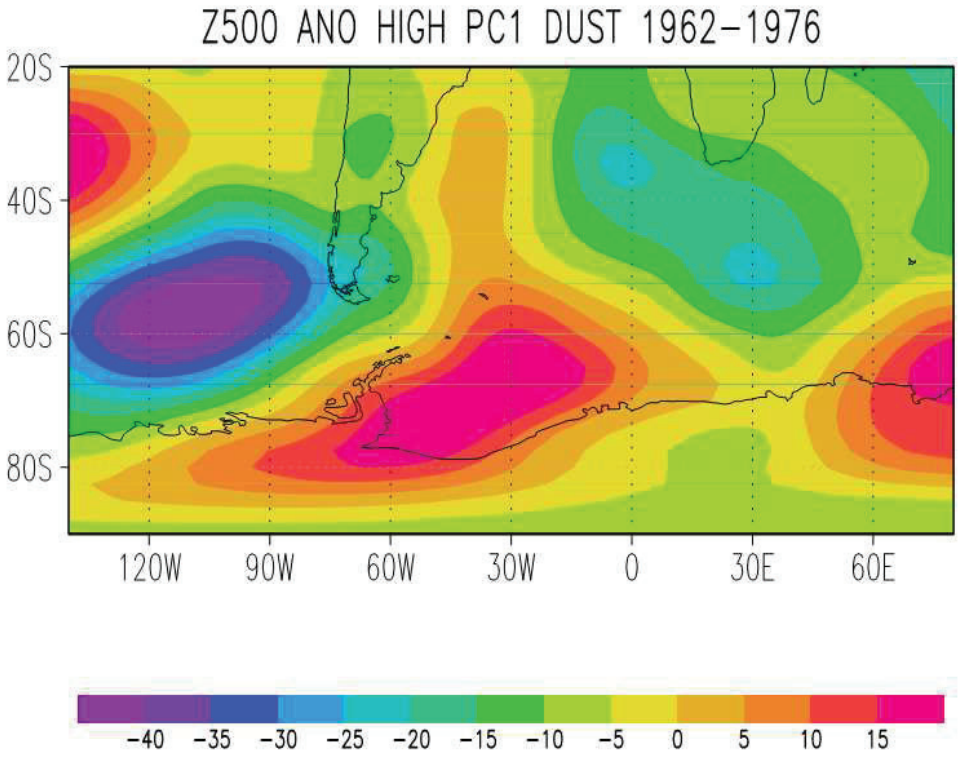

(a)

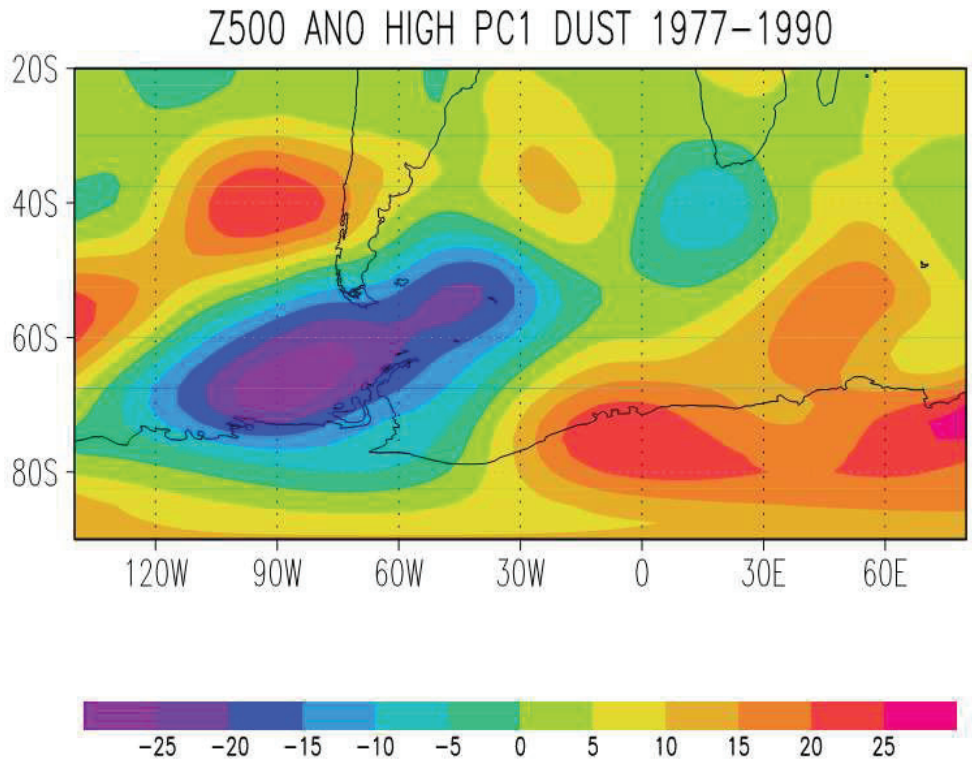

(b)

Figure 56: *Atmospheric circulation pattern associated to high values of the PCs of mineral dust between 56a 1962 and 1976 and 56b 1977 and 1990 (figure courtesy of N. Rimbu).*

the two time periods.

4.4 Oxygen isotopes

The composite map associated to high anomalies of δ^{18}O (Fig. 51) shows a pronounced dipolar structure. The low pressure anomaly over Weddell Sea lifts air masses while the high pressure anomaly subsides air masses over the South Atlantic. Air masses from the low pressure anomaly are moving from South America to the ECA. δ^{18}O is comprised in water vapor, that is either enriched or depleted in the heavier isotope ^{18}O, depending on the temperature (section 1.3.5, Dansgaard, 1964). Even though not exclusively, the Weddell Sea has been determined as one of the most frequent source regions for precipitation arriving at Neumayer Station (Schlosser et al., 2004). For this it is hypothesized that the Weddell Sea region is also important as a moisture source for the ECA.

Simmonds (2003) showed that between 1958 and 1997 cyclonic system density is higher in the Weddell Sea than for other regions west of the ECA. Since low pressure systems around Antarctica usually move eastward along the coast (King and Turner, 1997), this is an indication for the Weddell Sea as one source region. The Weddell Sea is however a region with sea ice throughout the year (e.g. Abram et al., 2013) leaving the open question of how the water vapor is entrained from the ocean into the atmosphere. Strong surface winds as can be produced by the low pressure anomaly in figure 51 over the Weddell Sea can cause polynyas in the sea ice. Accordingly, the exchange of latent and sensible heat can be enhanced, together with the enrichment of δ^{18}O in the water vapor in the atmosphere (e.g. Maqueda et al., 2004; Noone and Simmonds, 2004).

A second source region of water vapor that can be obtained from the composite map in figure 51 is the eastern coast of southern South America. From here,

air masses are transported by the strong winds that are induced between the high and the low pressure anomaly. These air masses are warmer and can therefore be responsible for the warmer events in the PCs of δ^{18}O as well. According to Kottmeier and Fay (1998), this region is, based on backward trajectories of up to five days, not a frequent source region (<10%) and for this the source in the Weddell Sea is probably stronger and transport of warmer air masses from the north is less likely.
In conclusion the Weddell Sea is most likely a source region for precipitation in the ECA.

4.5 Sea salt

All 4 cores show a maximum in sea-salt concentrations in winter. This is in agreement with other observations in Antarctica (e.g. Souney et al., 2002), and was explained by increased cyclonic activity, intensified meridional transport and generally intensified atmospheric circulation (e.g. Wagenbach et al., 1998a; Legrand and Mayewski, 1997). The values for sea salt in the first EOF (PC1>0.75) occur slightly more often in winter, but are in general evenly distributed over the year. Thus, all seasons contribute similarly to the composite map.The composite map associated with high positive values of sea salt PC1 (figure 52) shows a wave structure with alternating high and low pressure anomalies located at between 40° and 70° S.
Just north of ECA the main atmospheric flow anomaly is in southerly direction increasing the southerly transport of air and sea salt particles. The uptake of sea salt particles is associated with high wind speeds (e.g. de Leeuw et al., 2011), making this atmospheric circulation pattern favorable for the entrainment of sea salt aerosol into the atmosphere. Using a correlation analysis of a sea salt record with the sea level pressure and sea ice extend Souney et al. (2002) found that sea salt concentrations are highest in winter

and significantly correlated with the sea level pressure and the cyclonic activity in the Southern Ocean. No connection to the sea-ice extend was found. A similar result was found by Abram et al. (2013) suggesting that the wind speed variability, leading to higher sea salt emissions and faster transport, is more important for the interannual variations in sea salt than the interannual change in sea ice extent. The sea salt maximum in winter also indicates a wind speed dependency because at this time of the year low pressure systems have a higher frequency and intensity (Uotila et al., 2011). Cyclones usually move eastward and southward, indicating a direct transport from the ocean to the area of investigation. Note that this wind speed dependency will lead to high sea salt export no matter whether the source is sea ice or the open ocean.

Sea ice is a possible source for sea salt aerosols, at least in coastal areas (Abram et al., 2013). In the present study, the center of the low pressure anomaly is located in an area with sea ice neither in winter nor in summer. However, during the passage of the main air masses to the ECA, air is transferred over the sea ice regions and therefore sea ice cannot be excluded as a source for sea salt. Weller et al. (2011) found a negative correlation between sea salt concentrations and local atmospheric pressure anomalies at Neumayer Station. Indeed, easterlies are the most likely winds at Neumayer Station, indicating a cyclonic influence of local winds (section 3.5). Beside of emission, transport and deposition are relevant factors that can maintain the sea salt concentration in coastal Antarctica, and especially deposition is highly influenced by local features as wind and topography (section 3.5). However, these local features cannot be resolved with the NCEP-NCAR reanalysis data and the EOF most likely filtered these features out of the analysis.

For sea salt concentrations the conclusion is therefore that emission is the most important factor visible in the pattern determined by high values in the

PC of sea salt. However, transport is also important due to the atmospheric life time of sea salt particles, that is less than a week (e.g. Abram et al., 2013) and the possible sea ice source that is passed during the passage from the source region in the Southern Ocean to the deposition area.

4.6 Mineral dust

When the positive phase of dominant pattern of mineral dust variability is strong a pronounced negative pressure anomalies occurs southwest of South America (figure 53), in coherence with upward motion and convergence at the surface. Previous model studies by Albani et al. (2012), Li et al. (2010) and chemical studies (Wegner et al., 2012) showed that Patagonia is the main source for mineral dust in Dronning Maud Land. For this, high variability from the mineral dust concentrations is most likely determined by the source. McConnell et al. (2007) used NCEP-NCAR reanalysis data to correlate temperature, relative humidity and sea level pressure in monthly resolution to mineral dust concentrations. They found a high correlation of mineral dust concentrations with temperature and relative humidity in the source region, especially in spring. The observed pronounced maximum in $\sim$1970 is also present in the PC time series of mineral dust, but however not the decadal variability they found. This could be due to the shorter time interval of the data set used in the present study. In a model study, Mahowald et al. (2010) showed that the observed variability in dust concentrations could only be simulated successfully if the source strength was increased or decreased. A change in the transport strength could not modify the mineral dust variability. Model simulations by Albani et al. (2012) show that the dust load in the atmosphere originating from South America and the dust mobilization is highest in spring (September-November). This is coherent with the dust maximum observed in the original time series and the positive phase of the

dominant mode of mineral dust variability, which is most frequent in spring. The dominant mode of mineral dust variability of the four records considered in this study is mainly driven by the variability of mineral dust concentrations in the cores B38 and B39. This can be due to the location of the cores. B38 and B39 are both located close to the coast, each of them on a dome position. The other cores FB0702 and FB0704 on the other hand are located closer to the Antarctic plateau, and each of them on a slope. This slope can enhance the katabatic flow (Parish and Bromwich, 2007) resulting in an enhanced transport of mineral dust particles from the Antarctic plateau. Fernandoy et al. (2010) showed that the cores located closer to the plateau are probably influenced by snow advection from higher altitudes or by erosion. High katabatic winds may lead to heavy wind redistribution of individual snow fall events that may destroy the link between atmospheric dust aerosol concentration and the concentrations in the surface snow from the drill site. Therefore, mineral dust transport by cyclones in the deposition area is only of minor importance and on the southern hemispheric scale the source strength is the main driver of the dominant pattern of mineral dust variability in the four records considered in this study.

In conclusion, Patagonia acts as the source region for mineral dust aerosol deposited in the ECA and is also the key factor for events of high mineral dust concentrations. The conditions in the source dominate input of dust to ECA. Conditions in the sinking area are less important. This is supported by previous studies. The spatial variability of deposition is more controlled by the local topography.

5 Conclusion

In the present study, ice core constituents from four ice cores from the coastal Dronning Maud Land region have been quantified using a continuous flow analysis system. The time series of sea salt, mineral dust, sulphate and nitrate have then been used to investigate the spatial and seasonal differences from the four core sites.

The seasonal variability as well as the spatial distribution of the sea salt input is related to cyclonic activity that influences transport and deposition, whereas changing sea ice extent seems to play a minor role in line with other observations and modeling (Abram et al., 2013; Levine et al., 2014). For dust concentration in ECA the strength of the source seems to be the dominating factor. Katabatic wind flow is likely part of the transport pathways of dust and nitrate. Sulphate concentrations are closely connected to sea ice extend and the solar cycle.

In the second part of this study the analysis of the time series was taken from a local to a southern hemispheric scale. This was done using empirical orthogonal functions (EOF) and NCEP-NCAR reanalysis data. Only time series of δ^{18}O, sea salt and mineral dust in monthly resolution were used. Events were determined by a threshold of 0.75 sigma in the principal components of the EOFs. Only months that exceeded the threshold were used to calculate a composite of the anomaly pattern of the geopotential height and wind from the NCEP-NCAR reanalysis data set.

The analysis revealed that the selection of events is an appropriate tool to investigate changes in the atmospheric circulation pattern. Especially the source strength and source region of the particular ice core constituent could be obtained by this method. Nevertheless this methodology should be tested in further detail in the future by using more ice core records that ideally cover

a longer time interval. The planned drilling of an ice core at the Halvfarryggen will help to improve the data sets further and to obtain significant results with the introduced analysis.

In conclusion, the present study represents a new approach to use trace elements measured in ice cores as a proxy to reconstruct climate conditions and the source region of these proxies. Additionally, the local influences on the concentrations of ice core constituents could be reconstructed, and this known influence can be used to estimate the wind regime at the surface of the Antarctic ice sheet.

References

Abram, N. J., Curran, M. A., Mulvaney, R., and Vance, T.: The preservation of methanesulphonic acid in frozen ice-core samples, Journal of Glaciology, 54, 680–684, 2008.

Abram, N. J., Wolff, E. W., and Curran, M. A.: A review of sea ice proxy information from polar ice cores, Quaternary Science Reviews, in press, –, doi:10.1016/j.quascirev.2013.01.011, URL http://www.sciencedirect.com/science/article/pii/S0277379113000206, 2013.

Albani, S., Mahowald, N. M., Delmonte, B., Maggi, V., and Winckler, G.: Comparing modeled and observed changes in mineral dust transport and deposition to Antarctica between the Last Glacial Maximum and current climates, Climate Dynamics, 38, 1731–1755, 2012.

Bertler, N., Mayewski, P., Aristarain, A., Barrett, P., Becagli, S., Bernardo, R., Bo, S., Xiao, C., Curran, M., Qin, D., Dixon, D., Ferron, F., Fischer, H., Frey, M., Frezzotti, M., Fundel, F., Genthon, C., Gragnani, R., Hamilton, G., Handley, M., Hong, S., Isaksson, E., Kang, J., Ren, J., Kamiyama, K., Kanamori, S., Karkas, E., Karlof, L., Kaspari, S., Kreutz, K., Kurbatov, A., Meyerson, E., Ming, Y., Zhang, M., Motoyama, H., Mulvaney, R., Oerter, H., Osterberg, E., Proposito, M., Pyne, A., Ruth, U., Simoes, J., Smith, B., Sneed, S., Teinila, K., Traufetter, F., Udisti, R., Virkkula, A., Watanabe, O., Williamson, B., Winther, J.-G., Li, Y., Wolff, E., Li, Z., and Zielinski, A.: Snow chemistry across Antarctica, Annals of Glaciology, 41, 167–179, doi:doi:10.3189/172756405781813320, URL http://www.ingentaconnect.com/content/igsoc/agl/2005/00000041/00000001/art00024, 2005.

Bigler, M., Röthlisberger, R., Lambert, F., Stocker, T. F., and Wagenbach, D.:

Aerosol deposited in East Antarctica over the last glacial cycle: Detailed apportionment of continental and sea-salt contributions, Journal of G, 111, D08 205, doi:10.1029/2005JD006469, 2006.

Bigler, M., Svensson, A., Kettner, E., Vallelonga, P., Nielsen, M. E., and Steffensen, J. P.: Optimization of High-Resolution Continuous Flow Analysis for Transient Climate Signals in Ice Cores, Environmental Science & Technology, 45, 4483–4489, doi:10.1021/es200118j, URL `http://pubs.acs.org/doi/abs/10.1021/es200118j`, 2011.

Bory, A., Wolff, E., Mulvaney, R., Jagoutz, E., Wegner, A., Ruth, U., and Elderfield, H.: Multiple sources supply eolian mineral dust to the Atlantic sector of coastal Antarctica: Evidence from recent snow layers at the top of Berkner Island ice sheet, Earth Planet Sc. Lett, 291, 138–148, doi:10.1016/j.epsl.2010.01.006, 2010.

Castellano, E., Becagli, S., Hansson, M., Hutterli, M., Petit, J. R., Rampino, M. R., Severi, M., Steffensen, J. P., Traversi, R., and Udisti, R.: Holocene volcanic history as recorded in the sulfate stratigraphy of the European Project for Ice Coring in Antarctica Dome C (EDC96) ice core, Journal of Geophysical Research: Atmospheres, 110, n/a–n/a, doi:10.1029/2004JD005259, URL `http://dx.doi.org/10.1029/2004JD005259`, 2005.

Curran, M., van Ommen, T., Morgan, V., Phillips, K., and Palmer, A.: Ice core evidence for Antarctic sea ice decline since the 1950s, Science, 302, 1203–1206, 2003.

Dansgaard, W.: Stable isotopes in precipitation, Tellus, 16, 436–468, 1964.

Dansgaard, W., Clausen, H., Gundestrup, N., Johnsen, S., and Rygner, C.: Dating and climatic interpretation of two deep Greenland ice cores, Green-

land Ice Core: Geophysics, Geochemistry, and the Environment, edited by: Langway, CCJ, American Geophysical Union, Washington DC, 1985.

de Leeuw, G., Andreas, E. L., Anguelova, M. D., Fairall, C. W., Lewis, E. R., O'Dowd, C., Schulz, M., and Schwartz, S. E.: Production flux of sea spray aerosol, Reviews of Geophysics, 49, n/a–n/a, doi:10.1029/2010RG000349, URL `http://dx.doi.org/10.1029/2010RG000349`, 2011.

Delmonte, B., B., P., J.R., A., K.K., Basile-Doelsch, I., Maggi, V., and Lipenkov, V.: Dust size evidence for opposite regional atmospheric circulation changes over east Antarctica during the last climatic transition, Clim. Dynam., 23, 427âĂŞ438, 2004a.

Delmonte, B., Basile-Doelsch, I., Petit, J., Maggi, V., Revel-Rolland, M., Michard, A., Jagoutz, E., and Grousset, F.: Comparing the Epica and Vostok dust records during the last 220,000 years: stratigraphical correlation and provenance in glacial periods, Earth Science Reviews, 66, 63–87, 2004b.

Drews, R., Martin, K., Steinhage, D., and Eisen, O.: Characterizing the glaciological conditions at Halvfarryggen ice dome, Dronning Maud Land, Antarctica, Journal of Glaciology, 59, 9–20, 2013.

EPICA-Community-Members: Eight glacial cycles from an Antarctic ice core, Nature, 429, 623–628, 2004.

Fernandoy, F., Meyer, H., Oerter, H., Wilhelms, F., Graf, W., and Schwander, J.: Temporal and spatial variation of stable-isotope ratios and accumulation rates in the hinterland of Neumayer station, East Antarctica, Journal of Glaciology, 56, 673–687, 2010.

Fischer, H., Fundel, F., Ruth, U., Twarloh, B., Wegner, A., Udisti, R., Becagli, S., Castellano, E., Morganti, A., Severi, M., et al.: Reconstruction of millennial changes in dust emission, transport and regional sea ice coverage

using the deep EPICA ice cores from the Atlantic and Indian Ocean sector of Antarctica, Earth and Planetary Science Letters, 260, 340–354, 2007a.

Fischer, H., Siggaard-Andersen, M., Ruth, U., Rothlisberger, R., and Wolff, E.: Glacial/interglacial changes in mineral dust and sea-salt records in polar ice cores: Sources, transport, and deposition, Reviews of geophysics, 45, 2007b.

Goudie, A. S. and Middleton, N.: Desert dust in the global system, Springer, 2006.

Gupta, P., Noone, D., Galewsky, J., Sweeney, C., and Vaughn, B. H.: Demonstration of high-precision continuous measurements of water vapor isotopologues in laboratory and remote field deployments using wavelength-scanned cavity ring-down spectroscopy (WS-CRDS) technology, Rapid Communications in Mass Spectrometry, 23, 2534–2542, doi:10.1002/rcm.4100, URL http://dx.doi.org/10.1002/rcm.4100, 2009.

Hall, J. and Wolff, E.: Causes of seasonal and daily variations in aerosol sea-salt concentrations at a coastal Antarctic station, Atmospheric Environment, 32, 3669 – 3677, doi:10.1016/S1352-2310(98)00090-9, URL http://www.sciencedirect.com/science/article/pii/S1352231098000909, 1998.

Harrison, S., Kohfeld, K., Roelandt, C., and Claquin, T.: The role of dust in climate changes today, at the last glacial maximum and in the future, Earth Science Reviews, 54, 43–80, 2001.

Hezel, P., Alexander, B., Bitz, C., Steig, E., Holmes, C., Yang, X., and Sciare, J.: Modeled methanesulfonic acid (MSA) deposition in Antarctica and its relationship to sea ice, Journal of Geophysical Research: Atmospheres (1984–2012), 116, 2011.

Hobbs, P. V.: Introduction to atmospheric chemistry, Cambridge University Press, 2000.

Hoefs, J.: Stable isotope geochemistry, Springer, 2008.

Hsu, J.: Multiple comparisons: theory and methods, CRC Pressr, 1996.

Jacobi, H.-W. and Hilker, B.: A mechanism for the photochemical transformation of nitrate in snow, Journal of Photochemistry and Photobiology A: Chemistry, 185, 371–382, 2007.

Johnson, M. S., Meskhidze, N., Kiliyanpilakkil, V. P., and Gassó, S.: Understanding the transport of Patagonian dust and its influence on marine biological activity in the South Atlantic Ocean, Atmospheric Chemistry and Physics, 11, 2487–2502, doi:10.5194/acp-11-2487-2011, URL `http://www.atmos-chem-phys.net/11/2487/2011/`, 2011.

Jones, P. D. and Mann, M. E.: Climate over past millennia, Reviews of Geophysics, 42, RG2002, 2004.

Kaleschke, L., Richter, A., Burrows, J., Afe, O., Heygster, G., Notholt, J., Rankin, A., Roscoe, H., Hollwedel, J., Wagner, T., et al.: Frost flowers on sea ice as a source of sea salt and their influence on tropospheric halogen chemistry, Geophys. Res. Lett, 31, L16 114, 2004.

Kalnay, E., Kanamitsu, M., Kistler, R., Collins, W., Deaven, D., Gandin, L., Iredell, M., Saha, S., White, G., Woollen, J., Zhu, Y., Chelliah, M., Ebisuzaki, W., Higgins, W., Janowiak, J., Mo, K., Ropelewski, C., Wang, J., Leetmaa, A., Reynolds, R., Jenne, R., and Joseph, D.: The NCEP/NCAR 40-year reanalysis project, Bulletin of the American Meteorological Society, 77, 437–471, 1996.

Kaufmann, P., Federer, U., Hutterli, M., Bigler, M., Schüpbach, S., Ruth, U., Schmitt, J., and Stocker, T.: An improved continuous flow analysis system for high-resolution field measurements on ice cores, Environmental science & technology, 42, 8044–8050, 2008.

Kaufmann, P., Fundel, F., Fischer, H., Bigler, M., Ruth, U., Udisti, R., Hansson, M., De Angelis, M., Barbante, C., Wolff, E. W., et al.: Ammonium and non-sea salt sulfate in the EPICA ice cores as indicator of biological activity in the Southern Ocean, Quaternary Science Reviews, 29, 313–323, 2010.

King, J. C. and Turner, J.: Antarctic Meteorology and Climate, Cambridge University Press, 1997.

Kistler, R., Kalnay, E., Collins, W., Saha, S., White, G., Woollen, J., Chelliah, M., Ebisuzaki, W., Kanamitsu, M., Kousky, V., et al.: The NCEP-NCAR 50-year reanalysis: Monthly means CD-ROM and documentation, Bulletin-American Meteorological Society, 82, 247–268, 2001.

König-Langlo, G. and Loose, B.: The Meteorological Observatory at Neumayer Stations (GvN and NM-II) Antarctica, Polarforschung, 76, 25–38, URL `http://epic.awi.de/17763/`, 2007.

König-Langlo, G., King, J. C., and Pettre, P.: Climatology of the three coastal Antarctic stations Dumont d'Urville, Neumayer, and Halley, Journal of Geophysical Research, 103, 10 935–10 946, doi:10.1029/97JD00527, 1998.

Koopmann, J. D.: Calibration of a laser particle counter and mineral dust measurements in Antarctic snow pits, Master's thesis, Rheinisch-Westfälische Technische Hochschule Aachen Fakultät für Mathematik, Informatik und Naturwissenschaften, 2006.

Korhonen, H., Carslaw, K. S., Forster, P. M., Mikkonen, S., Gordon, N. D., and

Kokkola, H.: Aerosol climate feedback due to decadal increases in Southern Hemisphere wind speeds, Geophysical Research Letters, 37, 2010.

Kottmeier, C. and Fay, B.: Trajectories in the Antarctic lower troposphere, Journal of Geophysical Research-Atmospheres, 103, 1998.

Kreutz, K. J. and Mayewski, P. A.: Spatial variability of Antarctic surface snow glaciochemistry: implications for palaeoatmospheric circulation reconstructions, Antarctic Science, 11, 105–118, doi:10.1017/S0954102099000140, 1999.

Krinner, G., Petit, J.-R., and Delmonte, B.: Altitude of atmospheric tracer transport towards Antarctica inpresent and glacial climate, Quaternary Science Reviews, 29, 274 – 284, doi:10.1016/j.quascirev.2009.06.020, URL http://www.sciencedirect.com/science/article/pii/S0277379109002297, 2010.

Lee, H.-M., Henze, D. K., Alexander, B., and Murray, L. T.: Investigating the sensitivity of surface-level nitrate seasonality in Antarctica to primary sources using a global model, Atmos. Environ., 89, 757–767, 2014.

Legrand, M. and Mayewski, P.: Glaciochemistry of polar ice cores: a review, Reviews of Geophysics, 35, 1997.

Legrand, M. and Pasteur, E. C.: Methane sulfonic acid to non-sea-salt sulfate ratio in coastal Antarctic aerosol and surface snow, Journal of Geophysical Research: Atmospheres (1984–2012), 103, 10 991–11 006, 1998.

Levine, J., Yang, X., Jones, A., and Wolff, E.: Sea salt as an ice core proxy for past sea ice extent: A process-based model study, Journal of Geophysical Research: Atmospheres, 119, 5737–5756, 2014.

Li, F., Ginoux, P., and Ramaswamy, V.: Distribution, transport, and deposition of mineral dust in the Southern Ocean and Antarctica: Contribution of major sources, J. Geophys. Res, 113, 2008.

Li, F., Ginoux, P., and Ramaswamy, V.: Transport of Patagonian dust to Antarctica, Journal of Geophysical Research (Atmospheres), 115, D18217, doi:10.1029/2009JD012356, 2010.

Mahalinganathan, K., Thamban, M., Laluraj, C. M., and Redkar, B. L.: Relation between surface topography and sea-salt snow chemistry from Princess Elizabeth Land, East Antarctica, The Cryosphere, 6, 505–515, doi:10.5194/tc-6-505-2012, URL `http://www.the-cryosphere.net/6/505/2012/`, 2012.

Mahowald, N., Kloster, S., Engelstaedter, S., Moore, J. K., Mukhopadhyay, S., McConnell, J., Albani, S., Doney, S. C., Bhattacharya, A., Curran, M., et al.: Observed 20th century desert dust variability: impact on climate and biogeochemistry, Atmos. Chem. Phys, 10, 10–875, 2010.

Maqueda, M. M., Willmott, A., and Biggs, N.: Polynya dynamics: a review of observations and modeling, Reviews of Geophysics, 42, RG1004, 2004.

Marshall, G. J.: Trends in Antarctic geopotential height and temperature: A comparison between radiosonde and NCEP-NCAR reanalysis data, Journal of Climate, 15, 659–674, 2002.

Masson-Delmotte, V., Hou, S., Ekaykin, A., Jouzel, J., Aristarain, A., Bernardo, R., Bromwich, D., Cattani, O., Delmotte, M., Falourd, S., et al.: A Review of Antarctic Surface Snow Isotopic Composition: Observations, Atmospheric Circulation, and Isotopic Modeling*, Journal of Climate, 21, 3359–3387, 2008.

McConnell, J. R., Aristarain, A. J., Banta, J. R., Edwards, P. R., and Simões, J. C.: 20th-Century doubling in dust archived in an Antarctic Peninsula ice core parallels climate change and desertification in South America, Proceedings of the National Academy of Sciences, 104, 5743–5748, 2007.

Minikin, A., Legrand, M., Hall, J., Wagenbach, D., Kleefeld, C., Wolff, E., Pasteur, E. C., and Ducroz, F.: Sulfur-containing species (sulfate and methanesulfonate) in coastal Antarctic aerosol and precipitation, Journal of geophysical Research, 103, 10 975–10 990, doi:10.1029/98JD00249, 1998.

Neubauer, J. and Heumann, K. G.: Nitrate trace determinations in snow and firn core samples of ice shelves at the weddell sea, Antarctica, Atmospheric Environment (1967), 22, 537 – 545, doi:10.1016/0004-6981(88)90197-7, URL http://www.sciencedirect.com/science/article/pii/0004698188901977, 1988.

Noone, D. and Simmonds, I.: Sea ice control of water isotope transport to Antarctica and implications for ice core interpretation, Journal of Geophysical Research: Atmospheres, 109, doi:10.1029/2003JD004228, URL http://dx.doi.org/10.1029/2003JD004228, 2004.

Parish, T. and Bromwich, D.: Reexamination of the Near-Surface Airflow over the Antarctic Continent and Implications on Atmospheric Circulations at High Southern Latitudes, Monthly Weather Review, 135, 1961–1973, doi:10.1175/MWE3374.1, 2007.

Petit, J. R. and Delmonte, B.: A model for large glacial-interglacial climate-induced changes in dust and sea salt concentrations in deep ice cores (central Antarctica): palaeoclimatic implications and prospects for refining ice core chronologies, Tellus Series B Chemical and Physical Meteorology B, p. 30, 2009.

Prospero, J. M., Ginoux, P., Torres, O., Nicholson, S., and Gill, T.: Environmental characterization of global sources of atmospheric soil dust identified with the NIMBUS 7 Total Ozone Mapping Spectrometer (TOMS) absorbing aerosol product, Rev. of Geophys., 40, 1002, doi:10.1029/2000RG000095, 2002.

Reijmer, C., Van den Broeke, M., and Scheele, M.: Air Parcel Trajectories and Snowfall Related to Five Deep Drilling Locations in Antarctica Based on the ERA-15 Dataset, Journal of climate, 15, 1957–1968, 2002.

Renwick, J. A.: Trends in the Southern Hemisphere polar vortex in NCEP and ECMWF reanalyses, Geophysical research letters, 31, L07 209, 2004.

Reynolds, R. L., Yount, J. C., Reheis, M., Goldstein, H., Chavez, P., Fulton, R., Whitney, J., Fuller, C., and Forester, R. M.: Dust emission from wet and dry playas in the Mojave Desert, USA, Earth Surface Processes and Landforms, 32, 1811–1827, 2007.

Riedel, K., Weller, R., Schrems, O., and König-Langlo, G.: Variability of tropospheric hydroperoxides at a coastal surface site in Antarctica, Atmospheric Environment, 34(29/30), 5225–5234, doi:10.1016/S1352-2310(00)00322-8, URL `10013/epic.13190`, 2000.

Rimbu, N. and Lohmann, G.: Decadal variability in a central Greenland high-resolution deuterium isotope record and its relationship to the frequency of daily atmospheric circulation patterns from the North Atlantic region, Journal of Climate, 23, 4608–4618, 2010.

Röthlisberger, R., Bigler, M., Hutterli, M., Sommer, S., Stauffer, B., Junghans, H. G., and Wagenbach, D.: Technique for Continuous High-Resolution Analysis of Trace Substances in Firn and Ice Cores, Environmental Science &

Technology, 34, 338–342, doi:10.1021/es9907055, URL http://pubs.acs.org/doi/abs/10.1021/es9907055, 2000a.

Röthlisberger, R., Hutterli, M. A., Sommer, S., Wolff, E. W., and Mulvaney, R.: Factors controlling nitrate in ice cores: Evidence from the Dome C deep ice core, J Geophys Res, 105, 20 565–20 572, 2000b.

Röthlisberger, R., Hutterli, M., Wolff, E., Mulvaney, R., Fischer, H., Bigler, M., Goto-Azuma, K., Hansson, M., Ruth, U., Siggaard-Andersen, M., et al.: Nitrate in Greenland and Antarctic ice cores: A detailed description of post-depositional processes, Annals of Glaciology, 35, 209–216, 2002a.

Röthlisberger, R., Mulvaney, R., Wolff, E. W., Hutterli, M. A., Bigler, M., Sommer, S., and Jouzel, J.: Dust and sea salt variability in central East Antarctica (Dome C) over the last 45 kyrs and its implications for southern high-latitude climate, Geophysical Research Letters, 29, 1963, 2002b.

Ruth, U., Wagenbach, D., Bigler, M., Steffensen, J. P., Röthlisberger, R., and Miller, H.: High-resolution microparticle profiles at North-GRIP, Greenland: case studies of the calcium-dust relationship, Annals of Glaciology, 35, 237–242, doi:doi:10.3189/172756402781817347, URL http://www.ingentaconnect.com/content/igsoc/agl/2002/00000035/00000001/art00040, 2002.

Ruth, U., Barbante, C., Bigler, M., Delmonte, B., Fischer, H., Gabrielli, P., Gaspari, V., Kaufmann, P., Lambert, F., Maggi, V., Marino, F., Petit, J.-R., Udisti, R., Wagenbach, D., Wegner, A., and Wolff, E. W.: Proxies and Measurement Techniques for Mineral Dust in Antarctic Ice Cores, Environmental Science & Technology, 42, 5675–5681, doi:10.1021/es703078z, URL http://pubs.acs.org/doi/abs/10.1021/es703078z, pMID: 18754492, 2008.

Savarino, J., Kaiser, J., Morin, S., Sigman, D. M., and Thiemens, M.: Nitrogen and oxygen isotopic constraints on the origin of atmospheric nitrate in coastal Antarctica, Atmos. Chem. Phys., 7, 1925–1945, 2007.

Schlosser, E., Reijmer, C., Oerter, H., and Graf, W.: The influence of precipitation origin on the ^{18}O-T relationship at Neumayer station, Ekströmisen, Antarctica, Annals of Glaciology, 39, 41–48, 2004.

Schlosser, E., Duda, M., Powers, J., and Manning, K.: Precipitation regime of Dronning Maud Land, Antarctica, derived from Antarctic Mesoscale Prediction System (AMPS) archive data, J. Geophys. Res, 113, 2008.

Simmonds, I.: Modes of atmospheric variability over the Southern Ocean, J. Geophys. Res, 108, 1–30, 2003.

Simmonds, I., Keay, K., and Lim, E.: Synoptic activity in the seas around Antarctica, Monthly Weather Review, 131, 272–288, 2003.

Souney, J. M., Mayewski, P. A., Goodwin, I. D., Meeker, L. D., Morgan, V., Curran, M. A., Van Ommen, T. D., and Palmer, A. S.: A 700-year record of atmospheric circulation developed from the Law Dome ice core, East Antarctica, Journal of Geophysical Research-Atmospheres, 107, 4608, 2002.

Stauffer, B.: Das Isotopenthermometer im ewigen Eis: Mechanismen globaler Klimaschwankungen, Physik in unserer Zeit, 32, 2001.

Turner, J. and Pendlebury, S.: The international Antarctic weather forecasting handbook, British Antarctic Survey, 2004.

Uotila, P., Vihma, T., Pezza, A., Simmonds, I., Keay, K., and Lynch, A.: Relationships between Antarctic cyclones and surface conditions as derived from high-resolution numerical weather prediction data, Journal of Geophysical Research, 116, D07 109, 2011.

van Loon, H.: Interannual variations in the half-yearly cycle of pressure gradients and zonal wind at sea level on the Southern Hemisphere, Tellus, Series A- Dynamic Meteorology and Oceanography, 36, 76–86, 1984.

von Storch, H. and Zwiers, F. W.: Statistical analysis in climate research, Cambridge University Press, 2002.

Wagenbach, D., Ducroz, F., Mulvaney, R., Keck, L., Minikin, A., Legrand, M., Hall, J., and Wolff, E.: Sea-salt aerosol in coastal Antarctic regions, Journal of Geophysical Research-Atmospheres, 103, 1998a.

Wagenbach, D., Legrand, M., Fischer, H., Pichlmayer, F., and Wolff, E.: Atmospheric near-surface nitrate at coastal Antarctic sites, Journal of Geophysical Research, 103, 11–007, 1998b.

Wallace, J. and Hobbs, P.: Atmospheric science: an introductory survey, Academic press, 2006.

Wegner, A., Gabrielli, P., Wilhelms-Dick, D., Ruth, U., Kriews, M., De Deckker, P., Barbante, C., Cozzi, G., Delmonte, B., and Fischer, H.: Change in dust variability in the Atlantic sector of Antarctica at the end of the last deglaciation, Climate of the Past, 8, 135–147, doi:10.5194/cp-8-135-2012, URL `http://www.clim-past.net/8/135/2012/`, 2012.

Weller, R., Traufetter, F., Fischer, H., Oerter, H., Piel, C., and Miller, H.: Post depositional losses of methane sulfonate, nitrate, and chloride at the EPICA deep-drilling site in Dronning Maud Land, Antarctica, Journal of geophysical research, 109, D07 301, doi:hdl:10013/epic.19861.d001, URL `http://dx.doi.org/10.1029/2003JD004189`, 2004.

Weller, R., Woltjen, J., Piel, C., Resenberg, R., Wagenbach, D., König-Langlo, G., and Kriews, M.: Seasonal variability of crustal and marine trace ele-

ments in the aerosol at Neumayer station, Antarctica, Tellus B, 60, 742–752, 2008.

Weller, R., Wagenbach, D., Legrand, M., Elsässer, C., Tian-Kunze, X., and König-Langlo, G.: Continuous 25-yr aerosol records at coastal Antarctica - I: inter-annual variability of ionic compounds and links to climate indices, Tellus B, 63, URL http://www.tellusb.net/index.php/tellusb/article/view/16435, 2011.

Wesche, C., Riedel, S., and Steinhage, D.: Precise surface topography of the grounded ice ridges at the Ekströmisen, Antarctica, based on several geophysical data sets, ISPRS Journal of Photogrammetry and Remote Sensing, 64, 381 – 386, doi:DOI:10.1016/j.isprsjprs.2009.01.005, URL http://www.sciencedirect.com/science/article/B6VF4-4VPCVGH-2/2/4f2e51a185d5b424fb1b95febf1e1769, 2009.

Wilks, D. S.: Statistical methods in the atmospheric sciences, 1995.

Wolff, E., Rankin, A., and Röthlisberger, R.: An ice core indicator of Antarctic sea ice production, Geophys. Res. Lett, 30, 2158, 2003.

Yang, X., Pyle, J. A., and Cox, R. A.: Sea salt aerosol production and bromine release: Role of snow on sea ice, Geophysical Research Letters, 35, 2008.

A Comparison of IC and CFA measurements

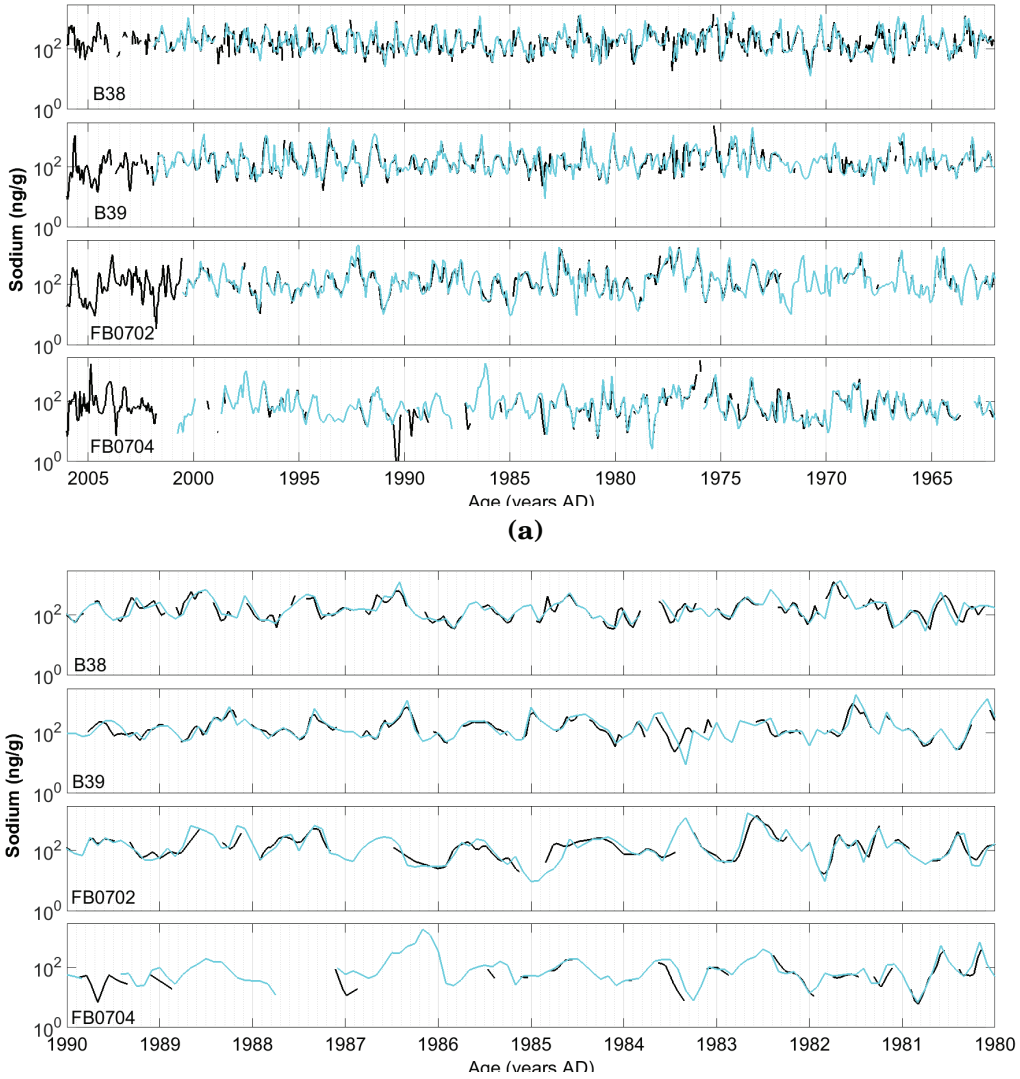

Figure 57: *Comparison of sodium concentrations quantified by CFA (cyan line) and IC (black line). (a) shows the full record, (b) the time series from 1980 to 1990.*

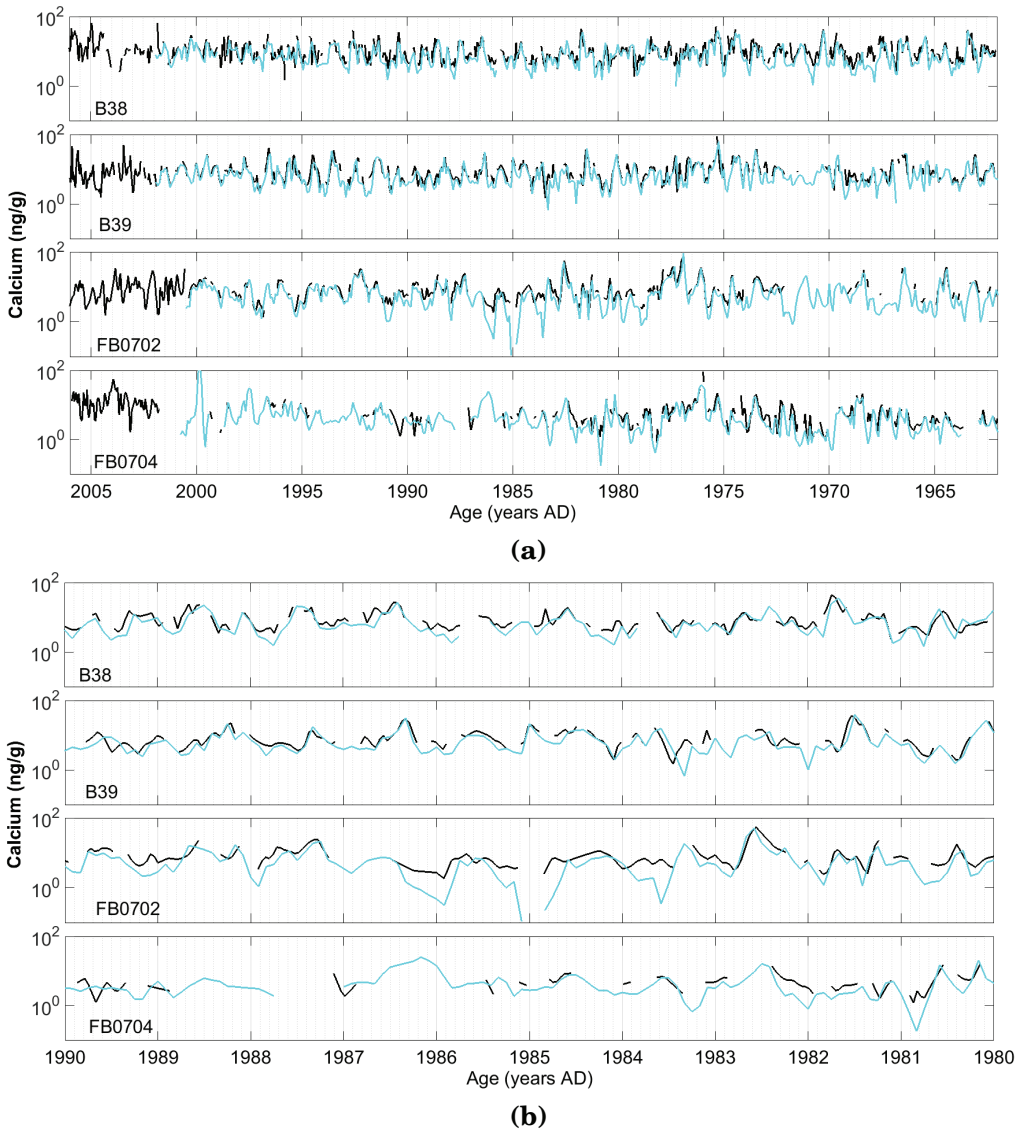

Figure 58: *Comparison of calcium concentrations quantified by CFA (cyan line) and IC (black line). (a) shows the full record, (b) the time series from 1980 to 1990.*

B Time series

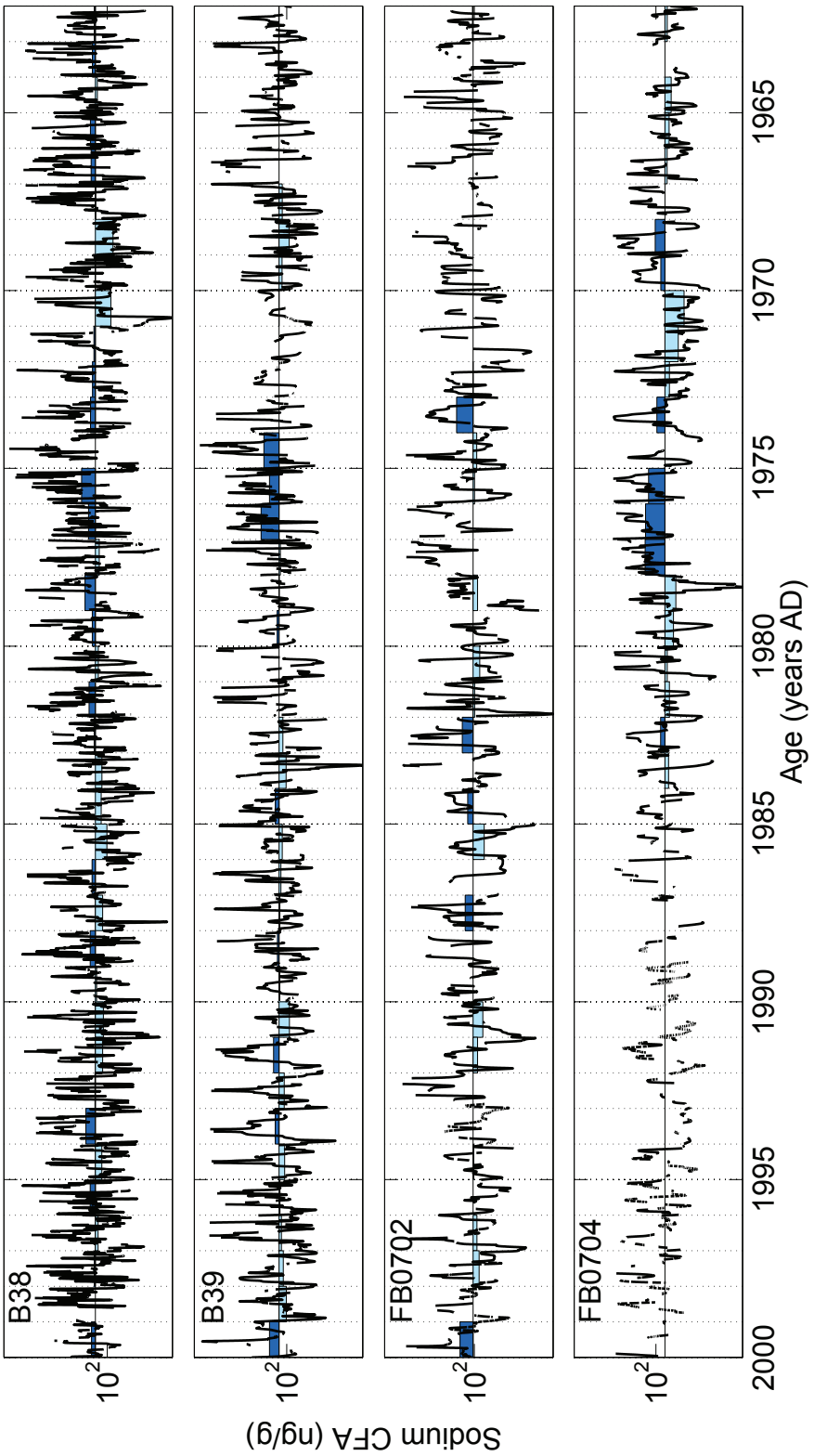

Figure 59: *Same as Fig. 16 but for sodium concentrations from CFA.*

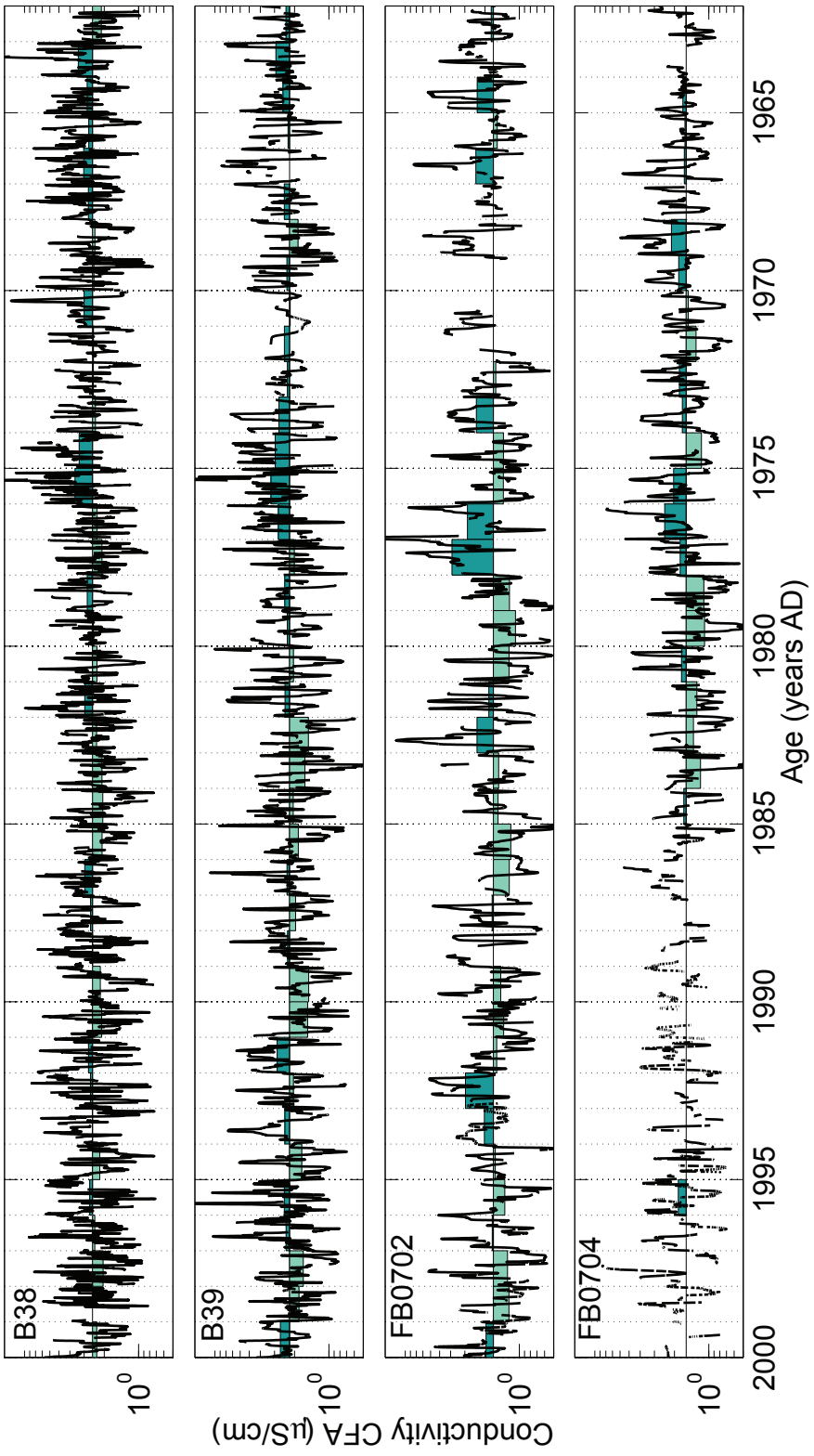

Figure 60: *Same as Fig. 16 but for conductivity from CFA.*

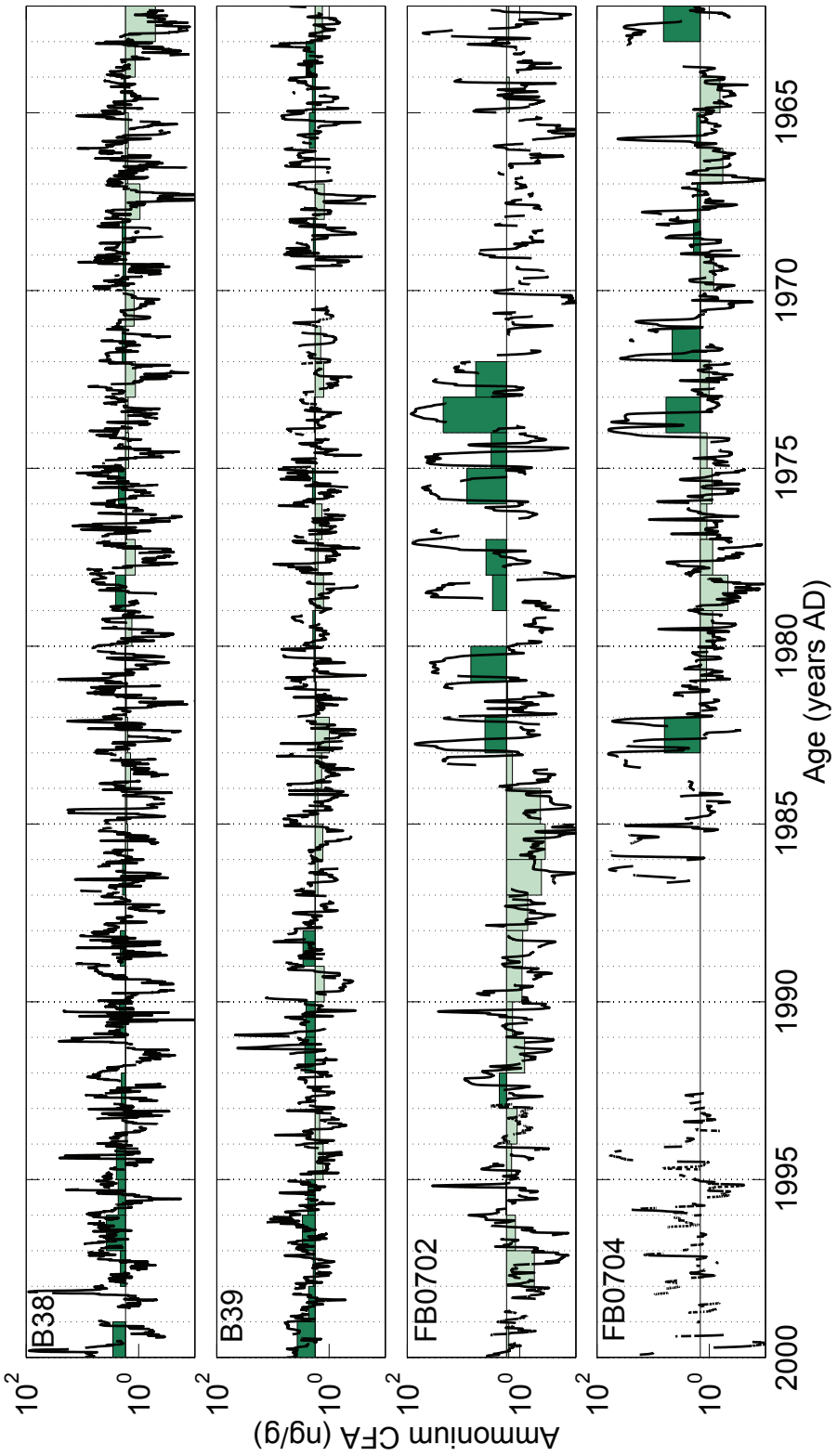

Figure 61: *Same as Fig. 16 but for ammonium concentrations from CFA.*

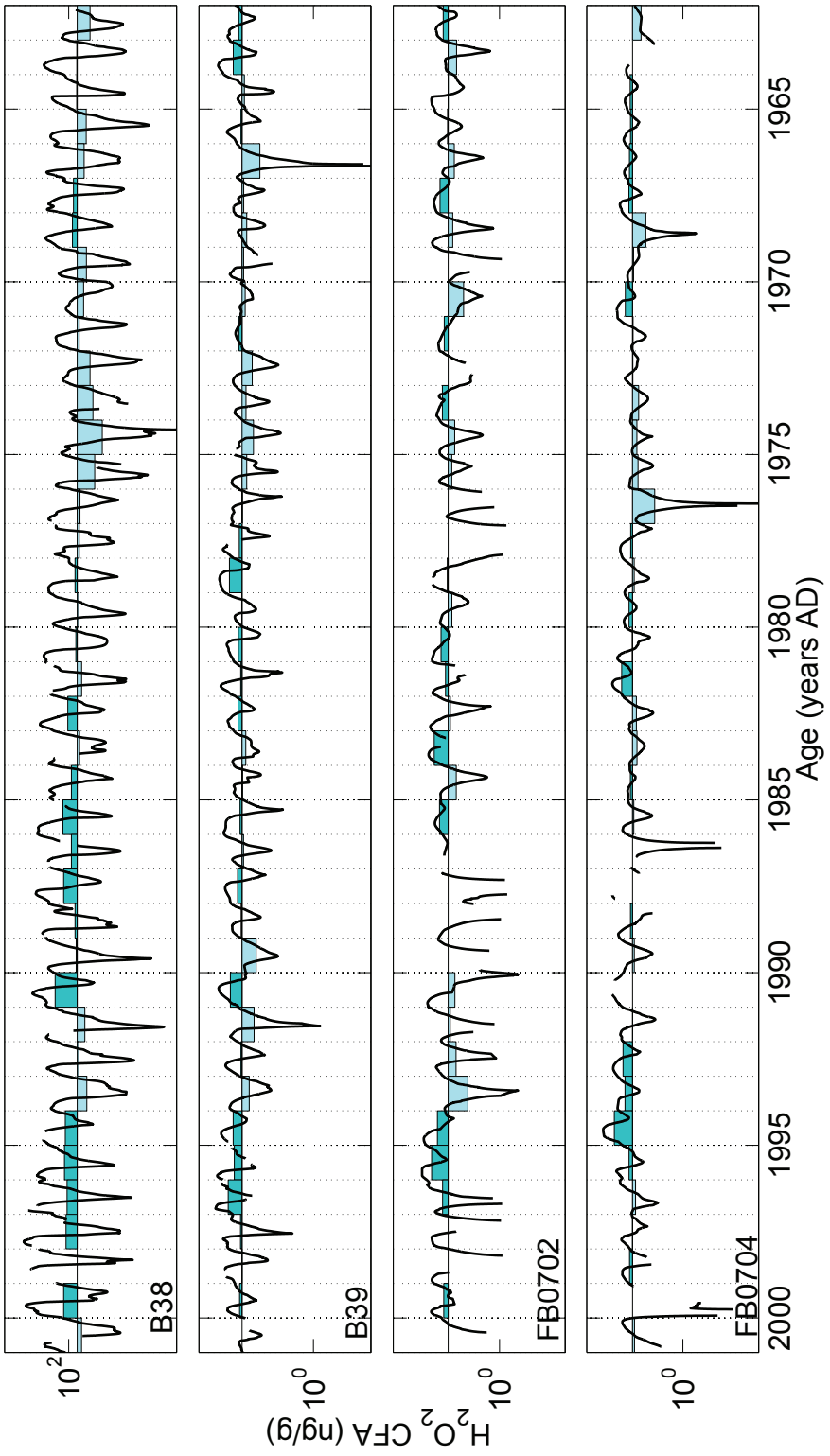

Figure 62: *Same as Fig. 16 but for oxygen peroxide from CFA.*

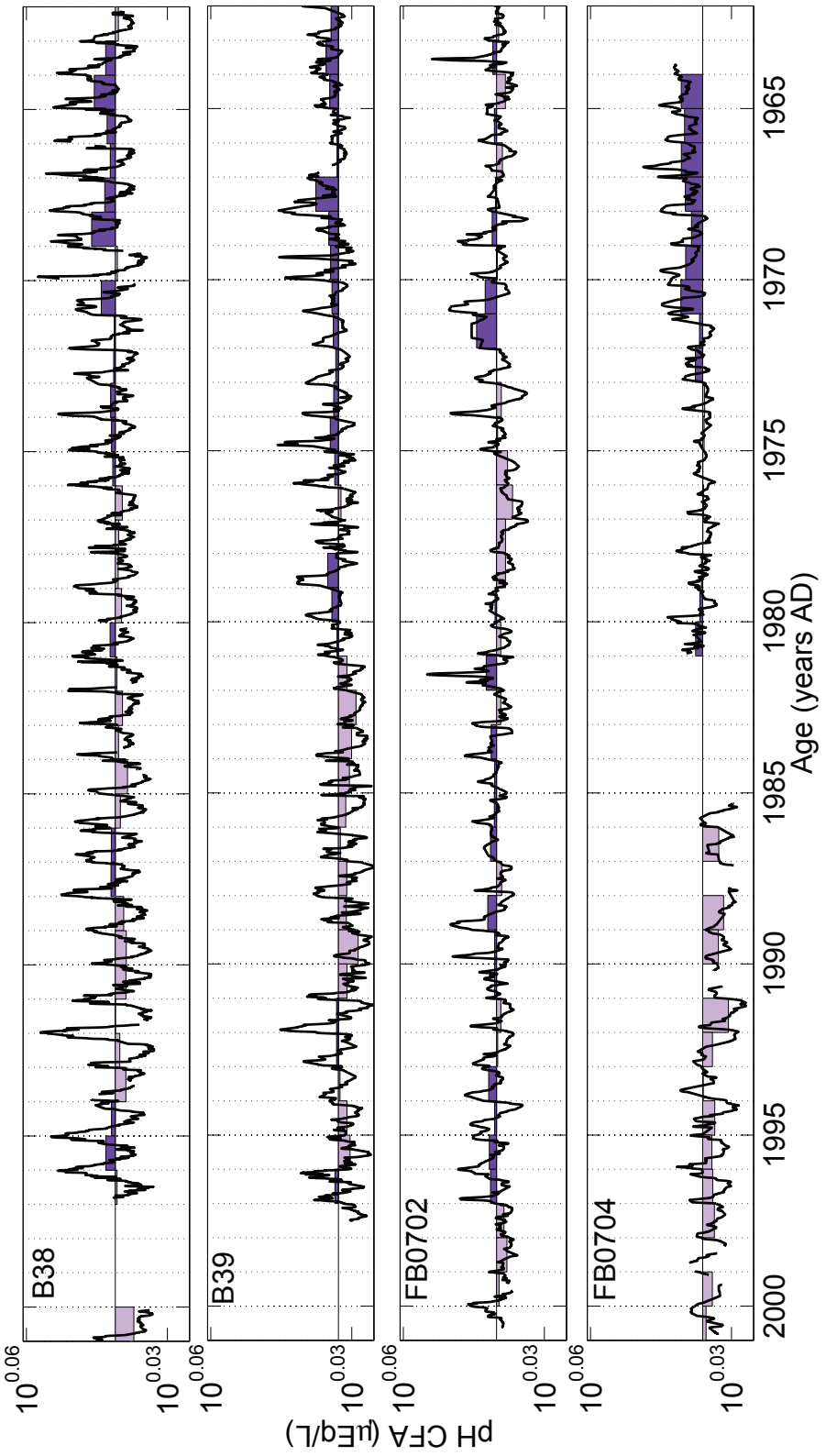

Figure 63: *Same as Fig. 16 but for acidity from CFA.*

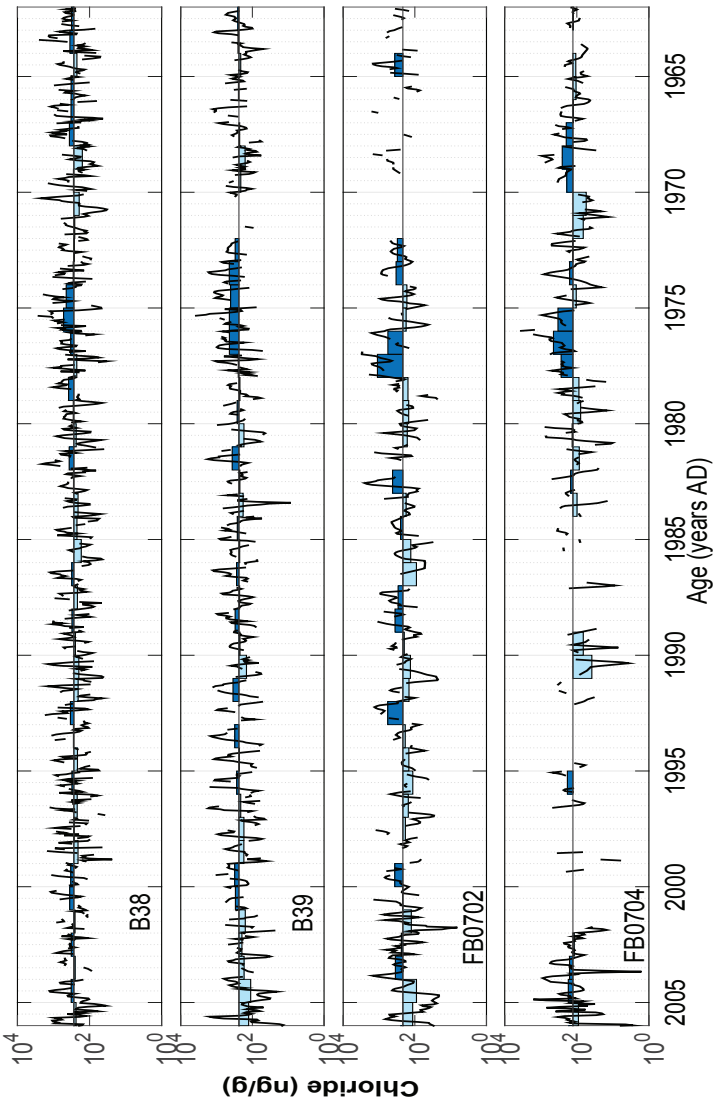

Figure 64: *Same as Fig. 16 but for chloride concentrations from IC.*

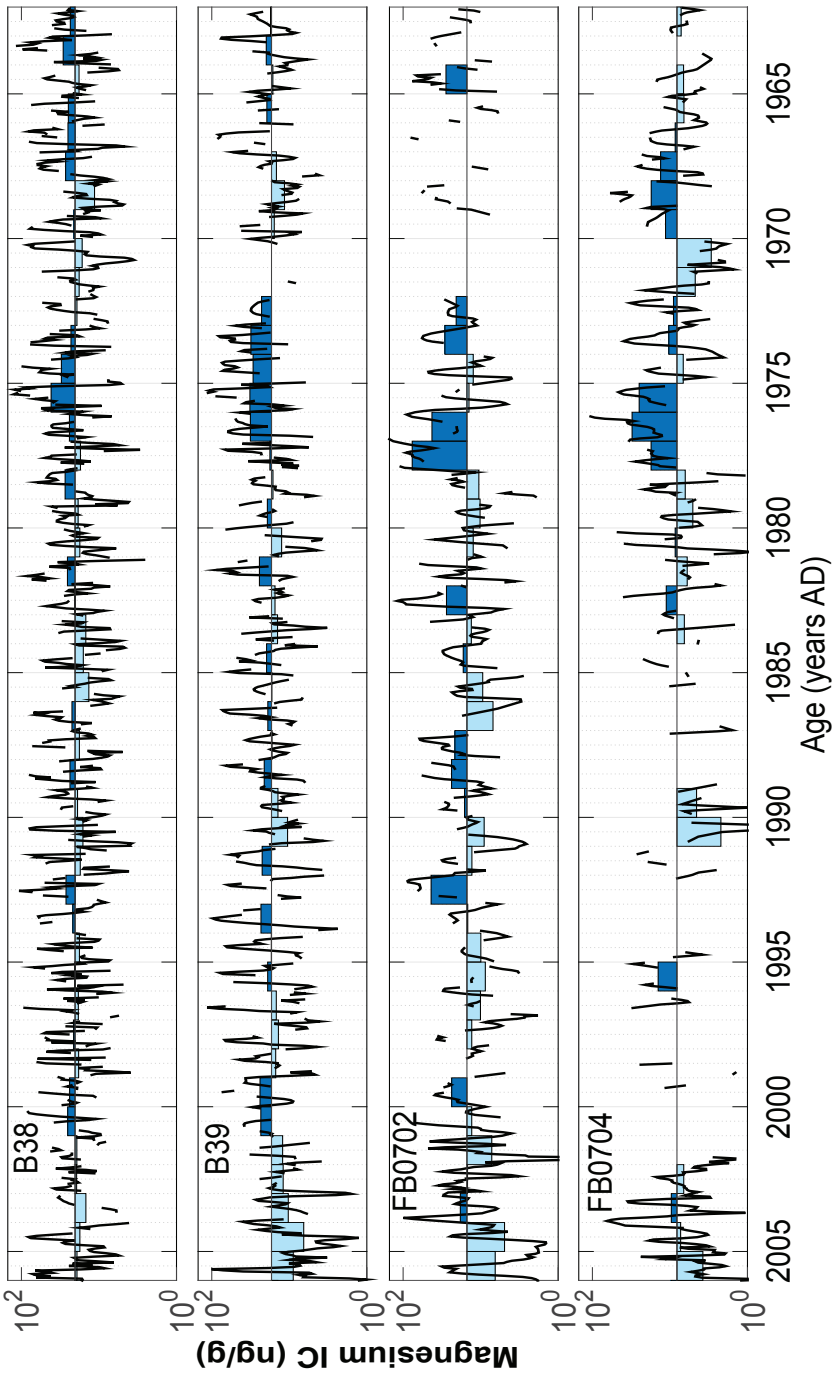

Figure 65: *As figure 16 but for magnesium time series from the IC.*

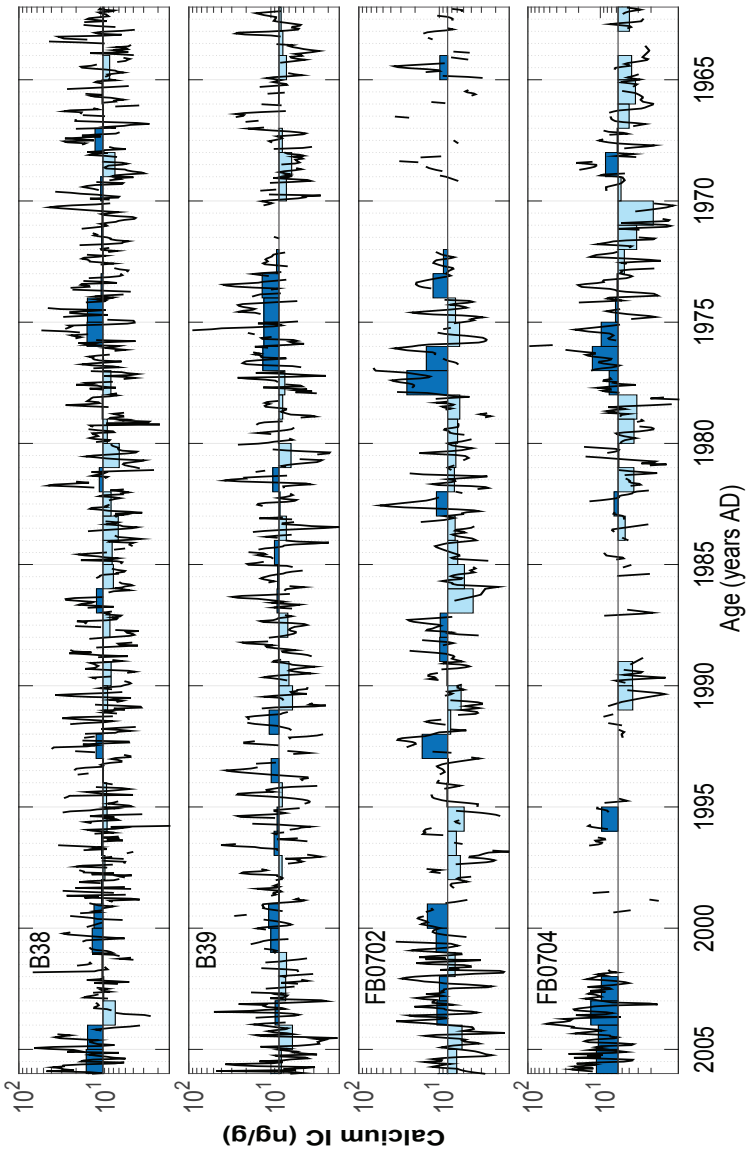

Figure 66: *Same as Fig. 16 but for calcium concentrations from IC.*

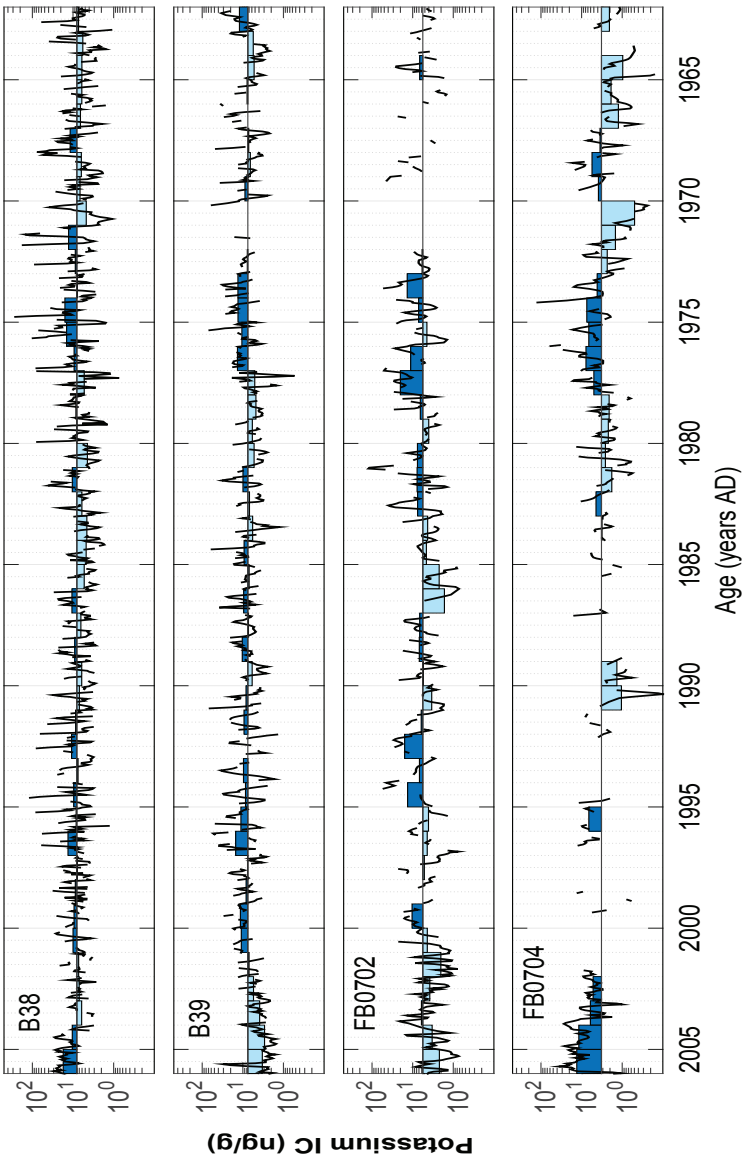

Figure 67: *Same as Fig. 16 but for potassium from IC.*

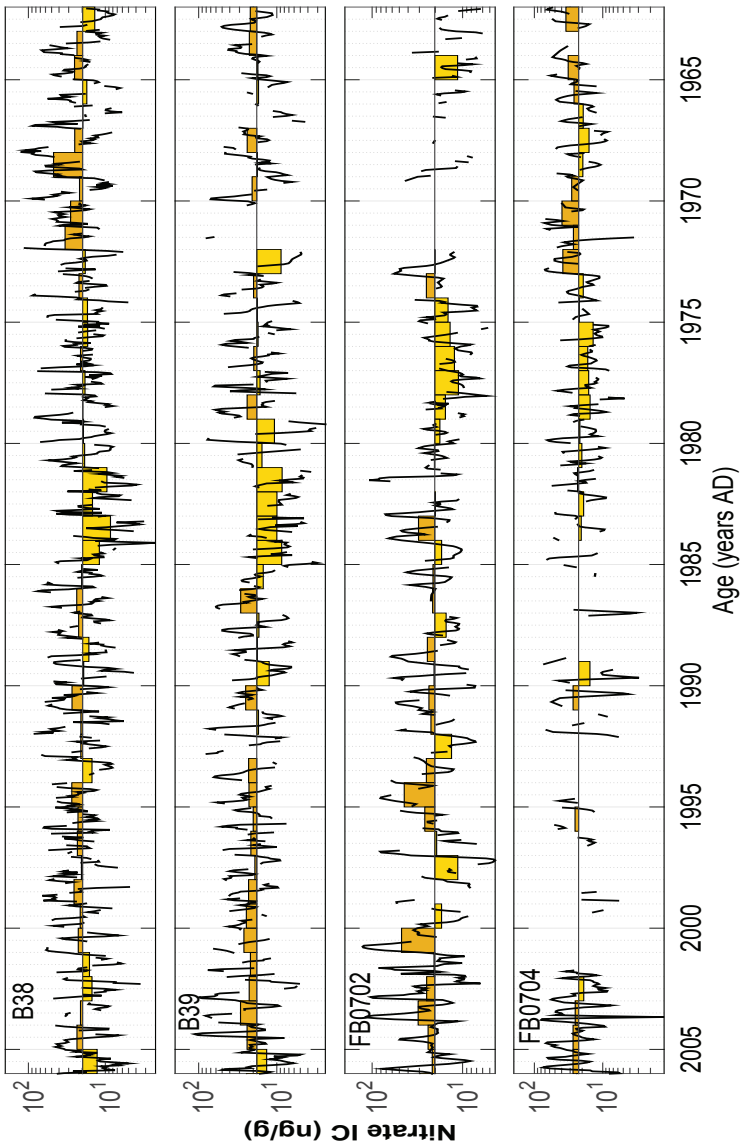

Figure 68: *Same as Fig. 16 but for nitrate from IC.*

C Seasonality

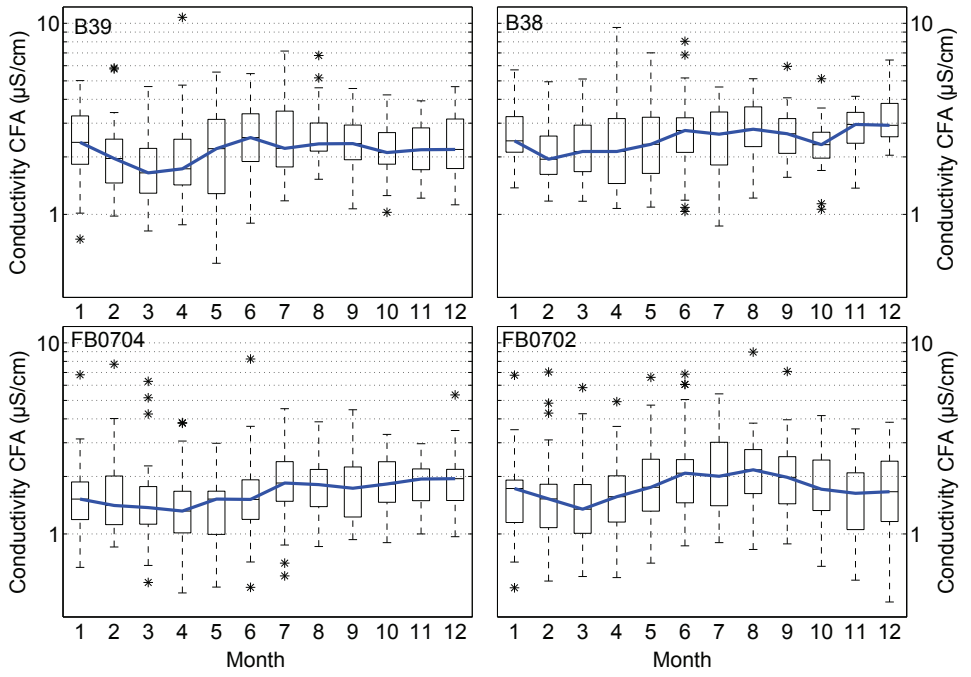

Figure 69: *Seasonally stacked conductivity record quantified by CFA (boxplots and blue line).*

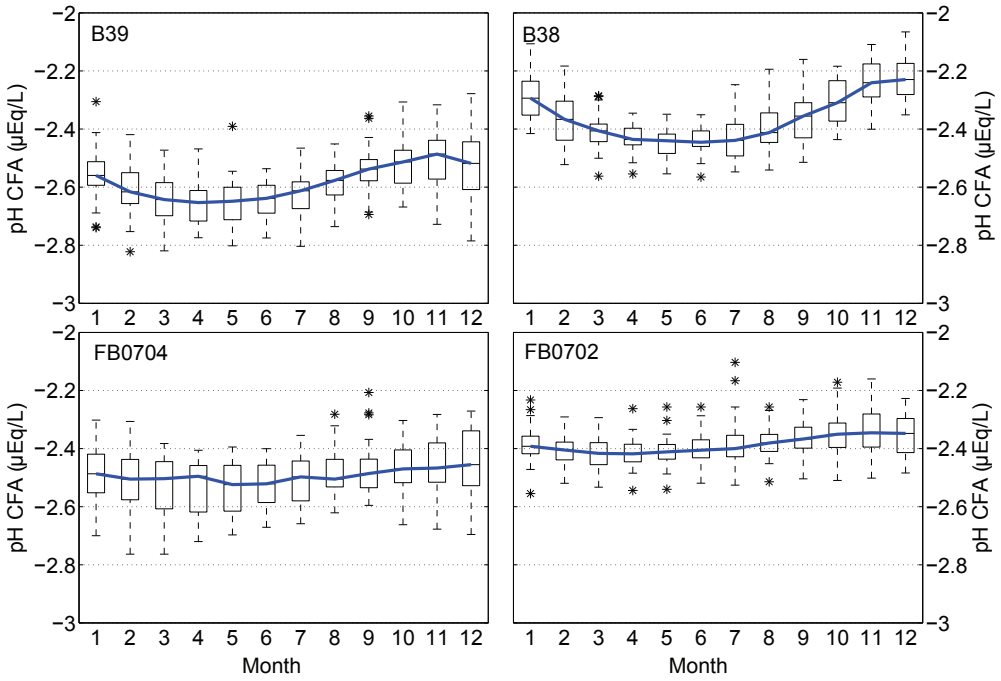

Figure 70: *Same as in figure 69 but for pH*

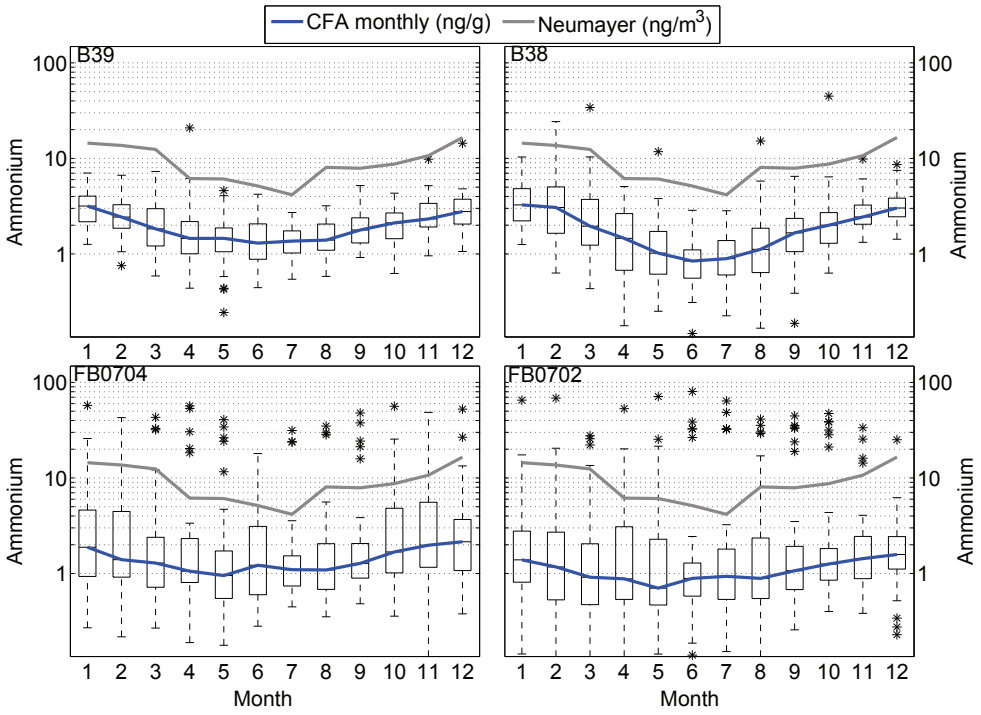

Figure 71: *Same as in figure 69 but for ammonium. Gray lines represent stacked data from Neumayer Station over the time period (1984-2006)*

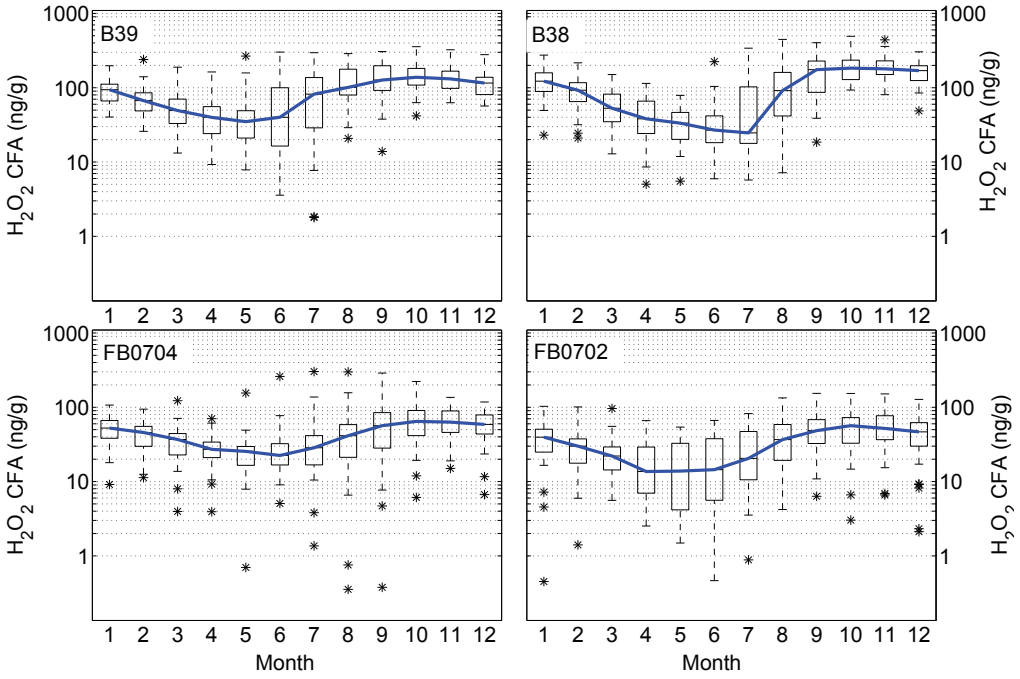

Figure 72: *Same as in figure 69 but for oxygen peroxide*

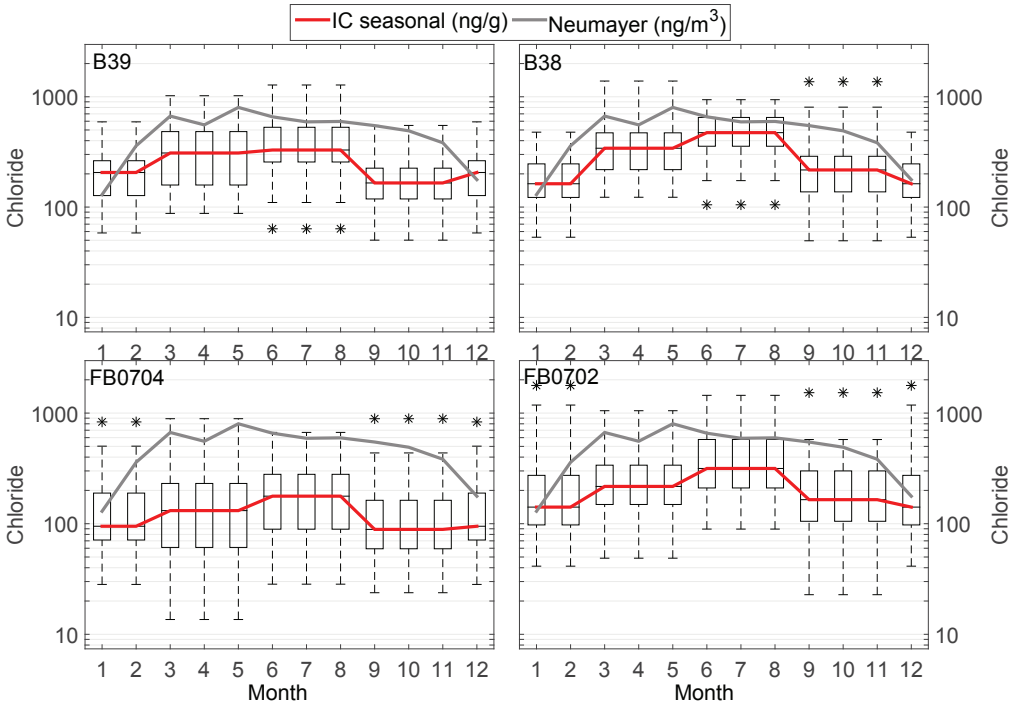

Figure 73: *Seasonally stacked chloride record quantified by IC (boxplots and red line). Gray lines represent stacked data from Neumayer Station over the time period (1984-2006).*

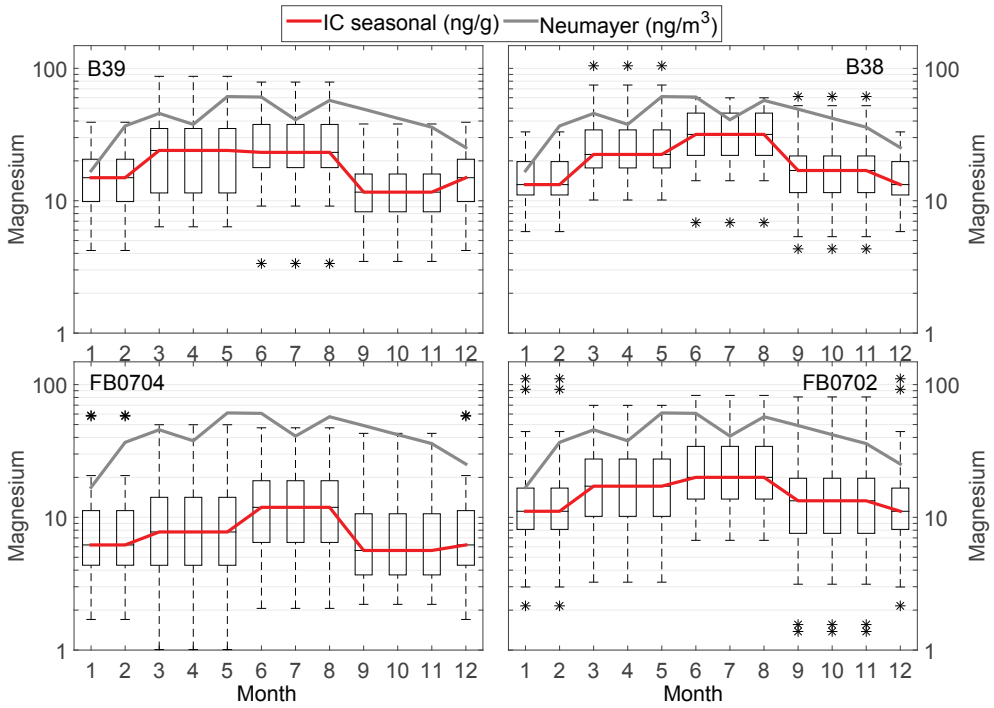

Figure 74: *Same as in figure 73 but for magnesium*

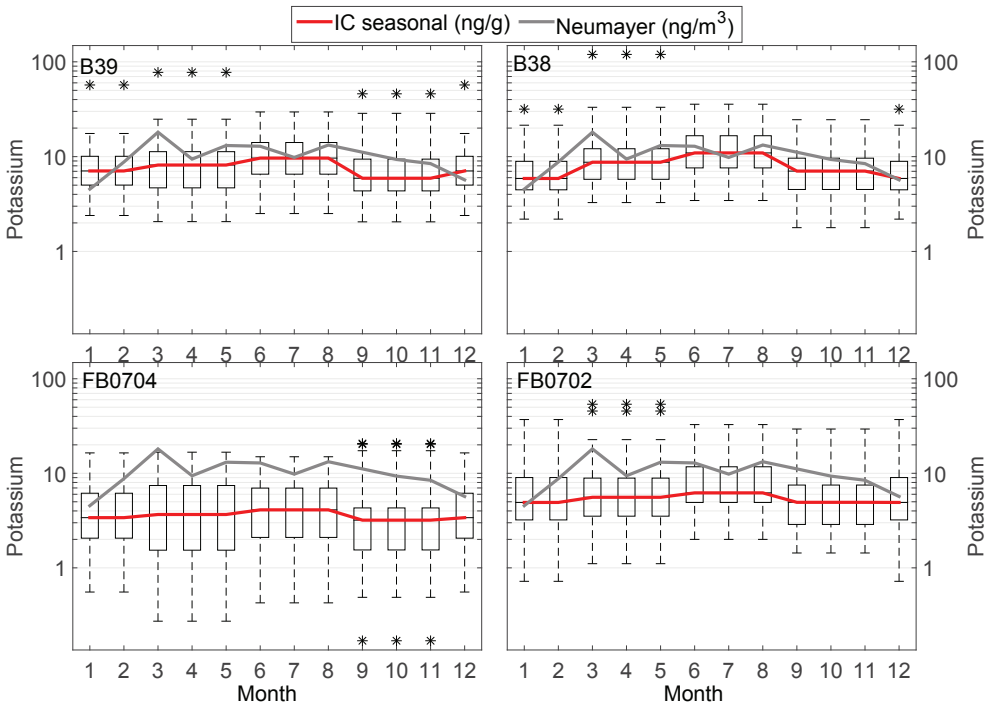

Figure 75: *Same as in figure 73 but for potassium*

Danksagung

Ich möchte mich bei den Menschen bedanken, die mich in den letzten drei Jahren begleitet haben.

Heinrich Miller für das Doktorvatersein.

Gerrit Lohmann für das Zweitprüfersein.

Anna Wegner und Rolf Weller für ihre unermüdliche Unterstützung.

Hubertus Fischer und Norel Rimbu für die tolle Zusammenarbeit.

Allen AWI-Glaziologen für die Diskussionen, den Kaffee, den Kaffee, den Kaffee, die MoMoKuchen und...

Dem POLMAR Team.

Allen am NEEM-Projekt beteiligten für die zwei tollen Saisons in Grönland.

Dem CFA-Team in Bern für die tolle Zeit in Bern und NEEM und die Unterstützung bei den Messungen:
Daiana, Gideon, Matthias, Olivia und Simon

Meinen Irren und meiner Familie für das gemeinsame Glücklichsein.
Anja D., Anja H., Anja H., Anne, Antje, Claudia, Dennis, Geri, Hanjo, Inga, Julian, Karsten, Katharina, Katrin P., Katrin W.., Lena, Lily, Line, Madlen, Maike, Mama, Markus, Mirka, Moni, Oli, Papa, Peter (bester Korrekturleser der Welt), Steffi S., Steffi W., Sven, Till, Tobi, Tony, Verena.
Und allen Neumayers.

Außerdem den Menschen, die die Musik in mein Leben bringen.
Ganz besonders Bela, Farin und Rod.

Da ist ein Licht, das lässt mich tanzen,
jede Nacht strahlt es mich an...
...denn der Wind trägt Lieder zu mir hin,
ich fang leise an zu singen
(Olli Schulz- Phosphormann)